Aalto University

School of Engineering

Jorge Armando Vega Lacy

Powder Bed Fusion for Electromechanical Plastic Components in High Voltage Electric Vehicle Applications.

Master's thesis

Degree Programme in Mechanical Engineering

In partial accordance to the degree requirements.

Supervisor: Professor Jouni Partanen

Turku, 17.08.2020

Abstract

Over the years, Injection Molding has been the ruling process to manufacture polymeric components for the automotive industry. By this process, excellent properties and fully dense parts can be achieved. Injection Molding can be pricey if a production batch size is not big enough to justify the high costs of the molds. With the increasing demand for Electric Vehicles, the need for plastic parts with a combination of good mechanical and dielectric properties could grow significantly. When low production volumes are required, Additive Manufacturing of polymeric components can be considered as an alternative to Injection Molding. For this to happen, the behavior of parts produced by Additive Manufacturing need to be tested in order to demonstrate their mechanical capabilities and as electrical insulators within a high voltage level, at which components and devices utilized in Electric Vehicle applications are tested.

In this work, tensile and electrical insulation specimens manufactured from polyamide (PA12) by Selective Laser Sintering (SLS) and HP- Multi Jet Fusion (MJF) in three build orientations were tested and compared to equivalent specimens produced by Injection Molding. For analyzing their mechanical properties, tensile tests were carried out according to the ISO-527 standard. To evaluate their efficiency as electrical insulators, voltage withstand (HIPOT) tests were performed to the specimens at a voltage level of 4kV AC and within a temperature range between 20 and 100°C.

The test results obtained by the tensile experiments denoted that the parts produced by Powder Bed Fusion for these experiments presented brittle behavior at fracture, with a maximum elongation at break between 10-26%. The maximum achieved tensile strength values represented almost 74% of the ones obtained by the injection molded equivalent specimens. As electrical insulators, the HIPOT test results showed that SLS specimens with a thickness of 2mm withstood a 4kV AC voltage load comparably as the injection molded parts. The Radiation- Absorbing Material present in the HP-MJF fusing agent could be a contributor for dielectric breakdown on the tested specimens. Therefore, the applicability of the HP-MJF process is questionable for high voltage environments and within the test conditions employed.

Keywords: Selective Laser Sintering, Multi Jet Fusion, dielectric breakdown, HIPOT, tensile test, Powder Bed Fusion, electrical insulation, electromechanical.

Acknowledgements

Abbreviations

ABS – Acrylonitrile butadiene styrene.

AM – Additive Manufacturing.

ASTM – American Society for Testing and Materials.

BAAM – Big Area Additive Manufacturing.

BEV – Battery Electric Vehicle.

CFF – Continuous Fiber Filament

CTI – Comparative Tracking Index.

EAB – Elongation at Break.

ESS – Energy storage system.

EV – Electric Vehicle.

EVA – Ethylene Vinyl Acetate Copolymer.

FDM – Fused Deposition Modeling.

FFF – Fused Filament Fabrication.

FLM – Fused Layer Modeling

HEV – Hybrid Electric Vehicle.

MJF – Multi Jet Fusion.

HV – High Voltage.

HSS – High Speed Sintering

IM – Injection Molding.

IR – Infrared.

ISO – International Organization for Standardization.

ORNL – Oak Ridge National Laboratory.

OEM – Original Equipment Manufacturer.

PA – Polyamide.

PBF – Powder Bed Fusion.

PBT – Polybutylene Terephthalate.

PEI – Polyetherimide.

PEV – Pure Electric Vehicle.

PHEV – Plugin Hybrid Electric Vehicle.

PLA – Polylactic acid

POM – Polyoxymethylene.

RAM – Radiation-Absorbing Material.

RP – Rapid Prototyping.

SLS – Selective Laser Sintering.

TPU – Thermoplastic Polyurethane.

UTS – Ultimate Tensile Strength.

Table of contents

1. Introduction

1.1 Objectives and motivation

This thesis has the goal of studying the electromechanical behavior of additively manufactured specimens when exposed to a high electric field and to tensile loading by comparing them with specimens manufactured by injection molding (IM). A voltage withstand test (HIPOT) is performed in electronic devices for electric vehicle (EV) applications during production. Therefore, this method is applied to evaluate if insulators produced by Selective Laser Sintering (SLS) and HP-Multi Jet Fusion (HP-MJF) are comparable to their injection molded counterparts. Mechanical properties play an equal role of importance for components that have the purpose of enclosing and supporting electrically conductive parts. Because of their importance, this thesis also compares mechanical properties by tensile testing. SLS, as a pioneering Powder Bed Fusion (PBF) process has been extensively studied, on the contrary HP-MJF is a relatively new process and a research gap has been identified in terms of studies that locate this technology on the map to produce parts for electromechanical applications.

This thesis aims to answer the following research questions:

- Are specimens manufactured by Selective Laser Sintering and Multi Jet Fusion comparable with injection molded parts and suitable to be utilized as electrical insulators within a defined test Voltage level utilized in the manufacturing of EV components?
- What are the main differences on mechanical properties between specimens manufactured by injection molding and by Powder Bed Fusion determined by short-term tensile testing?

1.2 Scope of this thesis

EV applications are too wide to be covered in a single thesis project. Therefore, this thesis is limited to study test specimens and not specific components that are present on a vehicle. Although, there is an overview of general requirements for plastics for EV applications included on section 3.1, not all the applications and requirements are covered in depth or included on the empirical section.

This thesis is based on a literature review of books, journal papers, articles, AM related websites, standards and material datasheets. A basic overview is given to AM technologies commonly utilized for processing plastics with higher emphasis on the technologies

included in the empirical chapters. The scope of this thesis is limited to voltage withstand and tensile characteristics of the samples without covering all the dielectric and mechanical properties that could be studied from a material for automotive applications. Further studies suggested to complement this work on Section 9.

1.3 Introduction and work structure

Additive Manufacturing (AM) involves a wide group of manufacturing technologies that are based on building solid objects layer by layer and directly from a digital model. In contrast with conventional manufacturing methods, with AM, it is not required to sculpt a shape from a block of raw material like with CNC machining. Neither is required to manufacture a mold or tool to shape a product like in injection molding (IM) or die casting. Due to its layer-based nature, AM offers the opportunity to create solid objects with minimal design and geometry limitations. In most of the cases, those geometries would be nearly impossible to be created by the conventional methods previously mentioned [1, 2].

AM originated as a prototyping technology focused on visual models for fit, function and form testing, and the processing speeds were low. The processes and equipment have improved drastically over the last decades in terms of quality and speed, so much that for some applications, AM is no longer a prototyping technology but the main process for end-use parts and for the serial production of small series of products, for instance hearing aids [1].

Vehicle manufacturers and component suppliers have been some of the earlier adopters of AM technologies for product development and manufacturing aiding tools. As most of the parts for vehicles are produced in massive volumes, injection molding is the most viable method for large scale production outputs at high speeds and high accuracy. AM cannot beat injection molding in terms of mechanical properties, speed, costs per unit and quality [1]. But it offers other advantages such as product customization, faster and cheaper design modifications, offers design freedom in terms of packaging components in reduced spaces and irregular geometries. At low production volumes, AM could provide parts at lower costs as there are no mold costs involved.

Powder Bed Fusion (PBF) is an AM sub-category of processes characterized by their capacity to transform raw materials in the shape of fine powders into three-dimensional solid objects by the aid of an energy source, which when applied towards the raw material, fuses together the powder particles. PBF, for example polymer Laser Sintering, has high potential to be utilized as a serial production method [3]. It does not require the addition of support structures when printing parts. Additionally, laser sintered parts possess a right balance of mechanical properties, long-term reliability and good precision [3].

Electric Vehicles (EVs) are complex products that utilize a series of electromechanical components in their propulsion systems for distributing, transforming or storing energy. Electrical energy is then transformed into mechanical energy and into motion transferred from an electric machine to the wheels of the vehicle. Most of those electromechanical systems contain electrically conductive parts that need to be supported and protected but also to be insulated from each other to avoid undesired electric contacts. For this purpose, polymeric materials are a suitable solution. They possess excellent dielectric properties, are economic and light-weight. When the batch size for producing parts does not justify the investment of an injection molding tool it is important to investigate how additively manufactured parts react to high voltages compared to injection molded components.

This thesis is oriented on making a comparative study between three different manufacturing technologies (Injection Molding, Selective Laser Sintering and HP-Multi Jet Fusion) in terms of tensile properties and voltage withstand. The tensile properties can provide a general idea of the mechanical behavior of the parts and the voltage withstand test on how the parts act as insulators under the stress of a high voltage level utilized during EV component production tests.

After this introductory section, section 2 provides a general background related to the growth in the demand for electric vehicles and an overview of common High Voltage (HV) components present in an EV.

Then, section 3 gives and introduction to thermoplastic polymers, the differences between amorphous and semi-crystalline polymers and general requirements for plastics that are utilized in vehicle electrification. As injection molding is the benchmark process on this work, section 4 describes the basics of injection molding as a process. Section 5 contains descriptions of the Additive Manufacturing technologies that are commonly utilized for processing polymers. The focus is given to Powder Bed Fusion processes, describing the process itself, some process parameters and materials. Section 6 digs into the work done by other researchers that have performed similar experiments for PBF parts and summarizes their main findings.

The empirical content of this thesis starts from section 7, it presents a comparative study between specimens manufactured by Injection Molding and SLS and MJF. Section 7 includes the methods and equipment utilized during the experiments to analyze tensile properties and high voltage stress of the specimens and the limitations of the testing procedures, the equipment and the devices utilized. Section 8 contains the main findings of the comparative study in a detailed manner with comparative graphs and discussion based on the literature reviewed in section 6. Section 9 summarizes, concludes the work done and contains suggestions for future work for a potential continuation on this thesis topic.

2. Background

The European Commission established that in order to reach the goal of 2°C resulting from climate change caused by greenhouse gas emissions, the transportation sector should cut emissions by 60% and by phasing out internal combustion engine vehicles from cities by the year 2050 [4]. It is estimated that by the year 2025, the amount of electric and hybrid electric vehicles circulating around the world will represent an approximate of 30% of the global vehicle fleet, with a 7.7% being battery electric vehicles (BEVs) and 23% hybrid electric vehicles (HEVs) [5]. According to the European Environmental Agency, only in the European Union the sales of BEVs increased by 51% and of plug-in Hybrids by 35% from 2016 to 2017 [6].
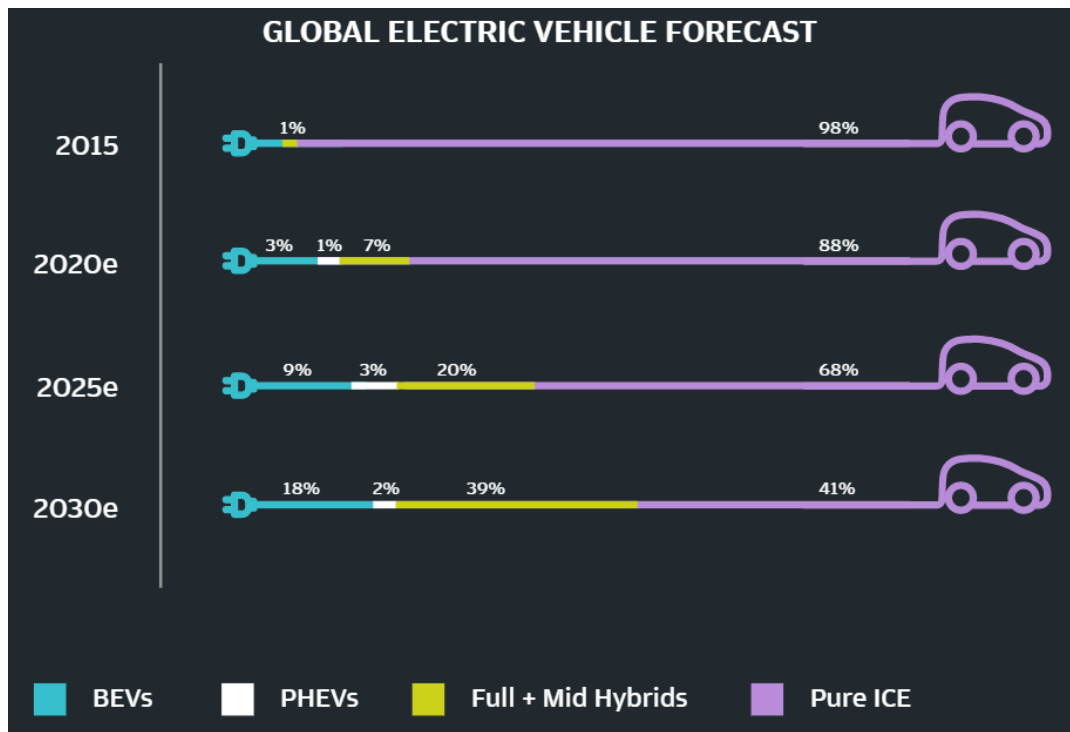
Figure 1: Electric vehicle forecast for 2025: J.P. Morgan estimates [5].

Vehicle manufacturers are constantly looking to develop lighter vehicles by switching to new materials for reducing fuel consumption, CO_2 emissions or, in the case of EVs, extend the range of the vehicle. One example of this is the BMW i3 electric car, that has a body structure manufactured from a carbon fiber composite [7]. By the utilizing thermoplastics good strength-to-weight ratio of components can be achieved. Plastic materials are traditionally transformed into functional components by injection molding, this process is capable to supply the large volumes required for automobile production. Such volumes, usually batches well above 1000pcs, are not always required during the product development phases of a component or when a product run is smaller but still is intended

to be an end-use part. For high volume manufacturing injection molding is the most competitive solution **[2]**, but injection molding can be an expensive process for prototyping purposes. An injection molding prototype requires a soft mold and making modifications to it result in added costs and extended time periods that are not desired when fast design changes are required.

Additive Manufacturing (AM) technologies offer the possibility to shorten the time spent on developing products due to the fact, that they can support the creation of faster design iterations by allowing designers and engineers to validate their concepts and create physical objects directly from a digital model imported to an AM machine in STL format. For small production volumes, AM is not limited to prototyping and can offer an alternative for serial production. AM cannot be considered a competitor against injection molding in terms of speed or achievable properties **[2]**. The highest advantage of AM can be described by quoting Neil Gershenfeld, from the MIT Center for Bits and Atoms who has said: "the revolution is not additive versus subtractive manufacturing; it is the ability to turn data into things and things into data" **[8]**. Consequently, it is important to emphasize the potential of AM as an innovation-enhancing technology and not as a replacement for existing processes.

On the other hand, it is important to understand how some parts created by AM technologies utilized for plastics (SLS and MJF) behave compared to injection molded ones in applications where injection molding is the most conventional solution. The need for elaborating this study surges from the will to increase the knowledge for AM technologies at the Product Development department at Valmet Automotive. The results will help as a starting point when selecting a suitable process between SLS or MJF for prototypes or for small production series for components present in EVs.

2.2 EV Powertrain HV Components

According to the EN 13447:2001 standard **[9]**, an electrically propelled road vehicle is a vehicle that utilizes and transforms electrical energy to generate mechanical energy by using one or more electric machines with the goal of generating traction. Road electric vehicles englobe a wide variety of topologies and architectures that utilize electric machines as their main or supplementary traction source. When electric propulsion systems are mixed with other sources of propulsion, the vehicle is considered a hybrid electric vehicle (HEV) **[9]**. When the propulsion system is purely based on electricity that is utilized to transfer power to the wheels of the vehicle, the vehicle is considered a pure electric vehicle (PEV). This section describes some of the main components utilized in electric vehicles without going into details of the different topologies and architectures that determine the differences between pure electric vehicles and several existing types of

hybrid electric vehicles. For practicalities, only battery electric vehicles are included as the main components are common between HEVs and PEVs. Fuel cell vehicles or topologies that do not use batteries to store energy are not included in this thesis.

According to the MBN LV123 standard [10], which is directly based on the German Association of the Automotive Industry standard VDA LV123, the typical HV components of an electric vehicle are an Energy Storage System (ESS), a power distribution unit (PDU), inverters for switching from DC to AC when an induction motor is utilized, a transmission with electric accessories such as an electric pump with motor, loads caused by running accessories such as an A/C compressor or HV heater. A DC/DC converter that allows the high voltage to be delivered to low voltage accessories such as the auxiliary battery of the vehicle. HV wire harnesses for AC or DC circuits, an on-board charger with inlet that in case of the usage of an AC power supply will be used to convert to DC to supply the ESS. The schematic representation in Figure 2 shows the different components mentioned before with two different alternative layouts depending on the type of external power source.
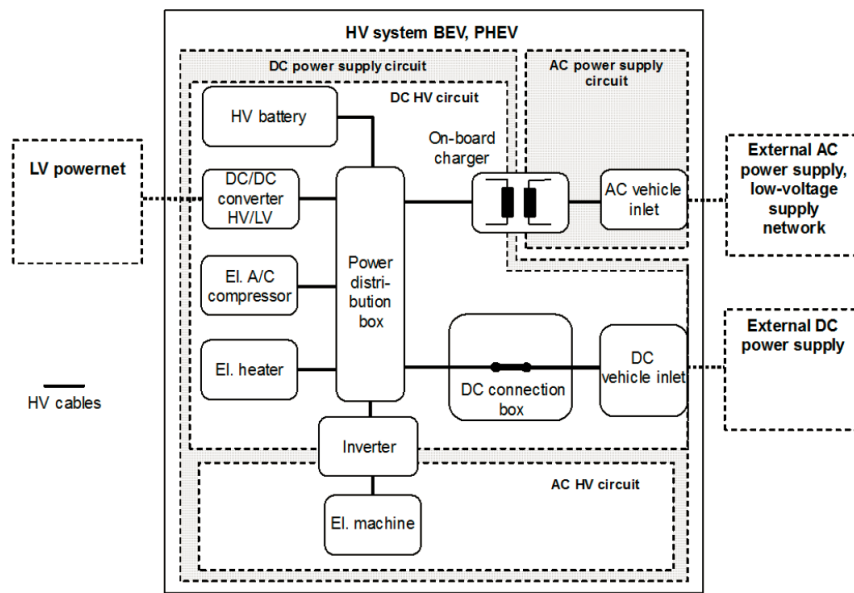
Figure 2: Schematic representation of the HV components in a BEV or PHEV. Extracted from [10].

Another aspect covered by the MBN LV123 is the list of typical parts that constitute a HV component. It could include a low voltage control unit, a low voltage connector for interface to the internal communications network of the vehicle, a ground connection, HV electronics and electric components, HV connectors, cooling connections, mechanical protection given by a housing or cover and a mechanical interface to mount to the vehicle for example, brackets and fasteners [10]. The focus of this thesis is on plastic parts that provide support, enclose and insulate smaller electrically conductive components inside of some of the main components mentioned above. As the number of HV components is wide

and each design can vary depending on the manufacturer and end application, the internal design or configurations of each HV component was not included in this thesis project.

The role of plastics in a HV battery pack or power electronics components is to provide mechanical packaging combined with electrical insulation for HV conductive components [11]. Some examples are presented in Figure 3, which shows two different plastic component sets, on the left upper side some battery cell repeater frames and manifold assembly from a Chevrolet Volt made from BASF Ultramid 1503-2 (PA66 30%GF) [11], on the right upper side a Nissan Leaf's disassembled DC/DC converter (junction box) showing busbars and contactors supported by a plastic carrier plate that keeps them away from touching the metal enclosure or other conductive components. The lower picture in Figure 3 is a close-up view of the Nissan Leaf's junction box, which is manufactured by Denso Corporation according to [12].
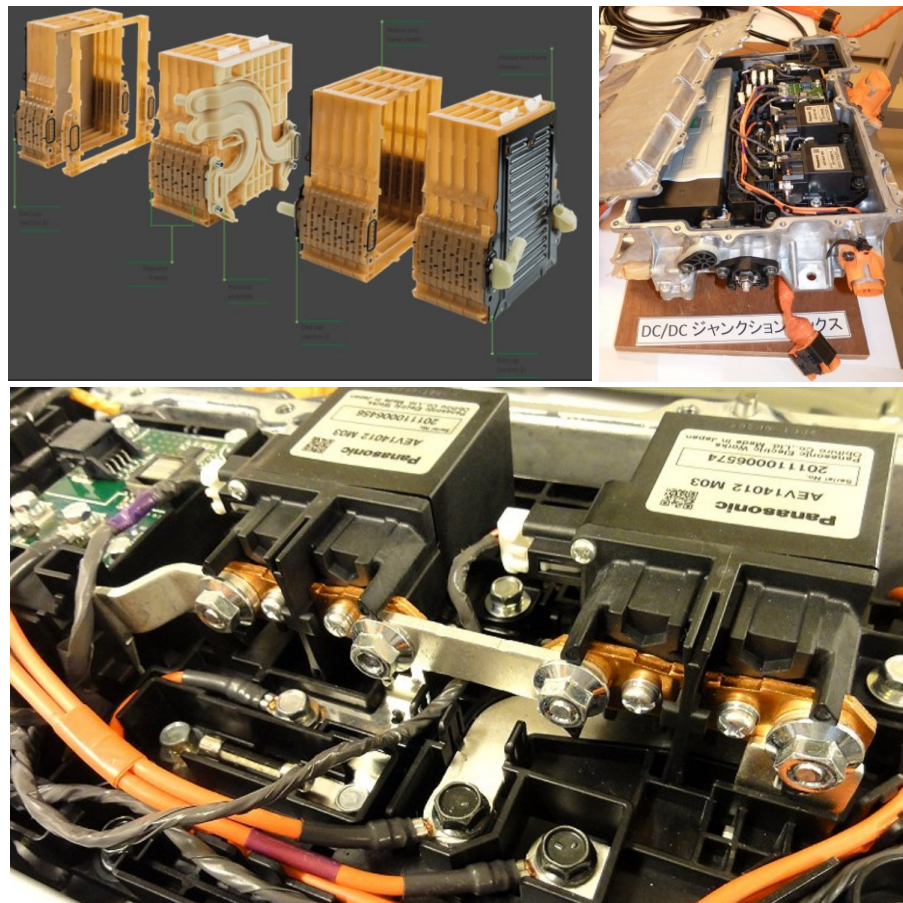
Figure 3: (Upper left) Battery cell repeater frames from a Chevrolet Volt [13]. (Upper right) Disassembled junction box of a Nissan Leaf. (Lower center) Close-up picture of the busbars of the Nissan leaf junction box [12].

3. Thermoplastic polymers

Polymers are the resulting long molecules of many monomers joint together physically or chemically. Polymers are organic materials and a lot of commercially available polymers can have more than 1000 monomer repeated units [14]. Polymers in general can be divided in three groups: thermoplastics, thermosets and elastomers. The general difference between those classifications is how their large molecules interact with each other when they are exposed to thermal changes.

Thermoplastics can be melted and solidified many times, while thermosetting polymers and elastomers, when they solidify, develop strong chemical bonds known as molecular cross-linking [14]. Cross-linking is irreversible and therefore, thermoset polymers do not soften when heated after they have been solidified without suffering degradation. Thermosets and elastomers cannot be processed by melting them. The terms plastic and polymers are commonly utilized interchangeably but the main difference between them is that a plastic is composed by a polymer plus extra elements on them such as additives, colorants, fillers, etc. [15]. This section only covers thermoplastic polymers; therefore, thermoset polymers, thermoplastic-elastomers and elastomers are not encompassed further.

When thermally processed, the molecules of thermoplastic polymers do not create any chemical covalent bond between its carbon atoms but are held together by weaker intermolecular forces known as Van-der-Waals forces [16]. Therefore, they can soften when the molecules are excited by heat, under mechanical forces or when applying solvents to them. By adding those factors to the materials, the distance between their molecules grows and consequently, the molecules tend to move with more freedom increasing ductility and flow [16].

Thermoplastics can be divided in two main groups according to their molecular structures: Amorphous and Semi-crystalline. Amorphous polymers do not form organized molecular chains. Their molecule chains remain in random order and tangled. They become brittle when below their glass transition temperature (T_g) and when above it they are ductile and soft. Amorphous polymers do not show a clear or defined transition between solid and liquid. Therefore, they do not reach a melting temperature (T_m) but rather a temperature where processing them is easier called the flowing point (T_f) [3]. For amorphous polymers T_f is an unpredictable temperature that is mostly determined empirically [3]. In contrast, Semi-crystalline polymers do form ordered molecular structures based on their crystallinity but are called semi-crystalline because they have some proportion of amorphous in them and part of their molecular structures are organized randomly creating amorphous regions mixed within the ordered structures (see Figure 4) [16, 17]. When semi-crystalline polymers reach their glass transition temperature (T_g), their molecules increase their

mobility and turn ductile, if the temperature keeps increasing there is a sharp temperature point in which they reach their melting temperature (T_m), in that point they become liquid. For semi-crystalline polymers $T_f = T_m$ [3]. T_g defines a point where a polymer experiences a lot of changes in its properties, therefore it is important as a material selection parameter [14]. It is important to note that for semi-crystalline polymers, when cooling after melting at T_m and really close to it, the creation of crystals occurs, this is called the crystallization temperature. Polymers with short molecules can form crystals faster [3].

Figure 4 shows the difference between the molecular structures in amorphous and semi-crystalline thermoplastic polymers marking their amorphous and semi-crystalline regions. Another important thermal transition in polymers is the point when they start to decompose/degrade, it is known as Decomposition Temperature (T_z), it occurs in most of polymers above 300-350°C [3].
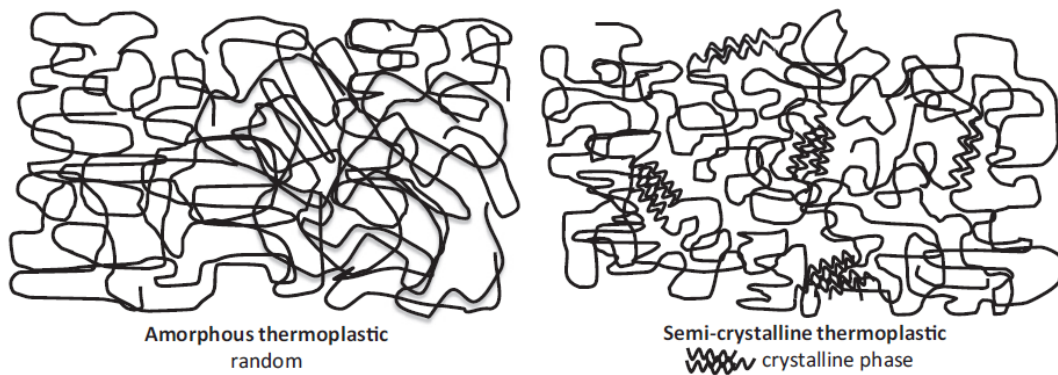
Figure 4: Amorphous and semi-crystalline structures schematic. Semi-crystalline regions are distinguished on the right-side schematic. Extracted from [3].

3.1 Requirements for Thermoplastics in EV Applications

One of the main issues in vehicles with Energy Storage Systems (ESS), specifically high energy density batteries, is the range that they can be driven before they need to be re-charged. A feasible alternative to extend the driving range of the vehicle is by decreasing the overall mass of the vehicle so that the power demand on the powertrain is lower and consequently, the overall energy consumption too. Utilizing plastics on battery related components can contribute to the reduction of mass and allow for highly integrated components. On the other hand, besides of strength-to-weight ratio there are additional requirements and properties to be considered when selecting materials that would be surrounding, supporting or enclosing High Voltage components as explained in the following sub-sections.

3.1.1 Flammability

A critical requirement for plastics surrounding, enclosing or in contact with electrically stressed items is flame retardancy. Even if batteries operate within a temperature range below 60°C [18] and ideally between room temperature and 35°C [19], if a fault occurs it can lead to fast temperature increments. Extreme abuse, shock and heat could lead to a thermal runaway with severe reactions involving the emanation of toxic gases, smoke and fire. In case of fire, the less materials contributing to combustion the better. Therefore, the usage of halogen-free (in the EU and Japan) flame-retardant plastics that fulfill requirements according to the UL94 flammability standard and be within the criteria of V-0 to V-2 is a common requirement [20]. The V-0 criteria rules that a specimen of a plastic material should not present flame for more than 10 seconds after burning it constantly in a vertical burning test for 20 seconds, neither the flame while burning can be as high as the clamp that holds the specimen or the droplets released by the melting specimen should ignite a cotton indicator placed under the specimen. Other UL94 classifications can be observed in Table 1 and are important to identify which materials can be utilized for certain applications.

Even if V-0 is required by many OEMs, each of their specifications could be different, and some battery pack components utilize materials that are among different UL94 criteria. In some cases, if a plastic component is confined inside of a metal enclosure, the flame retardancy requirements could be less strict and other UL94 grades can be accepted by the vehicle manufacturer. Some examples include the battery cell holders and battery modules of the VW Touareg 2010 and Porsche Cayenne 2010 hybrid models, which were manufactured from the resin NORYL™ SE110P (Polyphenylene Ether) produced by Sabic and rated UL94 V-1 [21].

Table 1: Flammability criteria extracted from the UL94 standard. [22].

Criteria conditions	V-0	V-1	V-2
Afterflame time for each individual specimen t_1 or t_2.	≤10s	≤30s	≤30s
Total afterflame time for any condition set (t_1 plus t_2 for the 5 specimens).	≤50s	≤250s	≤250s
Afterflame plus afterglow time for each individual specimen after the second flame application ($t_2 + t_3$).	≤30s	≤60s	≤60s
Afterflame or afterglow of any specimen up to the holding clamp.	No	No	No
Cotton indicator ignited by flaming particles or drops.	No	No	Yes

3.1.2 Electrical Properties

According to the ISO 6469-3 standard, in electrically propelled vehicles there are two voltage classes. Class A, or low voltage, which ranges from 0 to $30V_{AC}$ or 0 to $60V_{DC}$ and Class B, which covers the high voltages within a range between 30 to $1000V_{AC}$ and 60 to $1500V_{DC}$ [23].

According to the IEC/CEI 60644-1 standard, "insulation is that part of an electrotechnical product that separates the conductive parts at different electrical potentials" [24]. Electrically insulative materials do not allow charges to move freely when a force originated by an electric field is applied to them, in the case of polymers, the electrons stay strongly attached to their polymer chain, not allowing them to flow with the field unless the force generated by it is high enough to break the bond. When the electrons move current is conducted. Therefore, plastics are commonly utilized to insulate, carry and enclose electrically conductive components such as busbars, fuses, contactors and sensors to mention some examples and as in the examples observed in Figure 3. They possess low electrically conductive properties, although polymers could tend to conduct electricity minimally but often is due to impurities within their composition [14].

For components that require any kind of electrical insulation function, some of the most observed values in a material by engineers and designers are high dielectric strength, high insulation resistance and a Comparative Tracking index (CTI) corresponding to the highest voltage considered in standard tests, ideally belonging to Material Group I according to the IEC60112 test, which sets a value of 600V≤CTI [25, 26]. A high CTI value allows for packing components closer to each other with lower chances of conductive tracking [26]. Key properties to consider when selecting polymers for insulating components according to their application are shown in Figure 5 [27]. As observed in Figure 5, for high voltage (HV) applications, the dielectric strength plays a key role resulting from the possibility of a material losing its insulating properties when exposed to high electric fields.
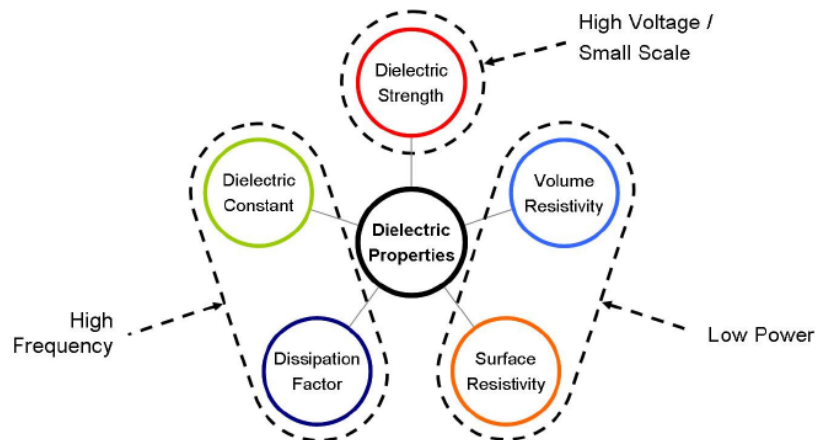

Figure 5: Dielectric properties for insulators according to their application. Extracted from [27].

3.1.2.1 Dielectric Strength

When exposed to stress caused by voltage, insulators can become conductors by losing their insulation properties, the voltage level for this to occur can be defined as the Breakdown Voltage or Dielectric Breakdown Strength of a material [28].

The dielectric strength of an insulator is the limit voltage after which, the insulator will present a Dielectric Breakdown. The Dielectric Breakdown at high voltages could present a burnt or carbonized local puncture where the failure occurred [14, 27]. According to the literature, it is difficult to identify a specific property in a material that could determine how suitable a material is as an insulator, this assumption is often achieved by empirical testing. The dielectric strength, according to the SI of units, can be expressed in terms of voltage per millimeters of thickness of the insulator (V/mm). It is common that a dielectric breakdown takes place in a zone with imperfections or voids in a material resulting from partial discharges formed due to air or gasses trapped within the voids that possess a lower dielectric strength than the polymeric material [14].

There are different factors such as aging, heat or mechanical stress that can contribute to the occurrence of a dielectric breakdown, in many cases it is common that not a single one contributes to it but a combination of many of them and its mechanisms [27]. Even if a dielectric breakdown is difficult to predict the mechanisms that contribute to it are electronic, thermal and electromechanical [14]. For instance, when performing dielectric strength tests with two electrodes it is possible to experience some deformation of the specimen under test because of compressive forces that result from the attraction that the electrodes develop to each other, this can contribute to a lower dielectric strength region [14].

3.1.3 Chemical and thermal resistance

Plastic parts that are in direct contact with battery electrolytes require to possess good chemical and heat resistance so that the components can keep maintaining their functions and integrity even if the operation temperatures are high [25]. In the case of components that belong or have to/any kind of liquid cooling system, a good compatibility with anti-freeze agents such as ethylene glycol or propylene glycol is a benefit.

In terms of heat resistance, a high heat deflection temperature is a considerable property to select a material for e-mobility applications. The exposure of polymers to temperature changes can cause geometrical distortions, softening, oxidation or embrittlement by thermal aging [24].

3.1.4 Moisture absorption

As moisture promotes electrical conductivity, it is important to point that plastics to be utilized as electrical insulators or to house electrical components should not be propense to absorb too much moisture. Some insulators, on the other hand quickly dry and get easily rid of any humidity with the heat produced by the current trying to flow through them. The exposure to water and high concentrations of stress could lead to the development of water trees, which are cavities filled with water or electrolyte that can cause water bridges between conductive parts, according to Drobny [14], water bridges do not cause a dielectric breakdown directly but can promote its development. Some testing methods for water absorption of plastics are defined by the ISO 62 and ASTM D570.

3.1.5 Mechanical and physical properties

Other important material selection requirements are low density to ensure low mass and properties such as high stiffness (Young's modulus), flexibility, puncture and impact resistance. For example, brittle materials could have more difficulties for absorbing energy from impacts and vibration in comparison to ductile ones. Polymers, in general, are flexible materials that respond slowly to forces applied to them and usually yield before fracture. On the contrary, brittle materials are affected immediately by loads and could fracture drastically without a clear transition between their yield and fracture points and without much extension [14]. As it was mentioned above, mechanical factors can induce or promote the breakdown of a solid insulator material. In the case of material brittleness with poor impact resistance, stresses applied to the polymeric material could lead to small cracks or fractures that could lead to dielectric breakdown as well [24].

The inner structure in the insulator material can also play an important role in meeting the dielectric strength values for an application, voids inside of a material can decrease the insulation properties of it [24]. When carrying electrically charged components the mechanical properties of polymers combined with their insulation properties have an important role for fulfilling safety and functional requirements.

Some examples of injection molded polymers that have been developed for vehicle electrification applications can be observed in Table 2. All the values contained in table 2 were taken from their manufacturers data sheets [29, 30, 31, 32].

Table 2: Examples of different polymers utilized in EV powertrain components and some of their relevant properties. Retrieved from: [29, 30, 31, 32].

Resin \ Characteristic	Amodel® HFFR-4133 (PPA)	Zytel® FR95G25V0NH (PA66/6TGF25)	Crastin® LW9030FR (PBT-IGF-GF30)	Noryl™ GFN1 (PPE + HIPS)
Density (g/cm^3)	1.45	1.4	1.55	1.17
Heat deflection temperature, 1.8MPa (°C)	300	236	205	115
Young's Modulus (MPa)	12000	8900	10200	4000
Dielectric Strength (kV/mm)	0.8mm →30	Not available	1mm → 29	3.2mm →18
Flammability UL rating	0.8mm → V0	0.4mm → V0	1.5mm → V0	0.75mm → V0
Water absorption (%)	0.28	4	0.35	0.06
CTI (V)	600	600	325	275
Manufacturer	Solvay	Dupont	Dupont	Sabic
EV Application	Enclosure and insulation for HV components.	Battery Housing and connectors [25].	Power electronics insulation and enclosures [25].	Battery cell spacers and holders [21].

4. Plastic injection molding basics

Plastic Injection Molding (IM) as a process has appeared since the last part of the 1800s, when the first injection molding machine was introduced to process cellulose nitrate. During the Second World War the process was developed for mass production and in 1946 the first screw injection molding machine was developed, which is the most commonly utilized type of machine nowadays [33, 34].

Plastic injection molding can be described as a cyclic process that can transform polymeric materials in the form of granules, with the aid of elevated temperature, pressure and a mold into different types of complex and identical finished products massively and with high dimensional accuracy. It has a wide range of applications that include consumer, automotive and aerospace products among multiple others. More than 30% of plastics existing worldwide are processed by injection molding and 50% of the equipment to process plastics is dedicated to injection molding [16].

IM is a repetitive process that starts by filling the hopper of the machine with polymer granules or pellets. Then they are inserted into the barrel. The barrel has heating elements that help for the material to reach the desired viscosity, this stage is called the plasticizing phase. The injection stage starts when the material is forced by the screw with a defined amount of pressure into the mold. The mold consists of two parts and contains a cavity. The cavity will be filled with the polymer to form the product, which will be a replica of the cavity's shape. While the material is kept inside of the mold cavity for cooling, pressure is applied for a short period of time, and sometimes more molten material is added to the part for shrinkage compensation, this pressure is known as holding pressure [17]. Injection molded parts in general present good density distribution, although some voids can be formed during cooling when air or gas bubbles get trapped in between the material once it has been solidified. Figure 6 shows a screw injection molding machine with its general components.
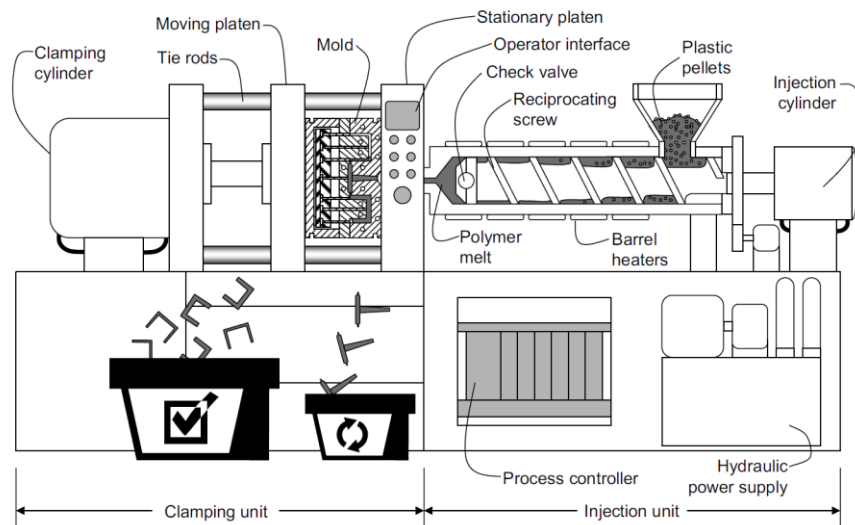
Figure 6: Screw Injection Molding Machine, extracted from [35].

IM as a process possesses advantages and disadvantages. Some advantages are: high-volume of production at a fast rate, repeatability, high dimensional accuracy, design flexibility, extensive possibilities for automation and low or no direct consumption of solvents or water. Most of its disadvantages are related to costs, setup and tooling lead times and equipment expenses. As the molds need to be manufactured from high strength tool steels, their machining for readiness could take from 12 to 16 weeks and are costly [34]. It is important to mention that injection molds, depending on the product, could be complex and can require many parts that wear over the time. For prototype runs and, in some cases, for serial production of small volumes there exist the possibility of making aluminum molds. The use of softer materials for tooling can reduce the lead time of the tool from many weeks to few days [34].

Within the automotive industry, injection molding is the most applied method for processing polymers for vehicles. The most utilized polymers for automotive overall applications are Polypropylene (32%), Polyurethane (17%) and PVC (16%). Other polymers like Polyamide (PA), ABS and POM are also widely used but in lower proportion [36].

4.1 Anisotropy of injection molded parts

The resulting properties of plastic parts processed by injection molding depend on many parameters. The stiffness, overall strength and dimensional accuracy depend on the anisotropy of the molded part, as well as on how the orientation of the molecules, additives, fibers or fillers of the material end located along the final part after molded. Other process factors and parameters affecting part quality can be the cooling rate, cavity design, injection speed and injection pressure among others [16]. Several parameters interact and have many dependencies with each other, parameter combinations may have different effects on part properties. They could be highly dependent on the material, for example, increasing the injection pressure and mold temperature can have positive effects on shrinkage and warping but higher injection pressure impacts negatively the ease to eject the part [34].

Some known mechanisms that affect the orientation of injection molded parts are the fountain flow effect, radial flow and flow induced by holding pressure while the part is cooling. The fountain flow effect depicted in Figure 7 is the result of the difference in temperatures between the mold cavity walls and the melted polymer going through a gate to fill the cavity. Usually, after the melt contacts the colder walls of the mold it solidifies immediately sticking to the walls and creating an effect that resembles when a water jet comes out from a fountain and goes out from it as a constant linear jet, then when reaching certain point at the top, it opens towards the sides to let the water fall back down and towards the sides due to gravity. In radial flow the material that goes through the gate starts stretching and expanding in a radial manner sticking first to the perpendicular walls next to the mold gates. Then the rest of the material starts pushing it to fill the cavity [16].
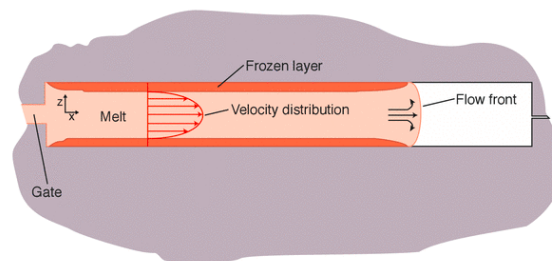

Figure 7: The fountain flow effect is one of the common mechanisms affecting anisotropy in injection molded parts. Extracted from [16].

5. Additive Manufacturing

Additive Manufacturing (AM) as a term, emerged from the term Rapid Prototyping (RP), which started in the second part of the 1980s. RP was employed to establish methods for rapidly allowing the creation of physical prototypes directly from digital data. The initial goal of these methods was to only test the functionality and fit of parts within an assembly or for product display purposes but with the evolution of the technologies involving those methods, it is currently possible to create functional parts and end-use products with them. As a result, Additive Manufacturing (AM) was established by the ASTM in agreement with the ISO as the term to refer to technologies that "add" material on a selective area to create a solid part [1, 37]. This section includes the different categories of the most common Additive Manufacturing technologies that allow the creation of plastic functional components, emphasizing on Powder Bed Fusion (PBF) technologies and materials.

Additive Manufacturing surges from the idea that parts can be produced by adding a layer on top of another previously created one to successively stack them with the purpose of building the desired part. This is achieved generally by stacking the layers in a vertical manner. Each layer is a cross-sectional cut of the final part with a pre-defined thickness dependent on the equipment capabilities.

In comparison with other well established and traditional manufacturing methods such as machining, which removes material to sculpt the final product. Additively manufactured objects tend to have fewer design limitations compared to their traditional counterparts because of the "layer by layer" process described above. On the other hand, as the parts are built by layers being stacked vertically, some features in some processes need to be supported by adding removable material to avoid sagging or overhang because the parts cannot be built "on air" [1]. AM optimizes the utilization of raw materials by adding material only in the locations where it is required. AM is a revolutionary technology not only because of its advantages over traditional subtractive methods, but because of the ability of producing objects directly from digital models and then obtain feedback from the additively manufactured object, creating a fast improvement loop [2].

From a design perspective, AM disrupts the principles of Design for Manufacturing, that have the goal of adapting the shape of a part to the limitations of a defined manufacturing process, therefore it is said that with AM "complexity is for free" [2]. Besides of the support structures, the only limiting factors for designing products for Additive Manufacturing is the designer's creativity and imagination [1]. AM allows designers and engineers to design for function and performance rather than for manufacturing. With AM the manufacturing equipment is more flexible to product changes, if compared to traditional manufacturing, where a set of dies, molds or cutting tools are specifically manufactured to fit a specific part geometry [2].

According to Gibson et. al. **[1]**, the generic step by step process of any AM process is represented schematically in Figure 8.

The basis of any AM method is the (1) CAD data of the part to be produced and its conversion from the native format of the software where it has been designed to STL (or AMF **[37]**) format (2). STL is the most common format that can be transferred to the AM manufacturing machine (3) for manipulation and preparation. Once the STL file is loaded in the machine user interface, it is then possible to do the machine setup (4), where the build parameters, for instance layer thickness, temperatures and speed, are defined. Afterwards, the build (5) is made automatedly and the part can be removed (6) from the machine when it is finished. After removal, the post-processing (7) phase starts, in which the part can be separated from its support material, deburred, or cleaned. The final step is the part end application or use, it might require some surface finish such as painting or assembly with other parts (8).
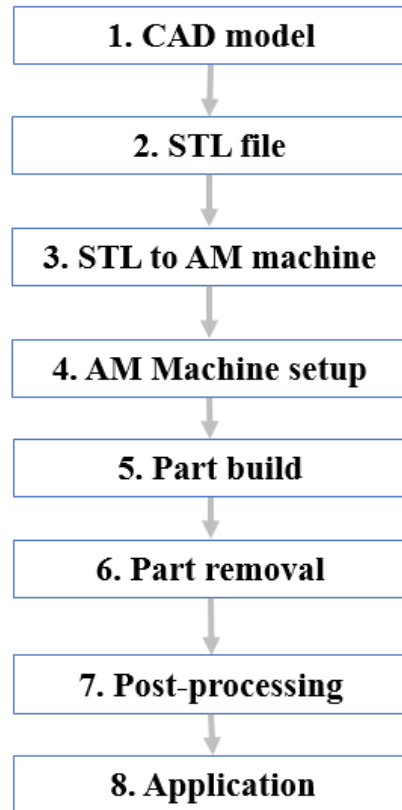
*Figure 8: Generic steps of the AM process. Adapted from **[1]**.*

5.1 Additive Manufacturing processes for polymers

The ASTM in collaboration with the ISO have developed the ASTM/ISO 52900:2015 standard, which divides additive manufacturing processes in 7 categories from which 6 are capable of processing polymers as summarized in Table 3 [37].

Table 3: AM processes for polymers according to the ASTM/ISO 52900:2015. Adapted from [37].

AM Process	Description	Suitable Materials	Raw material feedstock
Binder Jetting (BJT)	Uses bonding agents to keep granulated particles together. The bonding agent is dispensed through a nozzle over a build bed containing the material particles.	Metals, sands and polymers.	Powder, granulates.
Material Extrusion (MEX)	Molten material is extruded through a heated nozzle over a build bed to stack layers.	Polymers and composites.	Filaments and pellets.
Material Jetting (MJT)	Material droplets are deposited into a build platform with a printhead that contains a UV light source that cures the selectively deposited material.	Photopolymers and waxes.	Melted or liquid materials.
Powder Bed Fusion (PBF)	A heat source fuses selectively a material in the form of powder spread over a build platform.	Polymers and metals.	Powder materials.
Sheet Lamination (SHL)	Process sheet materials by cutting them in layers to join/bond them together to build and object in a vertical manner.	Thin metals, paper and polymers.	Sheet materials. Commonly in a spool/roll.
Vat Photopolymerization (VPP)	Liquid resin is contained in a vat and is cured selectively via a UV light.	Photopolymers. Thermoset polymers.	Liquid materials.

Each of the processes mentioned above have their own sub-categories, this thesis is oriented to **Powder Bed Fusion** processes for polymers and therefore, the further sections do not make mentions of other processes except for **Material Extrusion** and **Vat Photopolymerization** due to their relevance in the AM development and important presence in the AM industry.

5.1.1 Material Extrusion

The basic principles of the material extrusion process are based on heating a raw material, which is then located into a heat chamber to liquefy and then with pressure, the material is pushed through an extrusion nozzle with defined dimensions and shape. The material is then solidified and bonded to a build bed that moves upwards or downwards on the vertical Z axis (see Figure 9) while the horizontal directions X and Y are covered by the nozzle carrier. The goal of the movable build bed is to construct the part layer by layer and to bond the new material layer into the previously deposited layer until the complete structure of the part is finalized [1].

It is possible to solidify the molten materials only by the temperature difference between the heat chamber temperature and the environmental temperature for most thermoplastic polymers [1].

The raw materials that can be extruded can be in the shape of powder, granulates, pellets or filaments. When the material is not in the shape of a filament it can be pushed by gravity into the heat chamber, but an additional element must create the pressure to extrude the molten material through the nozzle. It can be done by a plunger, a screw or compressed gas, although these extruding systems are rarely applied in any commercial AM system [38].

When utilizing a filament material, the feeding system that moves the filament towards the heating chamber, creates the needed pressure to extrude the material through the nozzle simultaneously, in a similar manner as in a hot glue gun.

5.1.1.1 Fused Deposition Modeling (FDM)

Among material extrusion methods, the most widely utilized is Fused Deposition Modeling (FDM), which was developed by the American company Stratasys and got its patent granted in 1992, their patent expired in 2009. Consequently, in the following years there was an explosion of consumer-friendly and low-cost desktop machines flooding the material extrusion-based equipment market [39]. To avoid patent infringement, some manufacturers commercialize their machines as Fused Filament Fabrication (FFF) or Fused Layer Modelling/Manufacturing (FLM) instead of FDM but they operate under the same principles as FDM machines with small variations.

Process description:

FDM utilizes heat to melt a material in the shape of a continuous filament (4 in Figure 9a) into a liquefier chamber (3 in Figure 9a) to then push it by a traction (pinch roller) mechanism (2 in Figure 9a) through an extrusion nozzle (1 in Figure 9a). The molten material is then deposited over the build platform, which is usually also heated, and located perpendicular to the axis of the nozzle. A gantry system then displaces the extrusion nozzle along the X and Y axes of the build platform in the locations where the material is required.
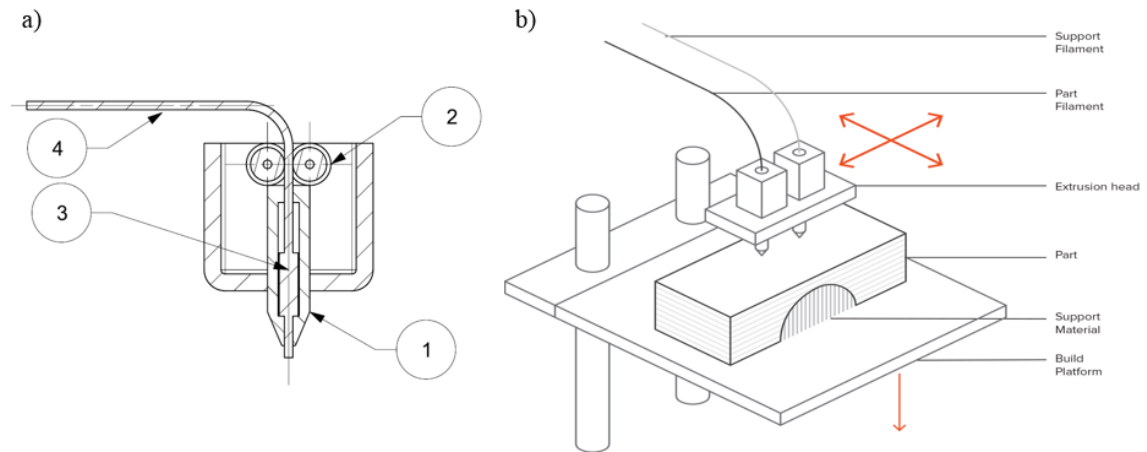
Figure 9: a) Simplified schematic of FDM extrusion nozzle adapted from [1, 38]. b) Simplified schematic of main FDM extrusion components, retrieved from [40].

Parameters and part quality:

According to Gibson et. al. [1], for most of parts, the first shape that an FDM machine starts plotting is the outline/perimeter of its cross section, which is printed at a lower speed to avoid drastic changes on the nozzle travel directions as speed changes may lead to geometric inaccuracies. The reason behind it is the synchrony variations between the travel of the nozzle along the horizontal plane and the nozzle extrusion rate. Fast directional changes can lead to have scarce or excess of material in some regions of the part. The infill on the part could be plotted at higher speeds as it is not determining the geometry of it but the orientation of the plotting on each layer can improve or decrease the overall strength of the part. Gaps between layers can lead to weak areas and overlaps can be used to fill gaps but they could result in part swelling. A good practice is to plot every extruded road in a cross-pattern to increase structural strength. The nozzle diameter determines the smallest feature to be achieved in the part. The strength of the part is strongly influenced by the layering setup that can lead to stronger or weaker areas within the part [1].

The mechanical properties of FDM parts are anisotropic depending on the printing orientation. For instance, Bagsik and Schöppner [41], made tensile tests with Ultem™9085

and Knoop and Shöppner [42] experimented with PA12 specimens. Both studies described that regardless of the raw material properties, the build orientation of their specimens strongly affected the end properties of their specimens while loaded in tension. Parts built in the Z direction (see Figure 25) have the lowest tensile strength values due to the weak fusion between layers and the X build orientation (see Figure 25) showed the best tensile behavior. In contrast, when the parts were loaded in compression the Z direction presents higher compressive modulus. Overall, material extrusion AM processes present the lowest mechanical properties in the normal direction of the layers, where two layers fuse with each other. It has been demonstrated experimentally that it is possible to increase the bonding between the layers and in consequence, their mechanical properties (approx. by 30%) by producing the FDM parts in an inert atmosphere. At high temperatures when melting the filament, the material can suffer degradation resulting from oxidation from contact with air [43].

Smaller nozzle diameters allow higher geometrical accuracy, but lower extrusion speeds and the opposite happens with large nozzle diameters. For parts produced by FDM it is advised to have a minimum feature size and wall thickness that are at least twice the nozzle diameter [1]. Electrical properties of FDM parts are as well anisotropic according to the printing orientation. According to Hoff et. al. [44] and Monzel et.al. [45], FDM parts present aligned voids in between layers that can lead to low mechanical properties and the same issues are a cause of lower dielectric strength. In the case of [44], it was noticeable that the orientation flat (parallel to the build platform) showed the poorest dielectric strength compared to vertically printed specimens for ABSM30 materials. Although they found that their experimental results are not completely aligned with the material datasheets published by the material manufacturer.

Materials:

FDM materials, as explained before are delivered in the shape of a continuous filament. FDM is highly compatible with amorphous polymers with low flow temperatures, low thermal expansion coefficient and low glass transition temperature (T_g) [46]. The main reason for suitability is that amorphous thermoplastics gradually suffer viscosity changes with increasing temperatures. FDM is less suitable for highly crystalline polymers. Semi-crystalline thermoplastics have better mechanical, thermal and electrical properties, as well as chemical resistance but tend to be more challenging in terms of homogeneous extrudability and their crystalline structures tend to promote faster shrinkage when cooling, making the adhesion between layers or to the build plate to the machine complicated [1, 46]. On the other hand, with the correct build chamber conditions, temperature control and process parameters semi-crystalline thermoplastics are possible to extrude successfully by FDM when the crystallization speed can be controlled [47].

The most common FDM material used on desktop machines is Poly Lactic Acid (PLA), it is one of the lowest in cost, it is biodegradable and biocompatible. On the contrary it does not perform well when exposed to high temperatures, has poor mechanical properties and low durability. It is suitable for form testing rather than functional testing for demanding applications. PLA can be found blended with particles of metals or wood mostly for appearance and texture, but this blends usually do not enhance the properties of the material significantly [48].

Different variants of Acrylonitrile Butadiene Styrene (ABS) such as ABSplus, ABS-M30 and ABS-ESD7 from Stratasys are intended for functional testing. ABS-M30 has better mechanical properties than standard ABS and is suitable for functional prototypes and end-use parts. ABSplus has similar mechanical properties as ABS-M30 but slightly higher dielectric strength. ABS-ESD7 is a variant of ABS-M30 but with electrostatic dissipative properties and a good alternative for applications in electronics [48].

Polyamides are semi-crystalline materials. However, there are many nylon materials available for FDM. For instance, PA6 and PA12 are available from Stratasys, they are tough and flexible, therefore suitable for functional parts with design features like snap-fits and living hinges [48]. Markforged offers nylon composite materials that blend PA12 with different Continuous Fiber Filament (CFF) variants, including carbon, kevlar and glass fiber reinforcements for adding stiffness to the raw PA12. Their technology consists of two nozzles, one deposits the polymer and the second one deposits the reinforcement. The glass fiber reinforced material is suitable for e-mobility functional parts if considering only stiffness, heat resistance and electrical insulation. Markforged also offers a series of materials called ONYX, these materials are composites based on "Tough Nylon" (PA6) plus chopped carbon fiber, it can be reinforced by their CFF systems. ONYX FR has UL94 V-0 rating for a minimum thickness of 3-4mm. Those materials are only compatible with Markforged machines [49].

Polypropylene, widely used for automotive applications and good electrical insulator is available by BASF as a polypropylene glass fiber blend sold as Ultrafuse PPGF30, it is stiff, withstands high temperatures but because of the 30% glass fiber content it cannot be processed with a regular extrusion nozzle, it requires a hardened one. BASF recommends not to use more than 80% infill to avoid warpage [50].

For high-performance materials, one example is Sabic's ULTEM™9085 which is Polyetherimide (PEI). ULTEM™9085 is UL94 V-0 halogen-free and it is intended for high demanding/performance applications where mechanical stresses are high. It is approved for transportation applications like commercial vehicles, automotive and airplane cabins. It can be utilized as an end-part material and can maintain mechanical properties at high temperatures [51].

5.1.1.2 Big Area Additive Manufacturing

Big Area Additive Manufacturing (BAAM) is a process developed by the Oak Ridge National Laboratory (ORNL). The innovative approach that BAAM has made to FFF is that it is a material extrusion process that instead of utilizing polymer filaments, uses commodity polymers in the shape of pellets. According to the ORNL, the same pellets intended for injection molding can be utilized for this technology. If compared with conventional FDM/FFF materials, the cost difference between low cost ABS filaments and pelletized ABS can be from 31USD/kg to 1USD/kg respectively **[52]**.

In terms of dimensions and speed, BAAM can print parts of 2.4x2.4x2.4m at a rate of 25kg/hr. The extrusion head on BAAM systems possesses a single screw similar to the ones that forces the material into a mold in injection molding machines, but the positioning of the extrusion nozzle within the work area resembles the same principle as in FDM, a gantry allows it to move in X and Y directions within the same plane and to build a new layer, the extrusion head rises vertically in the Z direction. The main potential application is intended to be big structures such as vehicle body structural components. As structural components are the main target of BAAM, the materials known to be processed by BAAM are mostly blends of discontinuous carbon fibers and engineering polymers such as ABS **[52]**.

5.1.2 Vat Photopolymerization

Vat Photopolymerization groups a series of processes that utilize photopolymers to create solid parts from liquid resins that are contained in a vat. Vat Polymerization includes the first 3D printing method to appear in the industry and established as Stereolithography Apparatus (SLA). Charles Hull, its creator, was able to 3D print the first SLA part in the 1980's. During that same decade he patented the SLA process. He developed the first 3D printer and founded 3D Systems, at that time it was the first and only 3D printing company in the world **[1, 53]**.

Process description:

In general, the process starts with a photopolymer layer contained in a vat in liquid form. In some cases, the part in this process is built "upside down", this means that the part is built from top to bottom in contrast to what is usually done in FDM, the part is "hanging" from the build platform instead of laying on top of it, although this is not a rule and in some machines the build platform moves downwards. The light source is located at the bottom or the top of the machine accordingly. The radiation emitted by the light source could be focalized towards the build platform through the vat containing the liquid resin, in that

cases the vat material is clear. When the light source illuminates the liquid material, it cures the first layer of the part, then the build platform/elevator is raised/lowered, and the vat bottom surface is uniformly recoated with a blade adding more liquid resin to build the next layer. It is important to mention that the radiation is selectively directed to the part and these processes require to the creation of supports structures that can be removed afterwards. The resin that is not touched by the radiation remains liquid.
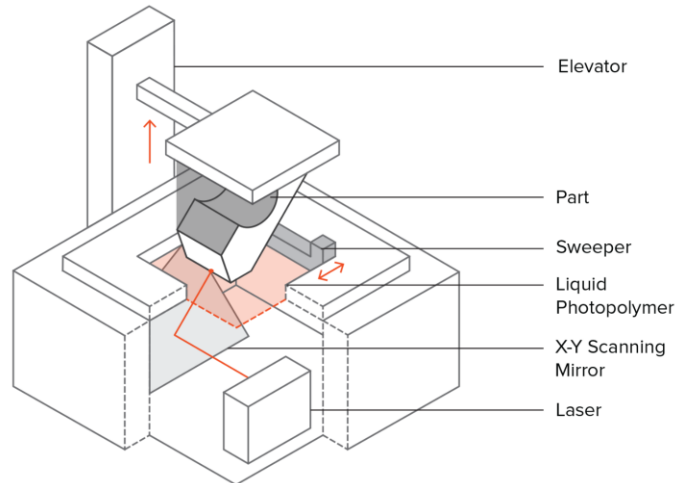
Figure 10: Schematic diagram of an SLA machine and its components. Extracted from [54].

Process parameters and part quality:

According to the literature reviewed in [55], relevant qualities present on finished SLA parts are smooth surface roughness and high dimensional accuracy, they have been studied extensively.

As the parts are built layer by layer, similarly as in FDM, the part contours always present steps that result from the joint of a previously made layer with the next one on top of it. The formation of steps is more evident in parts with large curved surfaces. The formation of steps can also have impacts on part costs due to the need of post-processing them to decrease the surface roughness values or achieve a better physical appearance. Studies compiled in [55], found that the surface roughness of an SLA part is highly impacted by the layer thickness of the print, part orientation and material properties.

The main factor affecting the overall dimensional accuracy of the parts, regardless if the radiation source is a laser or a lamp, is the volumetric shrinkage. Shrinkage occurs from the variable curing rates in different areas and different moments on the production process. When a series of monomer molecules form a polymer, the resulting polymer molecules usually have a lower volume and therefore the part, shrinks. The shrinkage of a layer affects a previously cured layer as the new layer, when joint to the previous one pulls it towards the shrinkage directions, and the process repeats within every layer of the part causing

residual stresses, curling and therefore, dimensional inaccuracy and part distortion [1, 55]. The curing reaction during photopolymerization is affected by different parameters such as laser power and scanning speed. In terms of mechanical properties, Vat Photopolymerization parts do not present isotropic behavior. The strength of the parts is low and therefore not utilized as finished products in demanding applications. According to Hoff et.al. [44], it was found that horizontally printed orientations resulted in lower dielectric strengths attributed to anisotropic curing that affects mechanical properties as well.

Materials:

The materials used in Vat Photopolymerizatioe are all in a liquid state and thermoset polymers. In contrast with thermoplastic polymers, they cannot re-melt after they are solidified from their liquid state. The photopolymer resins utilized in SLA are specially formulated for this process. All the SLA resins are based on epoxy or acrylate resins. The firstly developed resins were all based on acrylates but currently there is a wide availability of commercial resins that are mainly epoxy-based [1].

SLA resins can be divided according to two photopolymerization mechanisms: radical-initiated and cationic-initiated polymerization. Cationic-initiated include epoxides and vinyl ethers while radical-initiated cover acrylates. According to [55], the cationic based resins excel in terms of mechanical properties over acrylate resins, which can be strong but brittle. Cationic-initiated resins tend to keep curing even after removed from exposure to UV radiation.

There are commercially available resins that resemble the properties of some injection molding thermoplastics and possess good mechanical and heat resistance properties. However, photocurable resins are not suitable for long-term durability applications compared to injection molding parts, most of the materials available degrade and age over the time and their mechanical properties as well [1, 2]. Another aspect is the data available for flammability rating, from datasheets the compliance with UL94 is not available for most of the resins. On the other hand, in terms of dielectric strength there are resins, like the DSM Somos® ProtoTherm 12120, offering values between 15 and 16.5 kV/mm [86].

5.1.3 Powder Bed Fusion

Powder Bed Fusion (PBF) technologies are based on the processing of materials in the shape of powders. Besides of the shape of the raw material, these processes share the characteristic of utilizing a heat source to fuse powder particles selectively into a specific area of the build bed to form a part layer by layer additively. PBF processes differ from each other depending on the applied heat source and their approach to focus the heat source towards the powder as it can be point-wise, line-wise or layer-wise [1]. PBF is among the most suitable AM processes for end-part production resulting from good mechanical properties achieved and process capabilities for producing relatively high batch sizes.

The first developed PBF process was Selective Laser Sintering (SLS) by the University of Austin Texas. Later other variants based on it emerged. More recent technologies are Multi Jet Fusion developed by Hewlett Packard (HP MJF) and before that High-Speed Sintering (HSS) developed by Loughborough University.

This section goes through the process descriptions, parameters and materials for SLS and HP MJF and briefly on HSS.

5.1.3.1 Selective Laser Sintering (SLS)

Selective Laser Sintering (SLS) is widely utilized for direct manufacturing. It started with the intention of creating polymer prototypes, but the technologies and available materials can be utilized as final products. Some of the SLS part properties can be comparable to the ones of parts produced by traditional methods [1].

Process description:

SLS consists on constructing parts layer by layer by applying concentrated heat emitted by a laser into a selective area of a powder bed. When absorbing the energy emitted by the laser, the powder reaches the proper viscosity to fuse with adjacent powder particles. After cooling, those powder particles create a cross-sectional slice/layer of the part. When one layer is finished, the build bed is lowered according to the thickness of one layer. Then, new powder will be spread on top of the pervious layer by an application device. The same process is then repeated as many times as required until the part is finalized to be then cleaned or post-processed [1].

By the nature of the process, loose powder surrounds the part during the build. As a result, the powder acts as a support structure and therefore, no additional structures are needed to support any desired geometry. This is an advantage over other processes, it reduces the

needs for post-processing and the time invested into removing the support structures is eliminated. This principle also allows many parts to be nested on the processing chamber of the machine to maximize equipment utilization.

It is possible to reuse the remaining powder for future builds, but it is important to mention that the material degrades after being heated inside of the build chamber. To reuse material, it is advised to mix it with a higher proportion of new material to obtain good results [56].

SLS equipment

According to Schmid [3], equipment for Selective Laser Sintering consists of three main construction blocks; the Optics Module, a Build Chamber that contains the Build Area and a Powder Area. These construction blocks can be observed in Figure 11.

The Optics Module contains the laser and the systems required to focalize the radiation from the laser towards the selected area for fusion. These systems include a beam deflection mirror system, a correcting mirror and laser window. The correcting mirror has the function of adjusting the laser beam position. The laser beam has a round shape but when focused towards different positions on the build bed the laser shape becomes oval. Schmid [3] denotes that the highest accuracy in parts can be achieved in the center of the build bed. The Optics Module of an SLS machine should be isolated from the Build Chamber and Powder areas. Powder particles in the optic systems can lead to bad part quality due to dispersion losses [3].

The Build Chamber when closed is a compartment with a controlled atmosphere (filled with nitrogen) to avoid material powder degradation by oxidation [1]. For optimal sintering, it is important to pre-heat the powder material to achieve a desired temperature. The Powder Bed, which contains the part in progress, is located within the Build Chamber on top of a Build Platform, which lowers down gradually towards the Powder Area contained at the bottom of the machine. The walls and floor surrounding the Powder Bed are heated to keep a uniform temperature on it. To reduce the laser energy demands and promote an even powder melting, the top layer to be processed is kept near the melting temperature of the material (T_m) by heating it with an infrared lamp. Keeping a homogeneous temperature within the build chamber is critical to achieve good properties on finished parts. A homogeneous temperature decreases the probability of warping caused by thermal expansion and contraction [1]. The location of the parts within the powder bed can also contribute to warping because of cold spots [3].

The powder distribution for every layer is performed by three different types of devices depending on the equipment manufacturer; a counter-rotating roller, a blade or a double blade cartridge system. The main advantage of the roller is its robustness, support to promote a dense powder bed and can apply better powders with low flowability but could have some drawbacks like molten powder sticking to it. A blade is simple and allows good

surface finish with fine powders. A double-blade cartridge can apply the powder in both directions when travelling along the X and Y axes of the Build Chamber and while it travels it can deposit powder [3]. Figure 11 shows a schematic representation of the components an SLS machine and its main components.
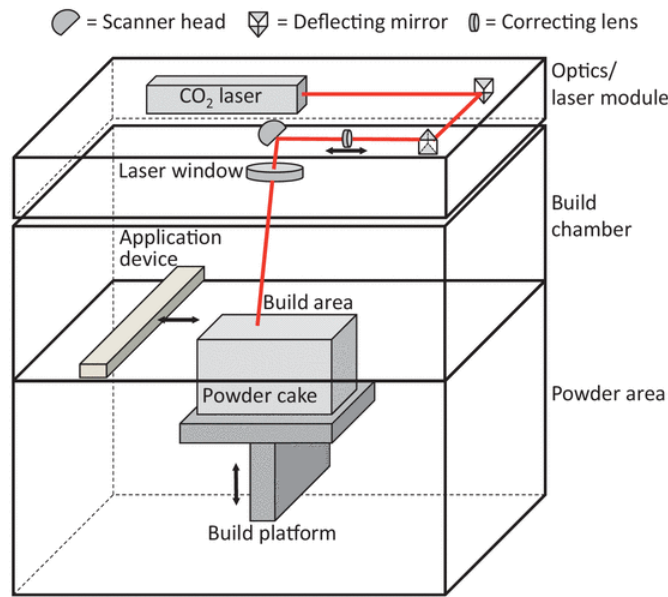
Figure 11: Schematic representation of the SLS machine components. Extracted from [3].

The main players manufacturing SLS equipment are EOS from Germany and 3D Systems from the USA. Some of the main differences between their machines are the material application on the Build Bed and powder supply methods [3].

Process Parameters and part quality

Selective Laser Sintering is a complex process which requires a combination of several conditions and parameters for successfully producing parts with good surface quality and properties. According to Gibson et. al. [1], the parameters that play the most important role in SLS are related to processing temperatures, laser-scanning and powder/material. Every single parameter or a combination of them can affect the end properties of the parts.

Temperature control combined with the proper laser power parameters have high impacts on the end properties of SLS parts. For example, high laser power values combined with an elevated temperature of the build bed can result in highly dense parts but can have affect the part the dimensional accuracy and vice versa, with low laser-power and low powder bed temperature, the accuracy can increase but the layers could not bond properly [1]. Non-uniform shrinkage, residual stresses and part curling could result from the combination of high laser power combined with a low temperature build bed [1]. A critical SLS parameter to be controlled is the temperature of the build chamber, that ideally, should always be

above the crystallization temperature (T_c) of the processed material. When too fast crystallization is allowed by fast cooling, warping occurs. The temperature range between a polymer melting temperature (T_m) and its temperature of crystallization in SLS can be identified as the "Sintering Window", which is a challenging temperature range to keep under control [57].

There are two types of scanning modes in PBF, contour mode and fill mode. The contour mode takes care of the dimensional accuracy of the part external contour. The fill mode takes care of filling the area within the part contour. With low laser power the scan speeds should be low also to achieve particle fusion [1].

The powder material has a crucial role on determining the properties of an SLS manufactured part. For example, when the powder bed is dense, higher mechanical properties and more dense parts can be achieved [3, 57]. Ideally, the shape of the powder particles should be spherical to maximize density and promotes the flowability, although most of the commercial PA12 powders have potato shape [57]. To achieve higher part densities, the material powders have particles of different sizes so that smaller powder particles can fill the gaps left in between bigger particles.

Materials

One of the main drawbacks of SLS is its narrow selection of commercially available materials if compared to processes such as FDM, SLA or to Injection Molding. Most of the parts produced by SLS are manufactured from PA12 or PA11, over 90% of the SLS parts are made from PA12 and its dry blends with other materials or additives [3, 57]. The main reasons for being PA12 a highly utilized material for SLS, are the possible combinations of properties ranging from material related to process related and the long time that the material has been experimented with the process. PA12 has been processed before for injection molding but the adaptations of it for SLS are mostly done mainly by two companies worldwide, Evonik and Arkema [3] and from them, the materials are commercialized by different companies. The biggest shares of the market belong to EOS and 3D Systems or subsidiaries of that two companies [3].

From 3D Systems SLS materials are commercialized under their DuraForm® brand which has a wide range of PA12, PA11 and blends with different properties. For instance, the standard PA12 DuraForm® is targeted to the production of functional end-use parts with flexible features such as snap fit joints. It is intended to be processable by any SLS machine regardless of its manufacturer. For extra stiffness DuraForm® GF and DuraForm® ProX® GF are a blend of PA12 with Glass beads for parts with higher stiffness requirements on operation at higher temperatures. As flame retardants the DuraForm®-FR1200 and DuraForm®-ProX®- FR1200, offer UL94 V-2 at a 5mm thickness or HB at 1.5mm, while the DuraForm®-FR100 is claimed to be rated UL94 V-0. Examples away from PA are

DuraForm® Flex (thermoplastic elastomer) and DuraForm TPU, both are rubber-like materials for manufacturing seals or other deformable components [58, 59].

EOS has a similar range of products, being PA2200 and PA2201 their general PA12 materials with balanced properties the main difference between them is the intense white color on PA2200 by the addition of titanium oxide (TiO_2) [3]. PA1101 is a PA11 material, PA11 in contrast with PA12 is derived from castor oil and offers superior elongation at break when compared to PA12 [3, 60]. PA2210FR is a halogen-free flame retardant UL94 V-0 polyamide 12 suitable for electronics and therefore a potential material for the use in electric vehicles [60]. EOS offers also a high-performance PEEK (Polyaryletherketone) with great mechanical properties (Young's modulus >4000MPa) and high temperature mechanical stability at 108°C. The downside of this material are the high costs and high processing temperatures, which that can only be achieved on a printer specifically designed for processing it (EOSINT P800) [3, 60].

Different process parameters combined with intrinsic and extrinsic material properties play a crucial role in the development of new materials suitable for SLS. Some examples of these properties are thermally dependent, such as having a wide sintering window or related to the shape and distribution of the powder particles, which contribute to better flowability and lower porosity of the parts as denoted in [57]. Therefore, some of the materials away from polyamides are mostly under research or utilized in small proportions. Some examples are: Polypropylene and some blends of it, POM, PBT, Polyethylene [61].

5.1.3.2 HP-Multi Jet Fusion (MJF)

Multi Jet Fusion (MJF) is a Powder Bed Fusion process that does not utilize a laser beam as a source of energy but IR radiation. It differs from Selective Laser Sintering mostly on the use of a printhead that contains the heat source, this printhead jets fusion and detailing agents on top of the material powder, those agents are based on the HP Thermal Inkjet Technology [62]. This process was introduced in 2016 and it is owned by the 2D printing manufacturer Hewlett-Packard, which has its roots on traditional paper printing. The MJF technology is intended to produce functional prototypes and end-use components and assemblies.

Process description:

According to HP [62], the process starts by spreading the first layer of uniformly pre-heated material powder over the build bed by the aid of a recoating system in the similar way as in SLS on one orthogonal direction, for example, along the Y axis. The first layer is pre-heated by an IR heat source mounted on a cartridge that contains as well, the multi-agent printing head with two agents and a second IR heat source, this cartridge travels along the

opposite orthogonal direction compared to the recoating system, for example the X axis as depicted in Figure 12 below.
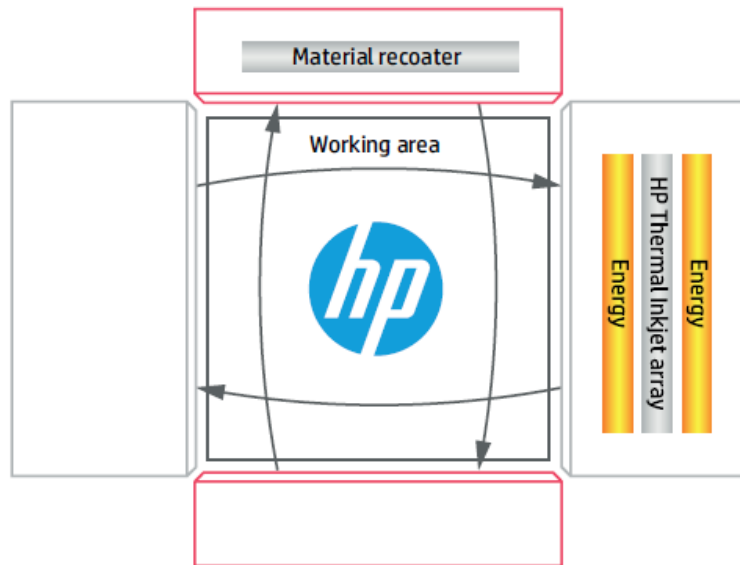

Figure 12: Schematic diagram of top view of build bed and HP MJF process. Extracted from [62].

Figure 13 depicts in detail the role of the application of heat and of the two different agents in the HP MJF process. On each pass, the printing cartridge, pre-heats, drops the agents and by utilizing a second IR lamp, it selectively fuses the area that represents one cross-sectional slice of the part. From the two agents one is a fusing agent ("F" (from Fusing) on Figure 13(c)), which is utilized to promote the fusion of the polymeric material. The fusing agent is selectively applied to the area in which reaching material coalescence is desired, as mentioned by O'Connor et al. [63], the fusing agent is a black ink containing an IR radiation absorbing agent with the goal of transforming the radiation into thermal energy. The second functional agent is described as a detailing agent. As shown in Figure 13(d) (depicted as "D" (from Detailing)), it is dropped on the external contour of the part to avoid fusion on that area and guarantee smooth and well-defined outer features of the part by not allowing loose particles surrounding the fused area to become attached to the perimeter of the layer being built. After each pass of the printing cartridge, the build bed is lowered by the same height as the layer thickness and another powder layer is spread over the build bed to create the next layer and the process repeats until the part is finalized. Usually the parts require post-processing by bead blasting and cleaning to remove the powder impregnated with the detailing agent that remains around the part contours without fusing to it [64].
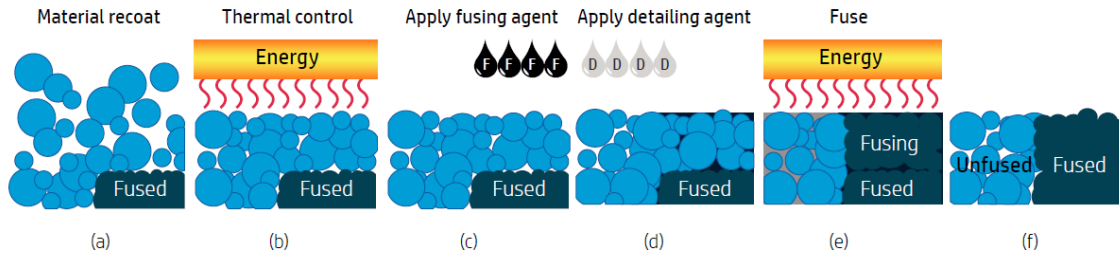
Figure 13: Schematic diagram of heat and functional agent application in HP MJF process. Extracted from [62].

Hewlett Packard claims **[62]**, that their MJF process can be up to ten times faster than point based SLS, faster than FDM and is suitable for relatively high volumes of production. It utilizes a layer approach and the temperature control by using a closed temperature loop the heat is focused to the areas that need fusion.

In terms of part quality, HP claims **[62]** that MJF can reach high isotropic parts and mechanical properties equivalent to the ones present in injection molding parts with balanced properties around the part geometry. As mentioned before and as described in section 6 ahead, AM parts present isotropic mechanical properties depending on their build orientation, being the Z printing direction (see Figure 25) the one with the poorest properties resulting from the inter-layer bonding, HP claims MJF is not affected by the printing orientation.

Process Parameters and Part quality:

MJF machines, have pre-defined and pre-tested sets of parameters that are defined according to the desired final output of the process in terms of mechanical, surface finish properties and dimensional accuracy required for the finished parts. HP in their MJF Handbook **[64]**, mentions the possibility of fine-tuning the pre-defined printing profiles for optimization by adjusting the irradiation level of the fusing IR lamp. The four sets of parameters are classified into Cosmetic, Balanced, Fast and Mechanical profiles. The main differences between them are the processing temperatures and the number of times the print head passes over one layer. For instance, the lower the process temperature the better cosmetic appearance and color distribution along the part. For higher mechanical properties and part density the higher temperatures are applied to the process on the mechanical printing profile. The fast printing profile reduces to half the times for the printhead to pass over one powder layer if compared to the Balanced and Mechanical profiles. The advantages and disadvantages of the different printing profiles are highly dependent on the material to be processed.

Materials:

While this thesis is written the material availability for HP-MJF is limited to polyamides 11 and 12. HP offers a PA12 that contains up to 40% content of glass beads to achieve higher stiffness but with an impact on ductility. HP PA12 powders can be highly recyclable and can be mixed up to 80/20% reused/new powder [64].

The dielectric properties of the materials are not disclosed in their publicly available datasheets, but HP has in its development roadmap plans to develop and launch thermoplastics (PA) with flame-retardant properties, elastomers and commodity plastics (polypropylene) by partnering with companies like BASF, Arkema, Evonik among others [62].

Similarly, as with SLS, the material development is challenging because of the complexity of the thermal control required to process different types of polymers successfully. The temperatures need to be carefully controlled to stay between the melting (T_m) and crystallization temperatures of the material to avoid an accelerated crystallization that could lead to part defects. Other crucial parameters are powder flowability, absorptivity of IR radiation and consolidation at melt [65].

Future developments:

MJF has promising future applications, as HP has wide experience in 2D printing technologies, they claim that their technology is capable to divide a 3D part in voxels while 3D printing, in a similar way as when a regular printer can print pixels and combine different colors into a piece of paper. A voxel is a 3D or extruded pixel with cubic shape. As described before, HP currently applies fusing and detailing agents into their process, but they are developing different "transforming agents" that will allow to control the properties of a part voxel by voxel. For instance, parts will be able to have different regions within the same part where an agent can be deposited to make that region electrically conductive, of a different color or have regional mechanical properties so that the part is more ductile, more brittle or stiffer over an area [66]. This will offer the potential of printing parts that meet different functional requirements in a single part of a single material. Currently the only application of the voxel principle is available for coloring.

Serial production application:

HP MJF is developed to be utilized in a serial production environment and the equipment itself is designed to produce several batches of parts continuously by including a processing station (right side in Figure 14) to clean and cool down the parts contained into a removable build unit that can be switched for an empty one for higher equipment utilization. One example of the serial production application of the technology is the use of HP MJF parts by BMW for the guide rail of the window of the i8 Roadster shown in Figure 15 [67]. As

mentioned before, AM can be a great tool for fast product development, according to [67], BMW developed the guide rail in only five days and the part possesses the properties that meet its requirements achieved by its shape, which could be challenging to be produced by traditional manufacturing methods.

Figure 14: MJF printer, processing station and material containers. Extracted from [68].

Figure 15: MJF window guide rail for a BMW i8 Roadster. Extracted from [67].

5.1.3.3 High Speed Sintering (HSS)

High Speed Sintering (HSS) was developed in the early 2000s by Neil Hopkinson at Loughborough University [69]. The process is close to Multi Jet Fusion, it utilizes an IR lamp as an energy source and a Radiation-Absorbing Material (RAM). According to [69], the main difference between MJF and HSS is that HSS does not use any fusion inhibiting agents during the process.

Process description:

The process consists on applying a thin layer of polymer powder (usually PA12) by a roller, which is integrated to the same assembly as the print head and IR lamp as depicted in Figure 17. The printhead applies the RAM on the region to be fused and is followed by the application of heat by the IR lamp, then the cycle repeats until the part is finalized [27]. The process is depicted schematically in Figure 16 below.
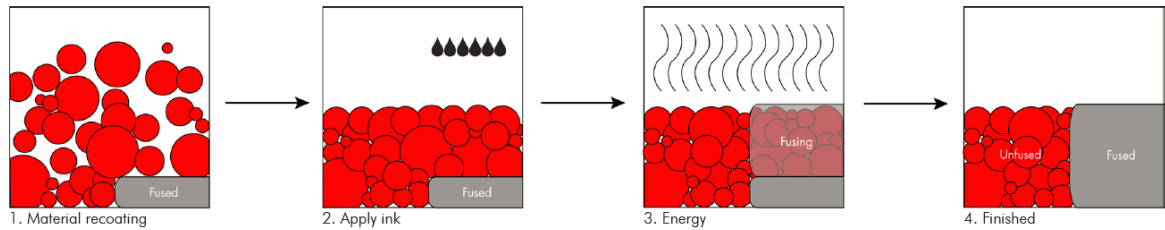
Figure 16: Steps in HSS process according to Voxeljet. Extracted from [70].
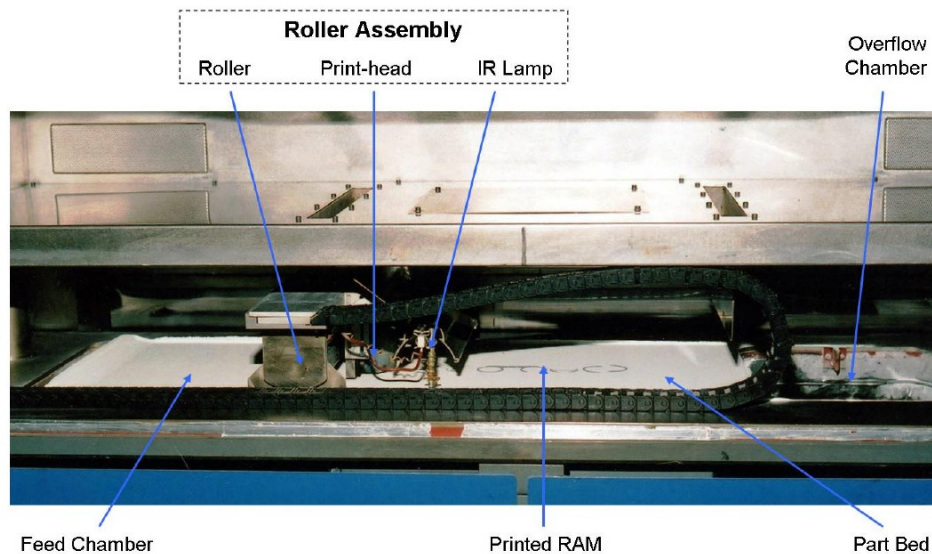
Figure 17: Main structure of HSS apparatus. Extracted from [27].

Currently, the HSS technology is licensed through Loughborough University to equipment manufacturers willing to apply it into their machinery, one example is Voxeljet. HSS can produce parts faster considering the process layer approach and at a lower cost by not utilizing a laser as in SLS [27].

Materials:

According to Voxeljet [70], the materials available for HSS are Polyamide (PA12), Polypropylene, Thermoplastic Polyurethane (TPU) and Ethylene Vinyl Acetate Copolymer (EVA).

6. Previous work

To establish a starting point on the expectations for the experimental part of this thesis, a brief literature review was performed to observe previous work made on comparing parts processed by Powder Bed Fusion with parts processed by Injection Molding and studies on the dielectric strength of additively manufactured parts. This section presents some of the findings on similar experiments.

6.1 Mechanical characterization of PBF parts by tensile testing

There are plenty of studies about investigating the short-term mechanical properties of parts made by additive manufacturing and how the influence of the different process parameters on these technologies affect the resulting mechanical properties of the tested samples. Emphasizing on SLS and according to Schmid **[3]**, studies about long term behavior of SLS parts should increase in number for the process to be adopted as a method to manufacture end-products.

SLS parts have been related to injection molded parts empirically by producing injection molded specimens and comparing the resulting values against the ones described by material data sheets. For instance, Van Hooreweder et. al. **[71]** studied structural and fatigue differences between as-built specimens made from PA12 powder by injection molding and by SLS in two different printing orientations (X and Z according to Figure 25). By utilizing already optimized process parameters, uniformly dense and uniformly porous parts were achieved. Their injection molded samples had a big void on one end of the specimens but full density along the rest of the part geometry, confirming that injection molding can produce dense solid parts with low porosity. Evident anisotropy was observed between the X and Z printing orientations, the Z orientation showed an elongation of only 4% while the X orientation presented a result of 7% compared to their injection molded specimen, which showed an Elongation at Break (EAB) of 97%. The SLS specimens presented brittle behavior when fracturing. According to Schmid (2018) **[3]**, laser sintered parts made from PA12 without reinforcement usually do not exhibit necking before breaking as shown in the stress-strain curve B on Figure 18 below, making them less prone to absorb energy before fracturing, in contrast with parts made by injection molding. On the other hand, an interesting finding of Van Hooreweder et. al. **[71]** was the higher Young's modulus from their SLS samples (X orientation 22% and Z orientation 26% higher than the IM samples), According to the authors the build orientation, part density and porosity had low effects on the fatigue behavior of the SLS specimens compared to the IM specimens utilized for the study. According to Schmid **[3]**, one reason for high Modulus

in Laser Sintered parts could be attributed to the bigger crystalline structures developed during the long cooling periods compared to IM, where cooling takes only few seconds.
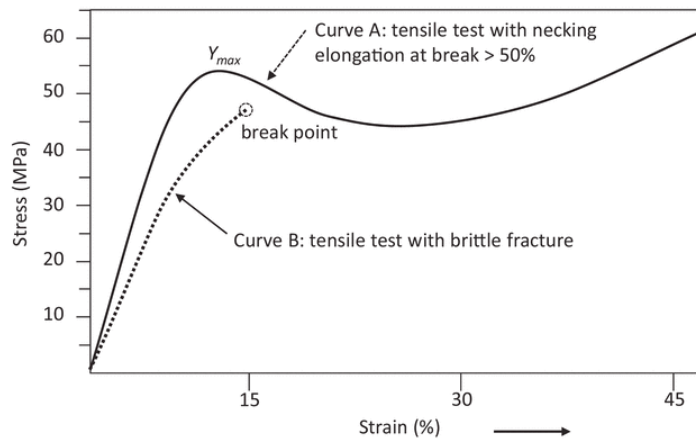

Figure 18: Strain-stress curves of a PA12 specimen (curve B) compared with an IM specimen (curve A). Extracted from [3].

Higher crystallinity can lead to more rigid characteristics but as SLS parts are porous, their voids can lead to the creation of stress concentrations that can lead to brittle fracture. For example, Flodberg et.al. **[72]**, performed a study for testing multi-purpose standard dumbbell-shape and cylindrical specimens manufactured with 3D Systems DuraForm ProX PA12 with and without carbon fibers to compare them with specimens produced by injection molding (only dumbbell shaped injection molded specimens) and SLS. Both specimen types were produced in horizontal and vertical orientations. Tensile tests for the dumbbell were performed at a speed of 50mm/min. The results of tensile testing showed lower tensile strength values (75% for Horizontal and 79% for Vertical Orientation compared to IM samples (100%)) for the unreinforced PA12 samples. In terms of Young's modulus, the values were really close for the unreinforced PA12 Horizontally printed specimens (98%). Contrary to the findings of Van Hooreweder et. al. **[71]**, the Vertically printed specimens outperformed the IM samples by 15%. The downside of SLS was again the EAB that for none of the orientations was above 6% (SLS Vertical orientation was 2.7%) of elongation presenting brittle breaking behavior. While the IM specimens elongated more than 17%. The authors noted high standard deviation between the average values of SLS unreinforced PA12 samples and attributed the variation on mechanical properties to high levels of porosity and internal voids within the parts and poor coalescence caused by a low energy density applied. Complete unfused powder particles were observable on the parts through microscopy instead of fully consolidated material.

Few studies about parts produced by MJF are available by the time this thesis is written. The available literature mentions slight differences between SLS and MJF specimens in terms of mechanical properties based on tensile testing. According to a performance and raw material study reported by Sillani et. al. **[73]**, the raw material characteristics between

the PA12 utilized for SLS (Duraform, PA2200) and MJF (HP 3D HR PA12) are similar in terms of flowability, size and shape distribution and thermal properties because both powders are manufactured by the company Evonik. By their tensile tests, it was found that the most significant difference in mechanical properties was for the Young's modulus, which resulted to be higher (approximately by an average of 34%) in SLS parts and attributed, as it was mentioned before, to the bigger crystalline structures formed by a higher period of time of exposure to high temperatures and the slow cooldown period in the SLS build chamber. MJF parts overall were less anisotropic depending on the printing orientation. The relative isotropic properties for MJF tensile specimens reported by Sillani et.al. were also reported by Morales-Planas et. al. [74] and O'Connor et. al. [63] confirming what HP claims regarding isotropic properties achieved with their patented technology.

6.2 Dielectric strength of PBF parts

Parts manufactured by injection molding and SLS have been studied as electrical insulators, on the contrary, by the time this thesis is written, no study has been found about testing parts manufactured by Multi Jet Fusion to investigate their behavior under electrical stress. This brief section discusses some of the findings of other authors regarding dielectric strength tests performed previously on specimens created by PBF processes.

If compared to injection molding, PBF processes, regardless of being SLS or MJF, present higher degrees of porosity and produce parts with lower density. It is documented in the literature that the porosity levels represented by percentage between SLS and MJF parts do not differ significantly between each other, both processes could produce parts with porosity levels up to 5% [63, 3]. The pores and voids in MJF parts could be randomly distributed within the part as reported by O'Connor et. al. [63] for specimens manufactured in Y orientation (according to Figure 25). Dielectric breakdown can be induced by the presence of voids or porosity, which can lead to fracture propagation resulting in the formation of conductive paths or simply by voids connected to each other. Individual pores can also contribute to the pre-degradation phenomenon of "partial discharges", which build over time and contribute to the appearance of electric trees, which are a cause of dielectric breakdown [14]. On the other hand, it was demonstrated by Morales-Planas et.al [74], while studying the water tightness of valve components produced by MJF, that leak tight components are possible after testing at a defined pressure (4.2MPa) as a result of low porosity but dependent on the wall thicknesses. They achieved better results for higher wall thicknesses between a range from 0.4 to 0.7mm. This contrasted other AM processes such as SLS, which they mention that even with the application of sealants, tested parts could only withstand 0.45MPa of pressure according to their references.

Additionally, it is important to mention the influence of the build orientation on dielectric strength. According to Hoff et. al. [44], build orientation can result in different dielectric strength characteristics. SLS specimens printed vertically, in X and Z orientations according to Figure 25, result in significantly lower dielectric strength values when compared to specimens built in Y direction. This printing orientations match with the results obtained for the leak-tight components in [74], where it is mentioned how vertical orientations tend to require more layers depending on the part geometry, this results on more interlayer gaps that lead to leakage for liquids. Therefore, the gaps could allow for current to leak through an insulator as well with a high enough electric field.

Another factor to consider is the presence of substances or additives that contribute to the reduction of dielectric strength. For instance, Thompson et. al. [27] made a comparative study emphasizing the difference between published injection molding data, SLS and HSS samples in terms of dielectric properties, among them dielectric strength. According to Thompson et. al. [27], the dielectric strength tested (with DC voltage) values between IM and SLS specimens are similar within a range of approximately 26-33kV/mm for samples 1mm thick. On the contrary, HSS specimens, which demonstrated to be denser than the SLS specimens, performed poorly presenting breakdown below 10kV/mm. The authors attributed the results to the presence of carbon black in the Radiation-Absorbing Material (RAM) and not to the porosity in the part.

7. Case study: PA12 mechanical and voltage withstand comparative study

This section contains a case study that compares the mechanical properties by tensile test and electrical insulation performance of Polyamide 12 specimens produced by three different manufacturing technologies, from which two of them are additive processes: Selective Laser Sintering and HP Multi Jet Fusion, and a conventional one: Injection Molding. These experiments were performed at Valmet Automotive premises.

Materials:

Since PA12 is the most utilized material for PBF processes and is an engineering thermoplastic that is available for Injection Molding it was decided to utilize this polymer for the study. For simplicity, the material was selected without fillings, beads or reinforcements. Even though this material does not fulfill all the requirements discussed on section 3.1, as mentioned in sections 5.1.3.1 and 5.1.3.2, the materials availabile for PBF processes are mostly limited to PA12. Additionally, it is one of the most common materials utilized when ordering functional prototypes at Valmet Automotive from external suppliers.

The PA12 materials for SLS and MJF were chosen based on the specimen supplier recommendation and availability. The material selection for the injection molded samples was based on finding an injection molded component made from PA12 existing in Valmet Automotive production to avoid mold costs and to cut the samples from that component. The material found was EMS-Grivory Grilamid TR55. The SLS material was EOS PA2200 and for HP-MJF it was HP3DHR PA12. Some of their properties are presented in Table 4.

Table 4: Tensile and electrical properties of tested materials [75] [76] [77].

Material / Property	EOS PA2200	HP 3DHR PA12	EMS-Grivory Grilamid TR55
Tensile strength (MPa).	[1]45	[2]48 (X, Y, Z)	[1]50
Tensile E-modulus (MPa)	[1]1700	[2]1700 (X, Y) [2]1800 (Z)	[1]2200
Elongation at break (%)	[1]20	[2]20 (X, Y) [2]15 (Z)	[1]>50
Dielectric strength (kV/mm)	Not available	Not available	31
CTI	Not available	Not available	600

[1]Tested acc. to ISO 527 at 1mm/min for E-modulus and 50mm/min for EAB. [2]Tested acc. to ASTM D638.

Additive Manufacturing equipment:

All the additively manufactured samples were ordered from Ajatec Prototyping OY as they had SLS and HP MJF capabilities available in the same facility. The machine to process the SLS samples was the EOS Formiga P100 shown in Figure 19. All the parameters were set by the supplier based on their regular operations and can be found in Table 5.

Table 5: Process parameters for specimen manufacturing by SLS in EOS Formiga P100. Courtesy of Ajatec Prototyping OY.

Parameter	Value
Layer height	0.1mm
Process chamber temperature (see Figure 19a)	169.5°C
Unloading chamber temperature (see Figure 19b)	135°C
Contour Laser Power	16W
Hatching Laser Power	21W
Contour Laser Speed	1500mm/s
Hatching Laser Speed	2500mm/s
Material proportion used/new powder	50%/50%
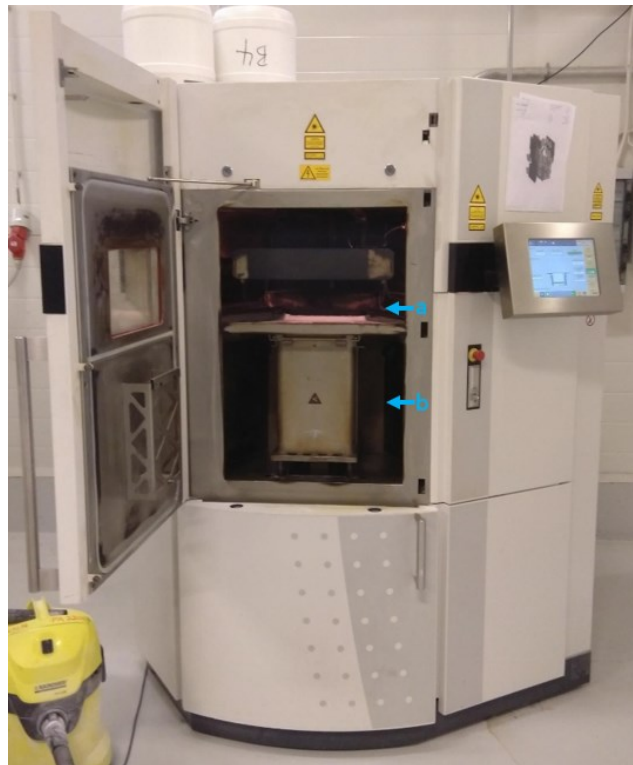
Figure 19: EOS Formiga P100 SLS machine. a: Process chamber. b: Removal chamber. Courtesy of Ajatec Prototyping OY.

The SLS parts were nested in three sets and mixed with parts from other customers (removed from Figure 20 to protect customer confidentiality) to optimize machine utilization as depicted in Figure 20.
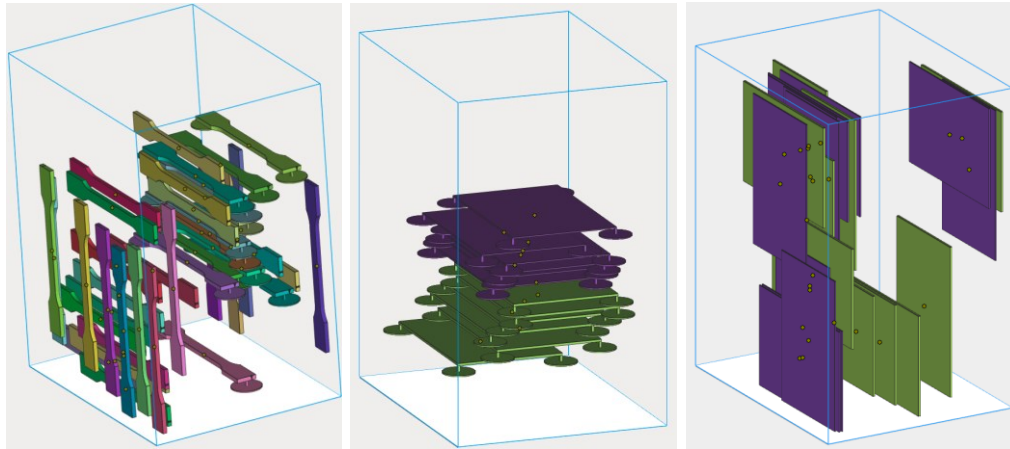
Figure 20: SLS nesting of specimen printing. Courtesy of Ajatec Prototyping OY.

The MJF samples were manufactured with an HP MJF4210 machine. The 3D printing station is shown in Figure 21. For HP MJF, the process parameters are not as detailed as with the EOS Formiga P100. As mentioned in section 5.1.3.2, HP has pre-defined four different printing profiles, for the testing specimens the "Balanced" printing profile with standard values was utilized for printing the parts with a default layer thickness of 0.08mm. The proportion between used and new powder material was 80% and 20% respectively.

Figure 21: HP MJF4210 3D printing station with upper lid open. Courtesy of Ajatec Prototyping OY.

As for printing parts by SLS, for HP MJF, the samples were nested to be printed in two batches on the machine as shown in Figure 22 (Components from other customers were removed from Figure 22 to respect the confidentiality of their projects).

Figure 22: HP MJF nesting of specimen printing. Courtesy of Ajatec Prototyping OY.

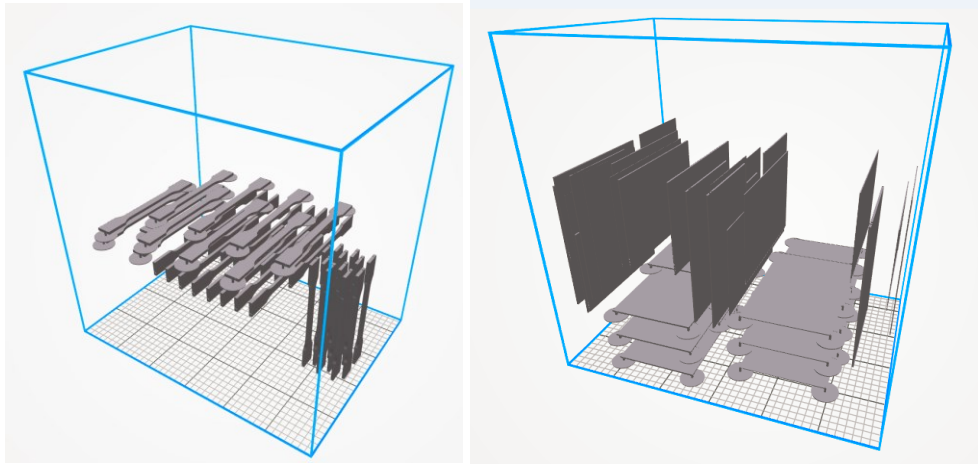All the samples were cleaned in the MJF processing station from remaining powder after printing (see Figure 23) and shot blasted with glass pearls grade 300-400μm to remove any non-sintered material around the parts.

Figure 23: HP MJF parts before cleaning and shot blasting. Courtesy of Ajatec Prototyping OY.

7.1 Tensile test

7.1.1 Testing method and equipment

The testing procedure was based on the ISO 527 standard, parts 1 [78] and 2 [79]. The ISO 527 standard specifies the testing speeds for Young's modulus determination to be 1mm/min and for elongation at break to be between 5-50mm/min. A speed of 50mm/min was selected based on the speed denoted in the datasheet of the injection molded PA12 material [77].

The machine for tensile testing was a Zwick Z010 universal testing machine with a load cell of 10kN. All the specimens' masses were measured with a Mettler PJ3600 DeltaRange scale for approximating their density. The volume of the parts was taken from the theoretical value from geometry contained in the CAD model of the parts.

7.1.2 Tensile specimen manufacturing

The specimens were prepared according to the ISO 527-2 type 1A geometrical specifications for tensile bars as depicted in Figure 24 [78]. The injection molded specimens were ordered from MSK Plast OY and were produced from an existing mold specifically available for tensile bar production. In comparison with the ISO standard dimensions, these injection molded specimens were 10mm shorter in total length and only one flow orientation was possible. The location of the gate on the mold can be observed in Figure 26. The molding process was set according to MSK Plast OY known parameters for PA12 Grilamid TR55. The parameters are presented in Table 6.
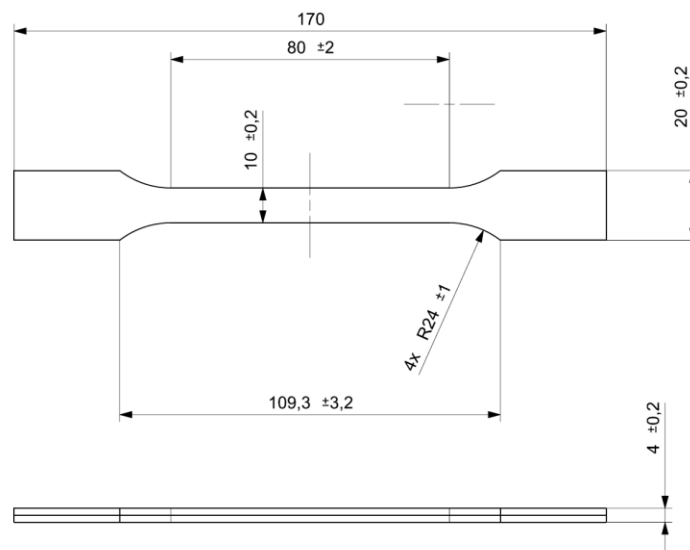
Figure 24: ISO 527-2 1A tensile bar dimensions. Adapted from [78].

The additively manufactured tensile test specimens were manufactured in 3 sets of 10pcs for each process. Each set of 10pcs included 3 different printing orientations as shown in Figure 25. As mentioned before, additive manufacturing parts present anisotropic properties depending on their orientation during production, therefore it was decided to test three common printing orientations.

Table 6: Process parameters for specimen manufacturing by Injection Molding. Courtesy of MSK Plast OY.

Parameter	
Nozzle/barrel temperatures	265/275/270/265/260°C
Injection speed	95mm/s
Clamping Force	1400kN
Material drying temperature/time	80°C/3h
Holding time	3s
Injection time	0.55s
Cooling time	25s
Mold temperature	80°C
Injection pressure	1140 bar
Holding pressure	60bar
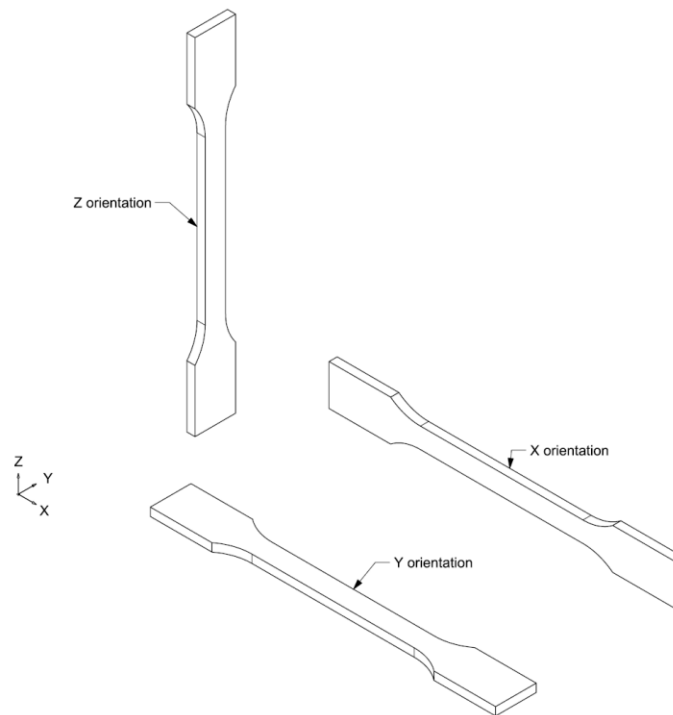
Figure 25: Printing orientation of SLS and MJF tensile specimens.
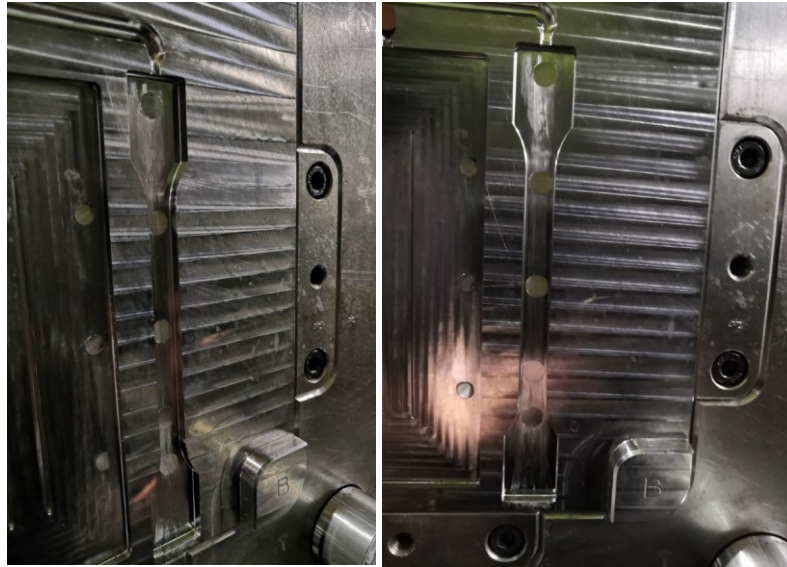
Figure 26: Injection molding cavity for tensile bars with gate location. Courtesy of MSK Plast OY.

The specimens were named based on manufacturing process (1 in Figure 27), printing orientation (2 in Figure 27) and an ascending running number (3 in Figure 27) was assigned to them for identification. Figure 27 shows an example of the nomenclature.

Figure 27: Tensile specimen identification numbering nomenclature.

7.1.3 Specimen conditioning

As per ISO 527 [78], all specimens were conditioned at 23°C at a relative room environmental humidity of 50% for a minimum period of 16hrs. The tensile tests were performed under the same conditions and in the same room where the parts were conditioned.

7.1.4 Limitations

The tests were performed without an extensometer device. Therefore, the results obtained for Young's modulus are not reliable for comparison with material datasheets and could only be used for comparison purposes within this thesis.

Although the materials processed by SLS, HP-MJF and Injection molding were all PA12, they were not the same exact material. Therefore, the comparison can only give approximate results. The sample size of 10 parts is not big enough to determine the statistic repeatability of the behavior of the parts outside of this thesis. The injection molding specimens were only possible to mold in one flow orientation, limiting the visibility of anisotropic properties developed in injection molding.

7.1.5 Test Setup

The setup of the tensile test was simply done by utilizing the spring action grippers of the Zwick Z010 machine and placing the tensile specimen between them as shown in Figure 28 below. The specimens were carefully located within the grippers to avoid any slippage or misalignment compared to the vertical axis of the transducer of the machine.
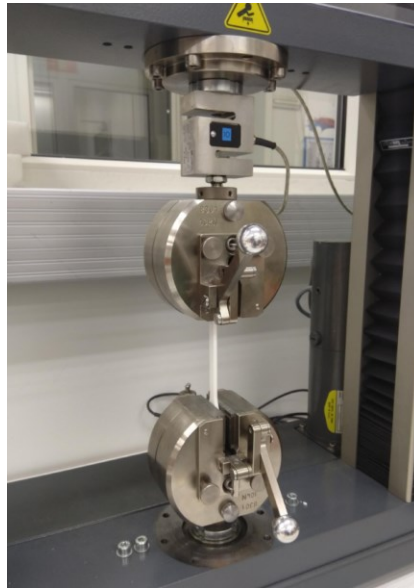
Figure 28: SLS tensile specimen mounted to Zwick UTS machine.

7.1.6 Test results reporting

The raw data from the tensile machine was exported, cleaned and processed with Microsoft Excel to generate stress-strain curves for each of the tested specimens and to group the diagrams by build orientation. The values for E-Modulus, Ultimate Tensile Strength and Elongation at Break were taken straight from the tensile testing machine reports. A comparative diagram can be found on section 8.1. All the stress-strain diagrams divided by process and printing orientation can be found in Appendix I.

7.2 Voltage withstand test

7.2.1 Testing method and equipment

A voltage withstand test (HIPOT test) was performed on the samples while increasing the test ambient temperature from 20°C to 100°C. Voltage withstand tests are non-destructive tests intended to ensure that an insulator is effective within voltage values above the tested device operation range. The results are reported as "Pass" or "Fail". The tests include a ramp up time to reach the test voltage and a hold time that is the time in which a continuous voltage is stressing the insulation.

One withstand test was performed for every ascending interval of 5°C to observe for leak current changes resulting from the temperature increasing. No stabilization time was allowed except for the highest temperature (100°C) because the climatic chamber tended to slow down the rise of temperature when approaching the target set temperature. Each HIPOT test was set for ramping the voltage from 0 to 4kV in 5 seconds and the withstand test lasted 60 seconds for every temperature step. The testing duration of 60 seconds was based on the ISO 16750-2 [80] standard, even though the test procedure in this thesis was not in accordance with it. The specimens were not exposed to a damp heat cycle as specified in [80]. The testing frequency was 50Hz as for European applications. The higher limit for leak current on the tester was set at 1mA to obtain a three-decimal resolution from the tester but if a 1mA leak current was achieved a second run of the test was performed with a leak current limit of 5mA, which according to the ISO 6469-3:2011 standard [23], is the maximum permissible touch current regarding the safety of the users of any device operating at a Class B Voltages. If the tester emitted a "Fail" result and leaked 1mA, a second test was performed to ensure the leak current could be above 5mA.

The test procedure was designed based on the internal testing capabilities and available equipment at Valmet Automotive. The voltage parameter was defined as 4kV based on a specification from an OEM from a previous project at Valmet Automotive that required a basic insulation level of 2.5kV AC but upon agreement was tested at 4kV AC. The climatic chamber utilized was a Vötsch VT4018 (shown in Figure 29 left) capable of rising the temperature 4°C per minute. For the voltage withstand test a GwINSTEK GPT-9804 HIPOT tester with a maximum AC voltage capacity of 5kV (shown in Figure 29 right).

Figure 29: Vötsch VT4018 climatic chamber (left) and GwInstek GPT-9804 HIPOT tester (right).

For a safe setup and to focus the voltage stress towards the specimens, a fixture was designed and manufactured. The fixture consisted on a frame and two electrodes, the upper electrode was spring loaded. The two electrodes were made from available copper with dimensions according to the Table 1 of the ASTM D149 standard (outer diameter=25mm, thickness=25mm, rounding radius=3.2mm) for performing dielectric breakdown testing [81]. For material cost reductions and manufacturability, the electrodes were made in two parts (items 3 and 6 on Figure 30 left). One part consisted on an M8 threaded rod and the second one was the electrode body. They were joined together by utilizing male and female threads on the parts respectively. The fixture can be observed in Figure 30. The frame for the fixture (items 1, 2 and 8 in Figure 30) was machined from POM plastic with a maximum working temperature of 140°C. All the parts were designed with Siemens NX11 and all the manufacturing was made at the prototype shop at Valmet Automotive in Uusikaupunki.
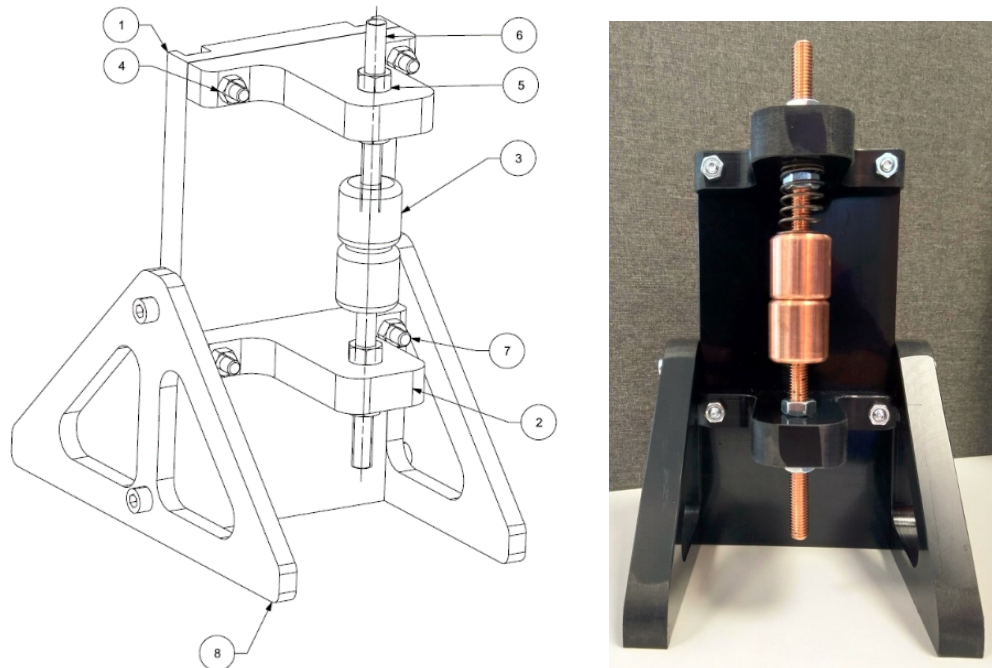
Figure 30: Schematic representation of testing fixture as designed in Siemens NX11 (left) and after readiness (right).

The test setup was made as depicted in Figure 31. The insulation specimen was located in between the two copper electrodes, the cables of the HIPOT tester were introduced through the side grommets of the climatic chamber. The high voltage cable was connected to the upper electrode while the lower electrode was connected to the ground cable of the tester. Special care was taken into avoiding any compression of the specimen between the electrodes. The electrodes with the help of the spring were only keeping the specimen in place, the gap between electrodes was adjusted by loosening the nut on top of the fixture (item 5 in Figure 30).

Figure 31: Testing fixture with HIPOT tester cables connected to it and insulation specimen located between the testing electrodes.

The failed specimens were observed under a Nikon MM-40 light microscope (see Figure 32) after testing for documenting possible punctures, carbonization or burn marks caused on the surface of the specimens. All the specimens' masses were measured with a Mettler PJ3600 DeltaRange scale for density approximation. The volume utilized for calculating the density of the parts was the taken from the CAD data of the specimens.
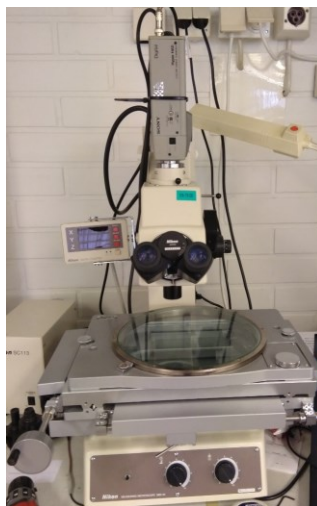
Figure 32: Nikon MM-40 light microscope utilized to review voltage withstand specimens.

7.2.2 Electrical insulation specimen manufacturing

In contrast with the tensile bars described in section 7.1.2, the specimens for the voltage withstand test were not geometrically following a specific standard but rather a recommendation from the ASTM D149 [81] according to the electrode size utilized. The standard recommends having a minimum material offset of 15mm all around the test electrode and this dimension was kept. Two sets of specimens were produced, the first set with a thickness of 1mm and the second one with a thickness of 2mm. The specimen quantities per set can be observed in Table 7 below. The printing orientations for the additively manufactured specimens were according to the ones shown in Figure 25.

Table 7: Specimen quantities according to their manufacturing process.

1mm / 2mm set configuration		
Manufacturing process	**Printing orientation**	**Quantity**
Injection molding	N/A	5/5
SLS	X	5/5
	Y	5/5
	Z	5/5
HP MJF	X	5/5
	Y	5/5
	Z	5/5

The additively manufactured specimens were planned and manufactured before the injection molded specimen manufacturing was decided. They were ordered in the same batch together with the tensile specimens. Initially, SLS and MJF specimens were ordered with dimensions of 150x100mm but it was only possible to obtain injection molded samples with dimensions of 110x55mm (see Figure 34). Subsequently, the additively manufactured specimens were carefully cut to the same dimensions to have uniformly dimensioned coupons.

The main challenge and dimensional limitation to produce the injection molded specimens was to find an economically viable solution as fast as possible. Therefore, fabricating a mold for the parts was discarded. There was scrap material from injection molded 2mm thick parts from a serially manufactured product at Valmet Automotive and the raw material was PA12 Grilamid TR55. The CAD model of the part was studied to find a suitable flat area. Ten specimens were cut out of ten scrap parts (due to confidentiality, the component picture is not included in this thesis). Due to the presence of reinforcement ribs and pockets the only possible dimensions were 110x55mm as discussed above. Figure 34 depicts the main dimensions of the final test specimens.

As mentioned, the thickness of the injection molded scrap parts was 2mm and to achieve a thickness of 1mm for the thinner samples, five pieces out of the ten 2mm coupons were milled for thickness reduction. A picture of three different coupons can be observed in Figure 33 below.
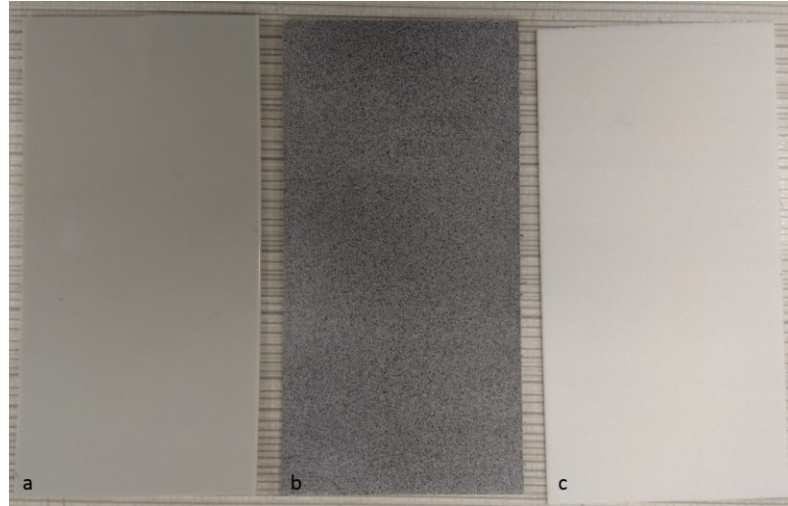
Figure 33: 1mm thick specimens manufactured be injection molding (a), HP Multijet Fusion (b) and Selective Laser Sintering (c).

The reason of making the specimens in a rectangular shape was to divide the part in two halves. One defined as the manipulation area on one end of the specimen to avoid touching the testing area and to avoid contamination of the area as it was performed by Thomson et.al. in [27] (see Figure 34). The sub-division of the areas were only marked by pen.
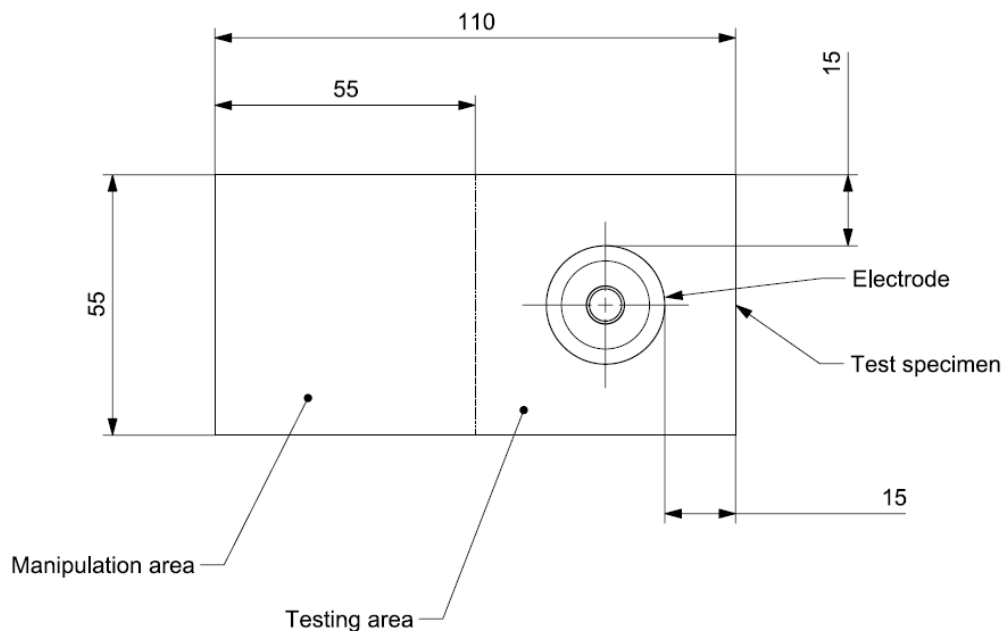
Figure 34: Schematic representation of specimens for voltage withstand test showing dimensions, position of the electrode within the specimen and area sub-division. Principle based on [27].

In the same manner as with the tensile specimens a nomenclature for identification of each specimen was assigned. It specifies the manufacturing process (1 in Figure 35), specimen thickness (2 in Figure 35), the printing orientation (3 in Figure 35 and according to Figure 25) and specimen number from 1 to 5 (4 in Figure 35). For injection molding no build orientation was assigned.

$$\underbrace{SLS}_{1}\underbrace{1mm}_{2}\_\underbrace{X}_{3}\underbrace{1}_{4} \quad \underbrace{MJF}_{1}\underbrace{2mm}_{2}\_\underbrace{Y}_{3}\underbrace{1}_{4} \quad \underbrace{IM}_{1}\underbrace{1mm}_{2}\_\underbrace{1}_{4}$$
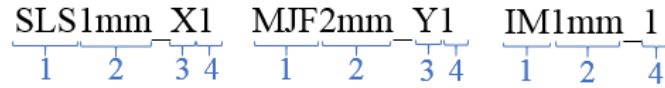
Figure 35: Nomenclature assigned for specimen identification per manufacturing process.

7.2.3 Specimen conditioning

Initially, the specimens were kept under laboratory conditions at a room temperature of 23°C and at a relative humidity of 50% but the tests were performed in a different location. Due to the length of each test per specimen (approx. 1 hr.), the specimens remained for long periods of time under an uncontrolled atmosphere at room temperature.

7.3.4 Limitations

The first limitation on this experiment was that the materials for each manufacturing process were all PA12, but they were not the exact same material, making the comparison reasonable but not fully equal.

As a second limitation for defining the test procedure was that the maximum operating temperature of the cables attached to the HIPOT tester that were inserted into the climatic chamber were graded for use at a maximum temperature of 105°C. This factor limited the maximum test temperature to 100°C. Originally it was desired to be 120°C. There were cables for applications on a maximum temperature of 125°C available to bridge the connection but they were graded only for 1kV. As a result, it was decided to perform the tests at a maximum temperature of 100°C to avoid damages to the equipment. The temperature considered during the test was the environmental temperature inside of the climatic chamber and not the surface temperature of the electrodes in contact with the insulation specimens.

It is important to add that AC HIPOT tests stress more the insulation material than DC voltage. AC and DC are equally good to detect a dielectric breakdown but the detection of current leaking through the insulation is not as accurate with AC as it is with DC HIPOT testing. AC HIPOT testing can give false failure results, due to the capacitance built between two conductors separated by an insulator resulting from the changes in direction from AC voltage [82].

8. Test results and discussion.

This section discusses the findings from the comparative study between conventionally manufactured PA12 specimens and the ones fabricated by Additive Manufacturing. It is divided in two sections, the first one includes the results from investigating the mechanical properties of standard test specimens obtained by tensile testing. The second section includes the findings from performing voltage withstand tests on 1 and 2mm electrical insulation rectangular coupons.

8.1 Tensile test results.

This section presents the results obtained from the tensile experiments performed utilizing comparative charts. The comparison was made between sets of 10 specimens manufactured by SLS, HP-MJF and Injection Molding. The additively manufactured specimens were built in three different orientations as depicted in Figure 25. The density of the parts was approximated by measuring the mass of the parts and using the volume directly from the CAD model to obtain a rough idea on part porosity. Porosity has a significant impact on mechanical properties as mentioned before. The calculated densities can be observed in Figure 36.
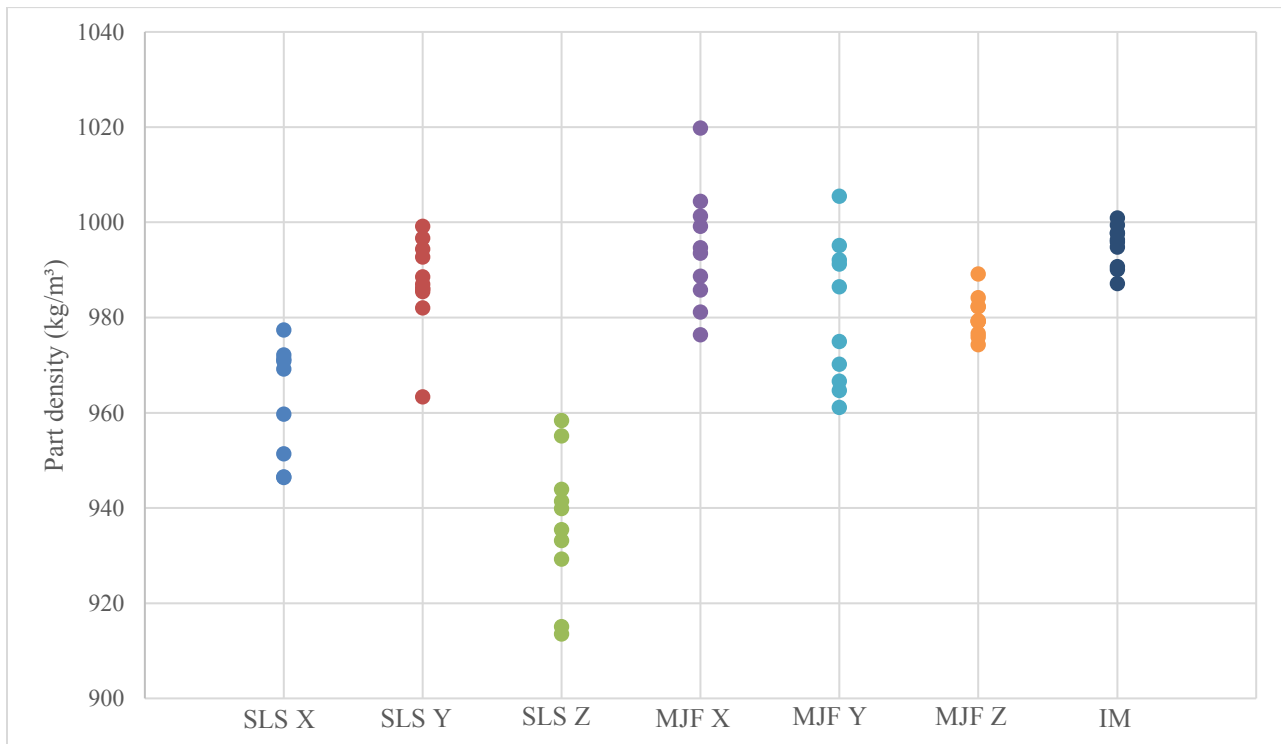
Figure 36: Calculated density of tensile specimens separated by manufacturing process and build orientation.

As it was expected and as depicted in Figure 36, the parts produced by SLS in the Z orientation showed to be the least dense from the whole specimen batch (with an average density of $936.5 kg/m^3$). This can be attributed to the gaps created in the interlayer junctions. As well, it can be observed that SLS parts do show higher anisotropy based on printing orientation when compared to MJF parts. The three sets of MJF specimens are relatively isotropic and in terms of density values and they were comparable to the injection molded specimens. It is interesting to find high uniformity between the MJF specimens printed in Z orientation, which had the lowest standard deviation (s) from the mean value (s=4.378) compared to the X and Y printing orientations (s=12.576 for X and s=15.185 for Y respectively). Y oriented SLS specimens resulted to be comparable with injection molded parts and showed a low standard deviation from the mean (s=5.595) if compared with the other SLS orientations (s=11.316 for X and s=14.795 for Z). Although the porosity percentage was not determined for this thesis, low part density can be a sign of voids and pores within the parts or gaps because of poor powder particle coalescence. Those defects, as it has been mentioned in section 6.1, can become fracture initiators due to stress concentrations within themselves and consequently can result in lower mechanical properties or part brittleness.

The average values for E-Modulus, Ultimate Tensile Strength and Elongation at Break are presented in Figures 37, 38 and 39 respectively.

	SLS - X AVG	SLS - Y AVG	SLS - Z AVG	MJF - X AVG	MJF - Y AVG	MJF - Z AVG	IM AVG
E-Modulus (MPa)	499,581	514,529	464,996	447,781	343,88	474,154	558,173

Figure 37: Average modulus of elasticity for 7 sets of tensile specimens divided by printing orientation and PBF process.

As it can be observed from Figure 37, the modulus of elasticity resulting from the tests are below the values presented in Table 4, which were extracted from the datasheets obtained from the

manufacturers of the raw PA12 materials. The tests were performed at the same speed as the ones depicted on the material datasheets from the injection molding material EMS-Grivory Grilamid TR55 PA12 (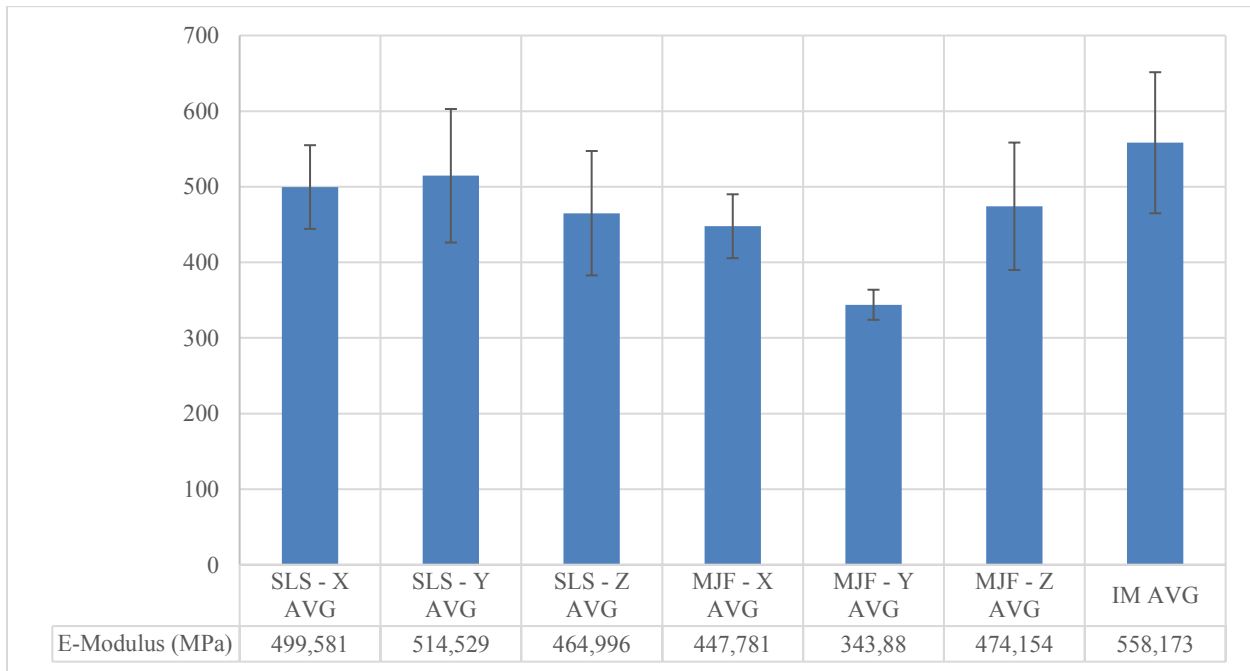1mm/min for Young's modulus and 50mm/min for EAB and UTS) [77]. One possibility for the low values could be attributed to the lack of an extensometer during testing, which is required by the ISO 527-1 standard. The E-modulus results obtained during these tests are not truly reliable for material selection but are good for comparative purposes between the processes in this thesis. The data obtained was disperse from the mean values, with high variability between the specimens within each group except for the MJF specimens built in Y orientation (s=19.913). The injection molded tensile bars showed to be far from mean values (s= 93.312).

From the PBF sets, the samples manufactured by SLS in the X and Y orientations obtained the highest Young's modulus values. They correspond to the 89.5% and 92.2% of the achieved modulus for the injection molded specimens respectively. On the contrary, the specimens manufactured by MJF in the Y orientation presented the lowest E-modulus values and only reached 61.6% of the modulus corresponding to the injection molded specimens. These results confirm what was described by Sillani et. al. [73], mentioning that the SLS process can produce stiff parts resulting from higher crystallinity induced by the longer time of exposure to higher temperatures and the long cooling periods. Another finding is the higher Young's modulus on the MJF specimens built in Z direction, in comparison with the ones printed by MJF in X and Y orientations. As it is mentioned by Sillani et.al. [73] and O'Connor et.al. [63], the weight of the newly fused layers on top of the previously printed ones plus the fusion agent, can promote a better interlayer bonding for the MJF process.

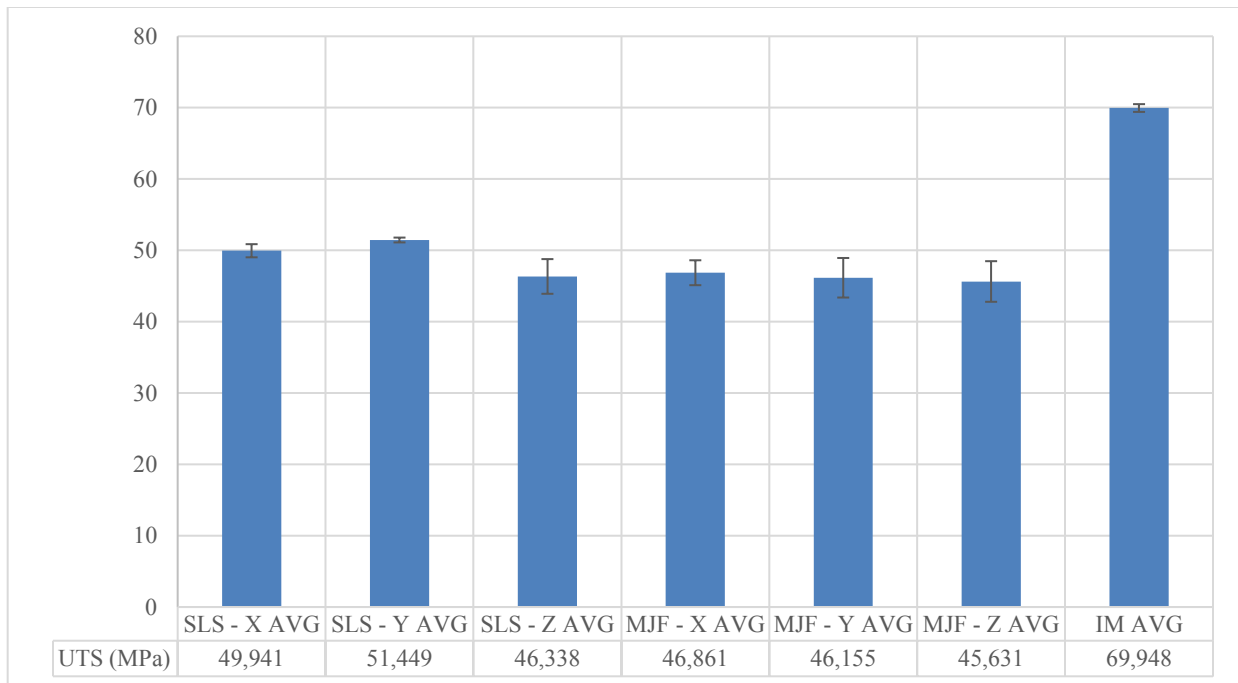|	SLS - X AVG	SLS - Y AVG	SLS - Z AVG	MJF - X AVG	MJF - Y AVG	MJF - Z AVG	IM AVG
UTS (MPa)	49,941	51,449	46,338	46,861	46,155	45,631	69,948

Figure 38: Average Ultimate Tensile Strength for 7 sets of tensile specimens divided by printing orientation and PBF process.

In terms of Ultimate Tensile Strength (UTS), Figure 38 presents the differences between all the specimens. For the parts produced by Additive Manufacturing, all the results were significantly lower than the ones obtained for the injection molded specimens. The standard deviations within the specimen groups are smaller if compared with the ones for modulus of elasticity presented in Figure 37. The low variations from the means could be attributed to the fact that the calculation of tensile strength is not dependent on utilizing an extensometer. Therefore, the UTS values are comparable to the tensile strength values from the material datasheets presented in Table 4.

From the additively manufactured specimens, the highest UTS values corresponded to the SLS specimens printed in Y orientation achieving 73.6% from the injection molded parts. The lowest value was obtained by the MJF specimens printed in Y orientation (66%) but not far from the results for the SLS parts printed in Z orientation (66.2%). When compared to the values presented in Table 4, the SLS parts reached higher values than the ones specified in their material datasheet corresponding to EOS PA2200, regardless of their build orientation. They presented relatively low anisotropy. SLS with Z orientation showed the poorest performance as documented in most of the literature and reportedly caused because of poor interlayer adhesion [3, 63, 73]. In contrast, all the MJF build orientations showed isotropic UTS values but all of them were 1-2MPa below the equivalent values on the material datasheet corresponding to HP3DHR PA12. The specimens produced by injection molding exceeded the UTS included in the EMS-Grivory Grilamid TR55 PA12 datasheet by 28.5% and were significantly superior than additively manufactured ones and with low variation (s=0.54).

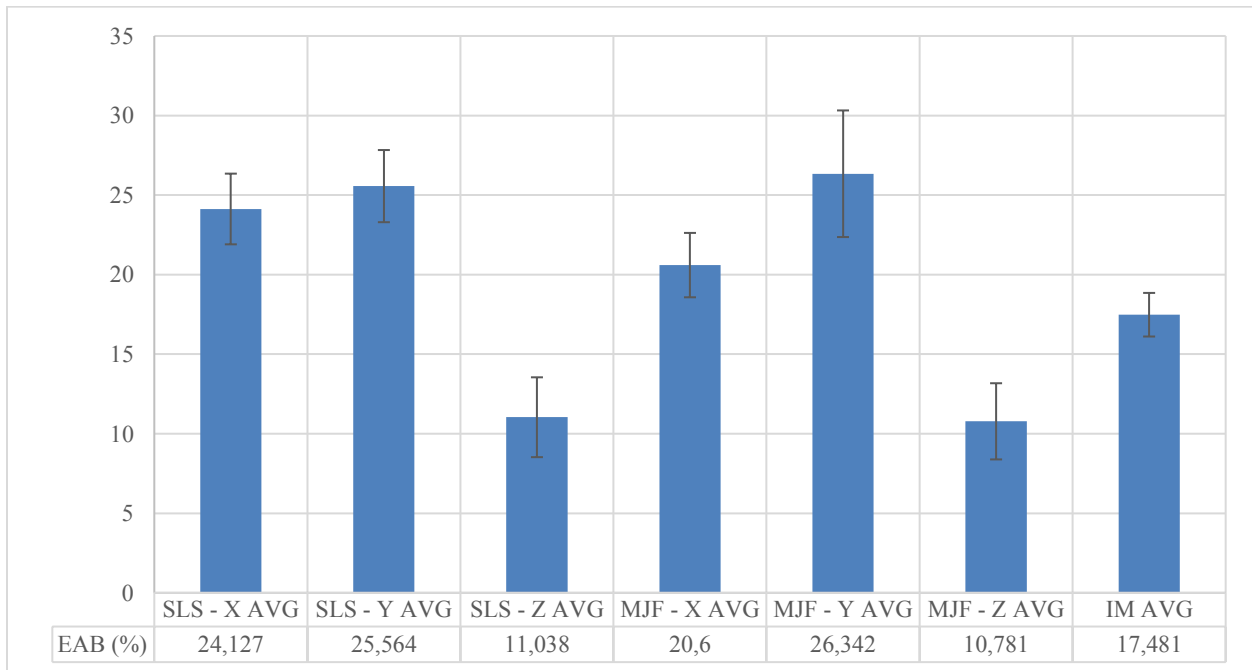|	SLS - X AVG	SLS - Y AVG	SLS - Z AVG	MJF - X AVG	MJF - Y AVG	MJF - Z AVG	IM AVG
EAB (%)	24,127	25,564	11,038	20,6	26,342	10,781	17,481

Figure 39: Average Elongation at Break for 7 sets of tensile specimens divided by printing orientation and PBF process.

Figure 39 presents the comparison for Elongation at Break (EAB), it can be observed from it that the highest values were not obtained by the injection molded samples as it was expected but rather by the MJF ones built in Y orientation. The specimens manufactured by injection molding performed poorly and below the expected values of >50% depicted in their raw material datasheet [77]. The injection molded specimens started to show necking (see Figures 41h, 41i, and 42g) but broke in a brittle and sudden manner. In contrast, in average the MJF with the Y build orientation presented the highest elongation at break, although they also obtained the highest standard deviation between all the specimen groups (s=3.978) while the injection molded specimens demonstrated less variation (s=1.37). MJF parts built in Y orientation surpassed the injection molding specimens but presented similar results to the ones corresponding to their SLS counterparts also printed in Y orientation, by a difference of 2.95% between each other. The results obtained for MJF technology do not correspond with the ones presented by studies performed by other authors, where the highest elongation corresponded to the specimens printed sideways (X orientation on this thesis, acc. to Figure 25) [63, 73].

For all the test iterations, stress-strain diagrams were obtained from the TestXpert software utilized by the Zwick Z010 universal testing machine. Figure 39 shows the first specimen of each set compared to each other, the rest of the diagrams can be found in Appendix I grouped by build orientation and by manufacturing process.
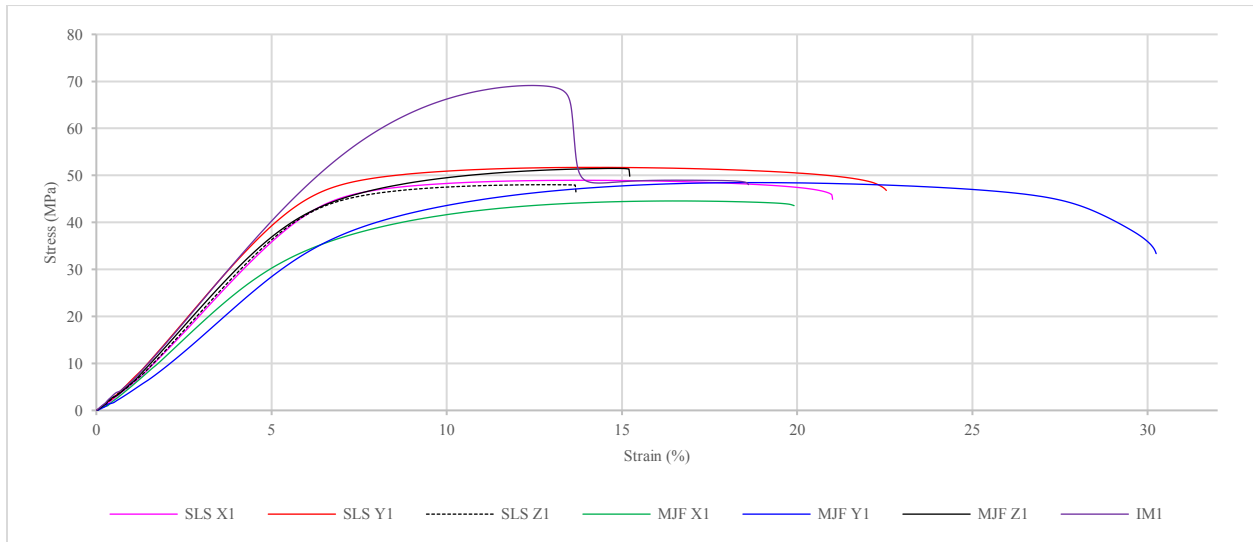
Figure 39: Stress-Strain diagram for set 1 of PA12 specimens manufactured by SLS, MJF and injection molding.

The stress-strain curves presented in Figure 39, show the mechanical behavior of the first set of specimens divided by manufacturing process and printing orientation. From the curves it can be observed the brittle fracture behavior of the specimens and their low elongation at break as mentioned earlier. The set of curves on Figure 39 was intentionally selected to show the high elongation of the MJF specimen built in Y direction identified as "MJF_Y1". All the set of injection molded specimens broke in a brittle and drastic manner with a characteristic snapping

sound when fracturing and at the center of the dumbbell shape. All the injection molded samples showed the start of necking as it can be identified in figures 39 and 42. It is known that materials with brittle fracture behavior are not the most optimal for absorbing energy from impacts [3].

By observing some of the specimens under the microscope, it was possible to see the coalescence between powder particles from the specimens produced by SLS and MJF. Figure 40a shows an injection molded specimen with a dense and uniform composition. The grain orientation resulting from the material flow after injected into the mold can be observed as vertical lines.
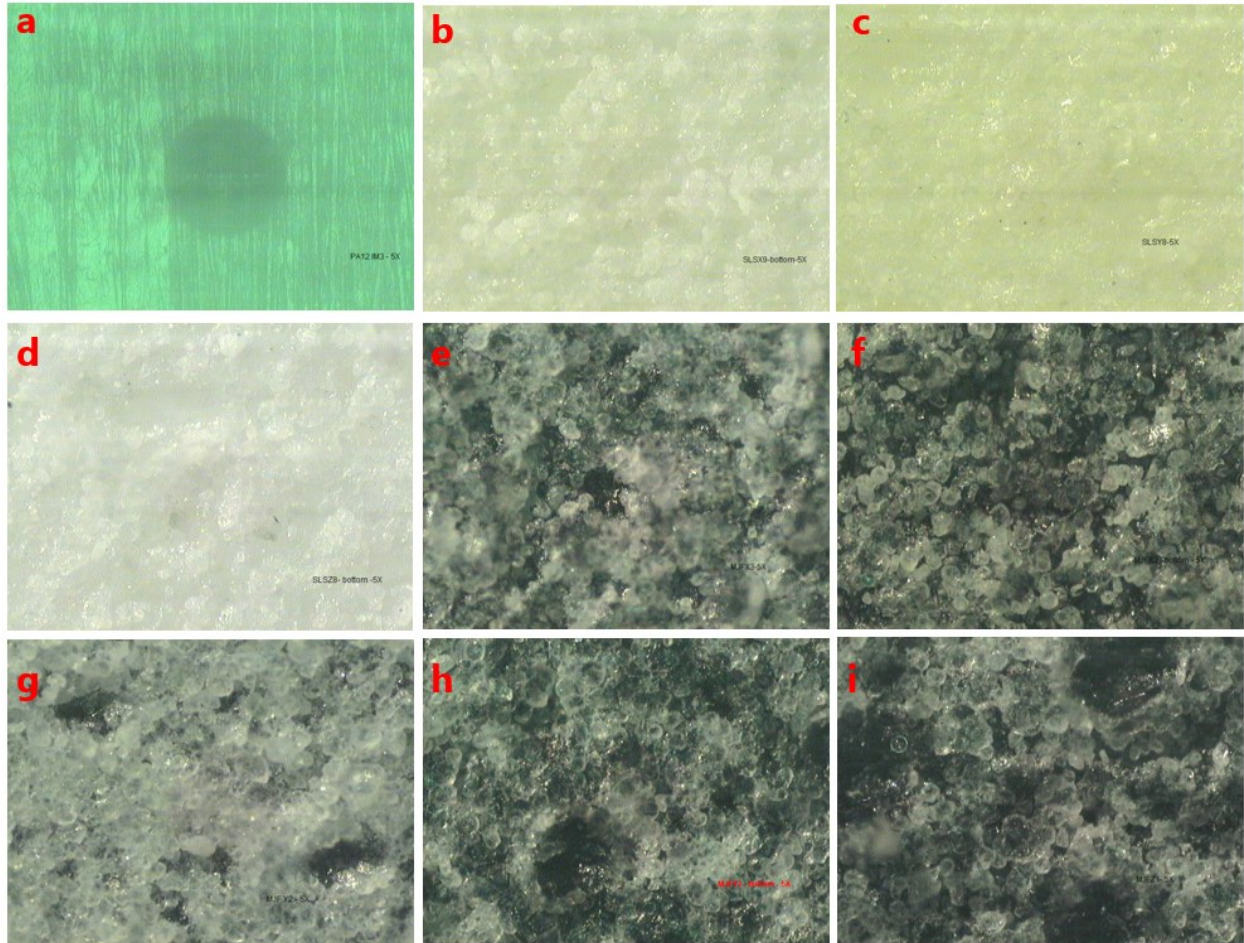
Figure 40: Specimens observed under light microscope with 5X objective. a: IM_3, b: SLS_X9, c: SLS_Y8, d: SLS_Z8, e: MJF_X3 side 1, f: MJF_X3 side 2, g: MJF_Y2 side 1, h: MJF_Y2 side 2, i: MJF_Z1.

After visual inspection with the light microscope, it was noticed that the SLS parts did showed good apparent coallesence between powder particles with the 5X objective as shown on Figure 40b, 40c and 40d. MJF specimens, in contrast, showed defined powder particles that remained without totally fusing (see Figure 40e, 40f, 40g, 40h and 40i). With the light microscope it was only possible to evaluate the external surfaces of the parts, therefore it was not possible to know how the powder was fused under the superficial layers. From the MJF specimens built in Y

direction presented in Figure 40, it can be observed the difference in surface color between the side of the part in contact with the powder bed (Figure 40g) and the one facing towards the print head (Figure 40h) which shows more evident traces of the black color from the fusion agent deposition.

Figures 41 and 42 depict the fracture areas of some of the specimens. An interesting observation was that the two MJF_Y specimens that had the highest elongation values started to show more ductile behavior before fracturing but this was not representative of the full MJF-Y specimen set as it was mentioned above. A comparison between the most ductile and an average MJF_Y specimens can be observed in Figure 41e and Figure 41f respectively.
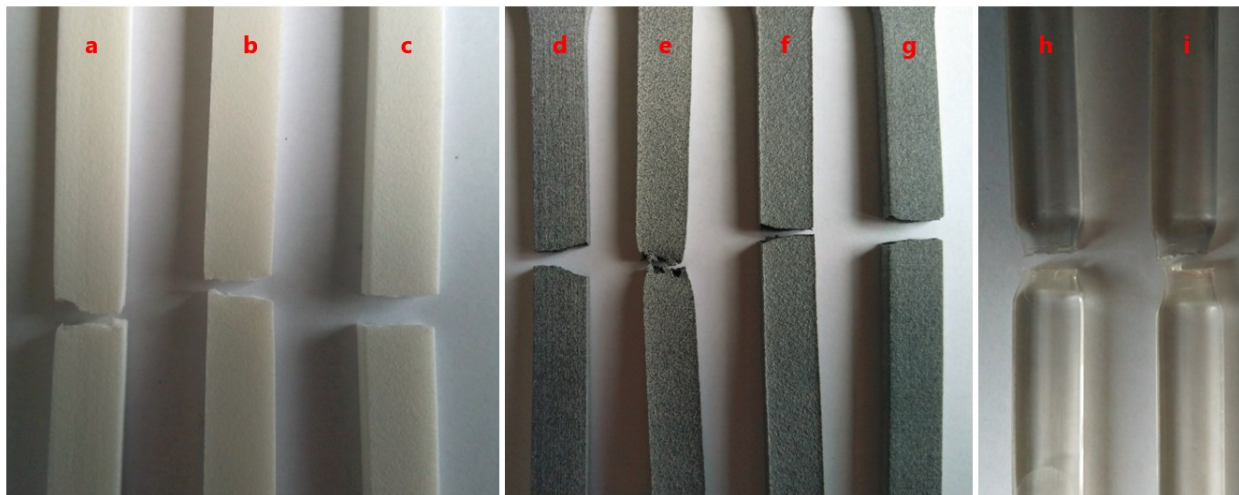
Figure 41: Fracture areas of specimens per manufacturing process and print orientation. a: SLS_X9, b: SLS_Y8, c: SLS_Z8, d: MJF_X3, e: MJF_Y2, f: MJF_Y3, g: MJF_Z1, h: IM_3 and i: IM_7.
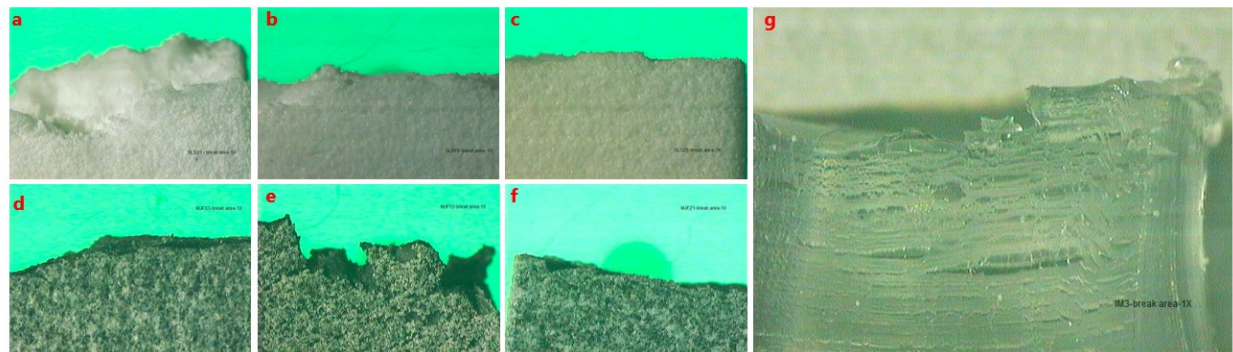
Figure 42: Fracture areas of specimens observed under the microscope with a 1X objective. a: SLS_X9, b: SLS_Y8, c: SLS_Z8, d: MJF_X3, e: MJF_Y2, f: MJF_Z1 and g: IM_3.

All the specimens manufactured by MJF presented capillarity in their uppermost surfaces that were parallel to the build platform of the machine. Figure 43 shows specimens printed in X and Y directions.

Figure 43: Capillarity present on MJF specimens printed in X (left) and Y (right) directions.

Unfortunately, the specimens were not marked and classified according to their location inside of the build chamber. As it is mentioned in **[3]**, the location of the parts inside of the powder bed is a crucial parameter that has a significant impact on the resulting mechanical properties specimens. Therefore, the variation of the results cannot be attributed to this factor but neither disregarded. For next studies that should be taken as a consideration.

8.2 Voltage withstand test results

This section presents the results obtained by performing multiple voltage withstand tests on PA12 rectangular specimens with 1 and 2mm thicknesses. A constant increase of temperature in steps of 5°C was applied during the test. The specimens manufactured by additive manufacturing were printed in three different orientations and the injection molded specimens were cut and machined from an existing component as described in section 7.2.2.

All the tests were performed first for all the sets with 1mm thickness. Each set consisted on five specimens. Figure 44 presents the summarized results measured by the tester in a bar chart as percentages of "Pass/Fail". The parts are grouped by manufacturing process and printing orientation, a "Pass" result meant the specimen withstood 4kV AC at all the temperatures from 20-100°C.
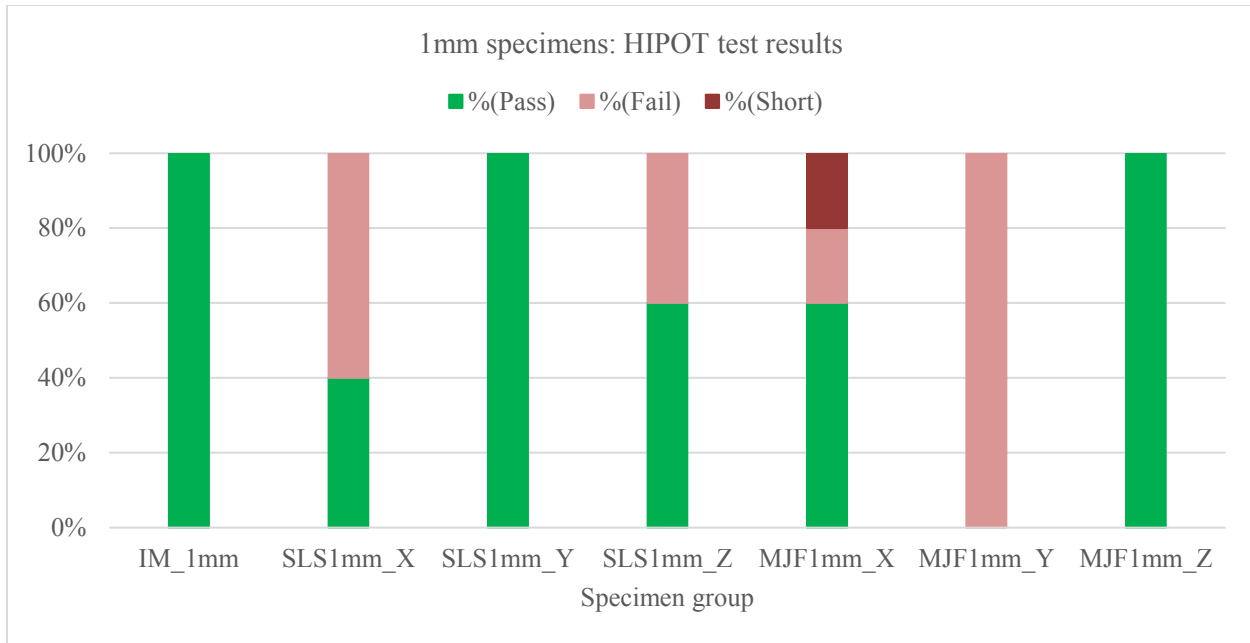
Figure 44: HIPOT test results for 1mm thick specimens presented as percentage, being 5 specimens the 100%.

As observed from Figure 44, for 100% of the 1mm specimens produced by injection molding, SLS in Y direction and MJF in Z direction the results obtained by the tester were positive. The outcome of the tester was "Pass" at a test voltage of 4kV AC and for all the temperature intervals from 20 to 100°C. On the contrary, from the 5 specimens with 1mm thickness produced by Multi Jet Fusion in Y direction, five out of five parts failed the test and allowed 5mA of current to leak through the material at temperatures between 20-30°C. SLS 1mm specimens produced in X and Z orientations had 60% and 40% of failure respectively, all of them at a test environmental temperature of 100°C. From the samples manufactured in X orientation by MJF, two specimens failed but for one of them the tester output was reported as "Short", which meant there was a direct conductive path between the electrodes through the insulation. The summarized table of the results for each sample containing the temperature at failure, voltage withstood, and leak currents measured at the end of each test cycle can be found in Appendix II.

In terms of leak current, the full set of five injection molded samples with a thickness of 1mm presented a stable behavior. They leaked low current values between 0.053 and 0.07mA from the 5mA defined limit and the leak current did not show significant changes at any environmental temperature between 20°C and 100°C. Figure 45 shows the average leak currents in function of the temperature rising. In contrast, the 1mm specimens manufactured by SLS and MJF did not show such stability and presented anisotropy depending on the printing orientation of the parts. Some important observation was that most of the MJF failed specimens presented breakdown close to or at room temperature. By this, the temperature to be discarded as a potential influential factor for the breakdown of the specimens.

Figure 45: Average values of leak current in function of temperature for all 1mm thick insulation specimens.

Only one MJF specimen printed in Y orientation (MJF1mm_Y2) was able to withstand three temperature steps without presenting immediate dielectric breakdown. The remaining four MJF specimens printed in the Y direction leaked 5mA and presented breakdown by puncture at the initial temperature of 20°C or within the five seconds voltage ramp phase at the start of the HIPOT test, before reaching the 4kV voltage level. Figure 46 (h, i, j and k) depicts some examples of punctured areas on MJF-Y specimens and their breakdown voltages are presented in Appendix II. Table 8 presents the general range of leak currents sorted by manufacturing process and build orientation. The leak current values showed to increase at the highest temperatures and if compared with injection molding, As mentioned before the SLS in Y and MJF in Z orientations were the best AM performers for 1mm thick insulators but compared with their injection molded equals, they leaked above seven times more current at 100°C although at room temperature were comparable.

Table 8: Leak current value ranges per 1mm specimen group.

Specimen group	Leak current ranges (mA)	Tested Environmental temp. ranges (°C)
IM1mm	0.053 – 0.07	20 – 100
SLS1mm_X	0.06 – 5	20 – 100
SLS1mm_Y	0.058 – 0.505	20 – 100
SLS1mm_Z	0.061 – 5	20 – 100
MJF1mm_X	0.061 – 5	20 – 100
MJF1mm_Y	0.24 - 5	20 – 30
MJF1mm_Z	0.061 – 0.51	20 – 100

Figure 46: 1mm thick electrical insulation specimens manufactured by SLS, MJF and IM observed with a 5X objective. a: SLS1mm_X1 top side, b: SLS1mm_Y1 top side, c: SLS1mm_Z1 top side, d: SLS1mm_X1 bottom side, e: SLS1mm_Y1 bottom side, f: SLS1mm_Z 1 bottom side, g: MJF1mm_X4 top side, h: MJF1mm_Y2 top side, i: MJF1mm_Y1 bottom side, j: MJF1mm_X4 bottom side, k: MJF1mm_Y2 bottom side, l: MJF1mm_Y1 bottom side, m: MJF1mm_Z2 top side, n: IM1mm_2 top side, o: IM1mm_2 bottom side.

All the specimens manufactured by additive manufacturing with 1mm thickness presented high anisotropy depending on the printing orientation. The specimens manufactured by MJF presented anisotropic dielectric behavior for the X and Z orientations, which was not totally expected, as they both were printed vertically but with different IR lamp path lengths. The 1mm thick MJF coupons produced in Y orientation that failed all the tests presented punctures and/or carbonization. In contrast with their SLS counterparts, which passed the tests at a 100%. By observing all the PBF parts under the microscope, it was evident that the powder particles in the surface of the parts were not totally fused regardless of the printing orientation. Poor coalescence between powder particles can be attributed to low power emitted by the heat source [71].

Figure 47 presents the results of the HIPOT tests performed to the 2mm thick specimens in the same manner as for the 1mm thick ones above.
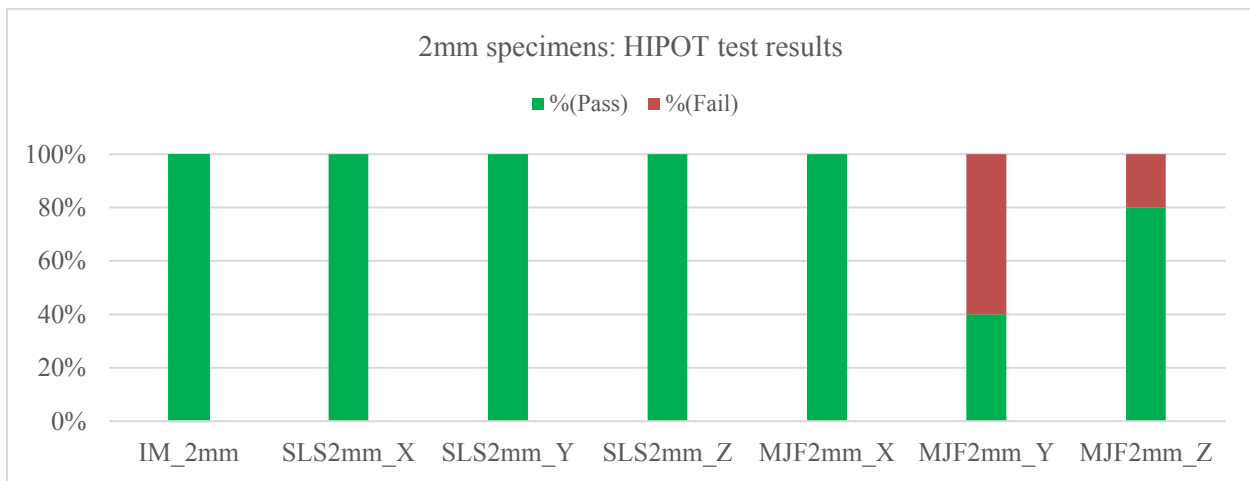
Figure 47: HIPOT test results for 2mm thick specimens presented as percentage, being 5 specimens the 100%.

As shown in Figure 47, the results obtained for 2mm specimens manufactured by injection molding and SLS are comparable. In the same manner, the MJF specimens printed in X orientation were 100% successful at 4kV AC and within the 20-100°C temperature range. On the other hand, one MJF printed in Z direction failed at 100°C without evident puncture and three of the MJF parts printed in Y orientation presented breakdown by punctures at temperatures between 75-100°C. At a thickness of 2mm, injection molded and SLS insulators are comparable. The results show isotropic behavior for SLS parts. MJF parts demonstrated improvements for the vertically printed specimens (X and Z) but Y oriented parts still presented a high failure rate. For specimens manufactured with a 2mm thickness, the overall leak currents were lower in comparison with utilizing 1mm thick samples. Equally as with their thinner counterparts, injection molded specimens were stable and did not show significant variations in leak current when the temperature increased from 20°C to 100°C, the highest leak current for an injection molded specimen was 0.061mA, approximately 81 times below the 5mA touch current safety limit established by ISO 6469-3:2011 [23].
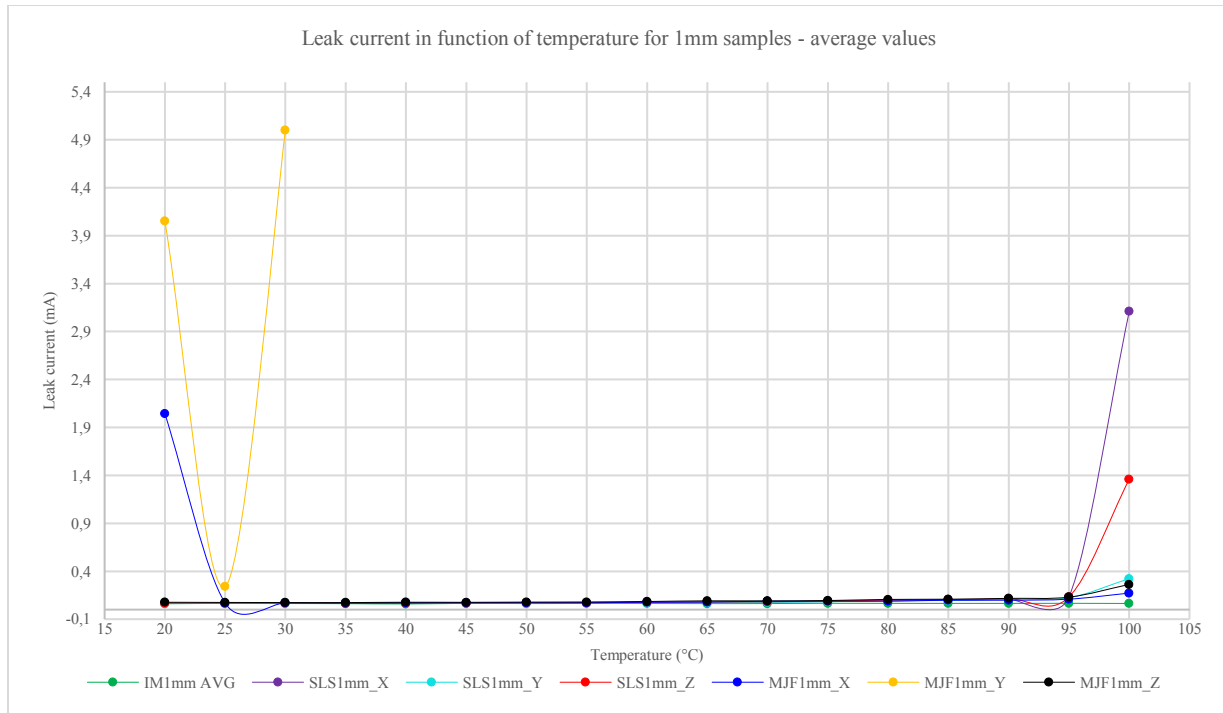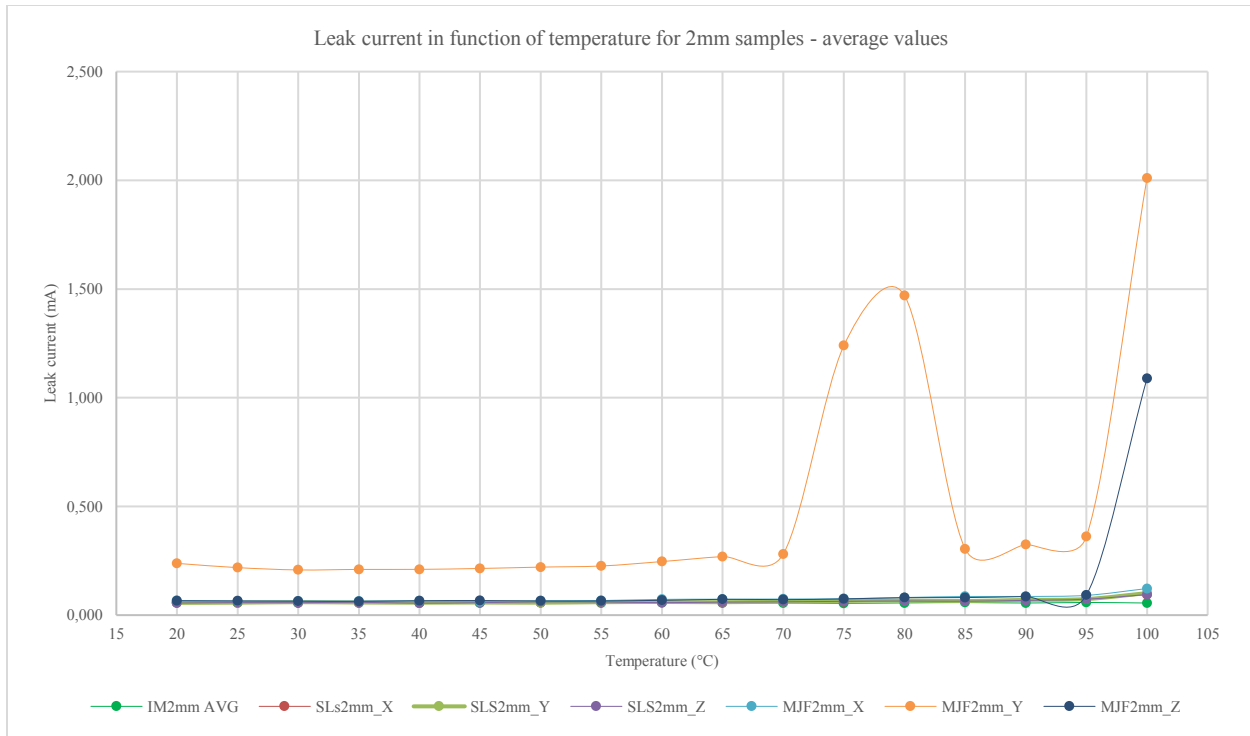
Figure 48: Average values of leak current in function of temperature for all 2mm thick insulation specimens.

On the other hand, between SLS 2mm thick specimens, there was degree of isotropic behavior when comparing the leak current values between different printing orientations but if compared with the injection molded parts in average leaked 1.8 times more current at 100°C, significantly lower than with 1mm thick specimens. The best performing group in terms of leak current for the MJF groups were the X and Z orientation, for the Z orientation the leak current at 100°C was 3.2 times higher than for the injection molded parts. For the Z orientation if the parts that failed were not considered, the leak current was within the range of 0.057-0.138mA, 2.2 times higher. These ranges are summarized in Table 9 and presented in Appendix II.

Table 9: Leak current value ranges per 2mm specimen group.

Specimen group	Leak current ranges (mA)	Tested Environmental temp. ranges (°C)
IM2mm	0.052 – 0.061	20 – 100
SLS2mm_X	0.052 – 0.106	20 – 100
SLS2mm_Y	0.052 – 0.13	20 – 100
SLS2mm_Z	0.052 – 0.1	20 – 100
MJF2mm_X	0.055 – 0.199	20 – 100
MJF2mm_Y	0.14 – 5	20 – 100
MJF2mm_Z	0.057 – 5	20 – 100

Figure 49 (a-f) shows better powder particle coalescence for SLS specimens if compared with the 1mm thick specimens presented in Figure 46. For MJF specimens it is still evident that some powder particles remained without fusing together at the surface of the parts and carbonized punctures were caused during the tests as seen in Figure 49 (h, k and m).
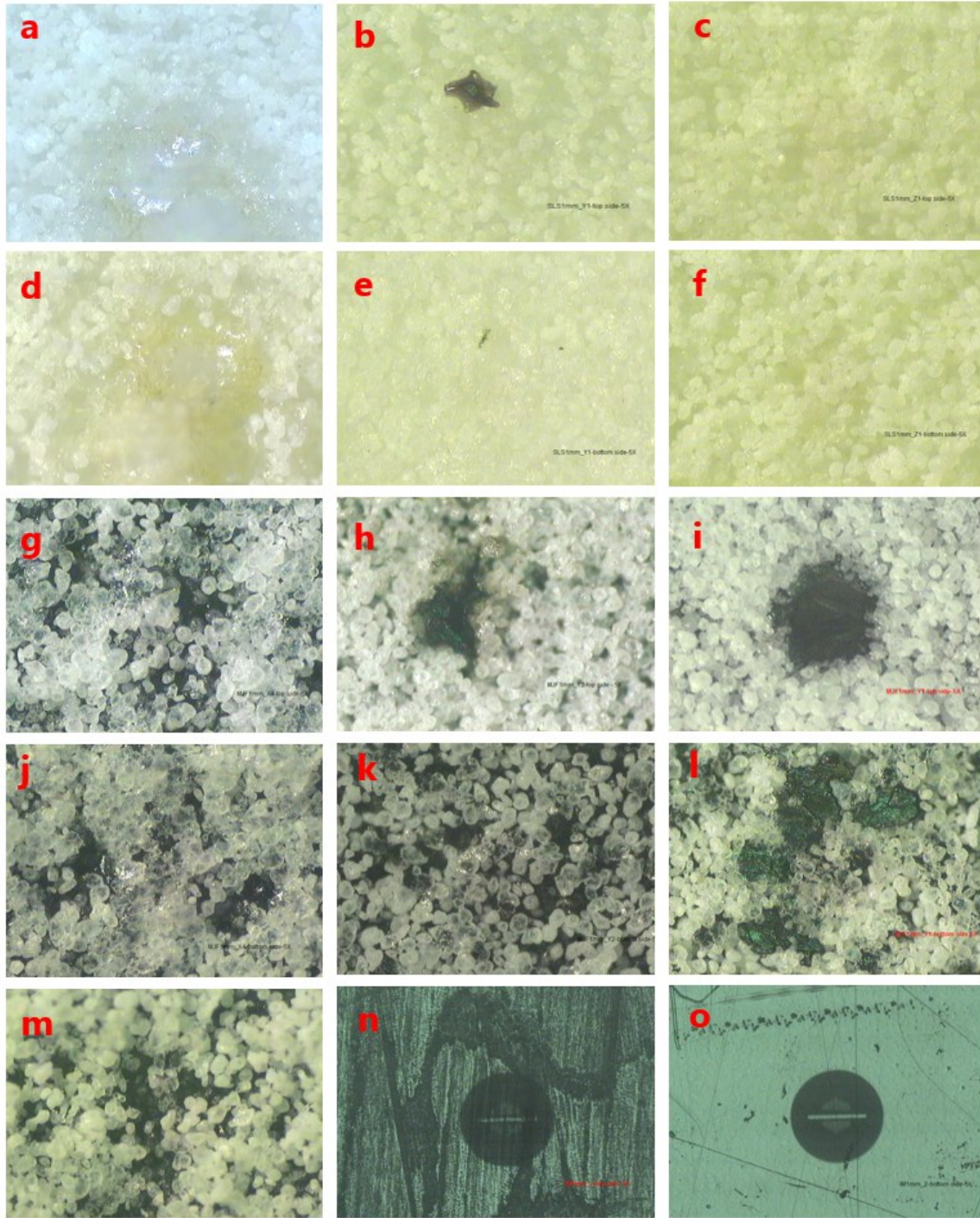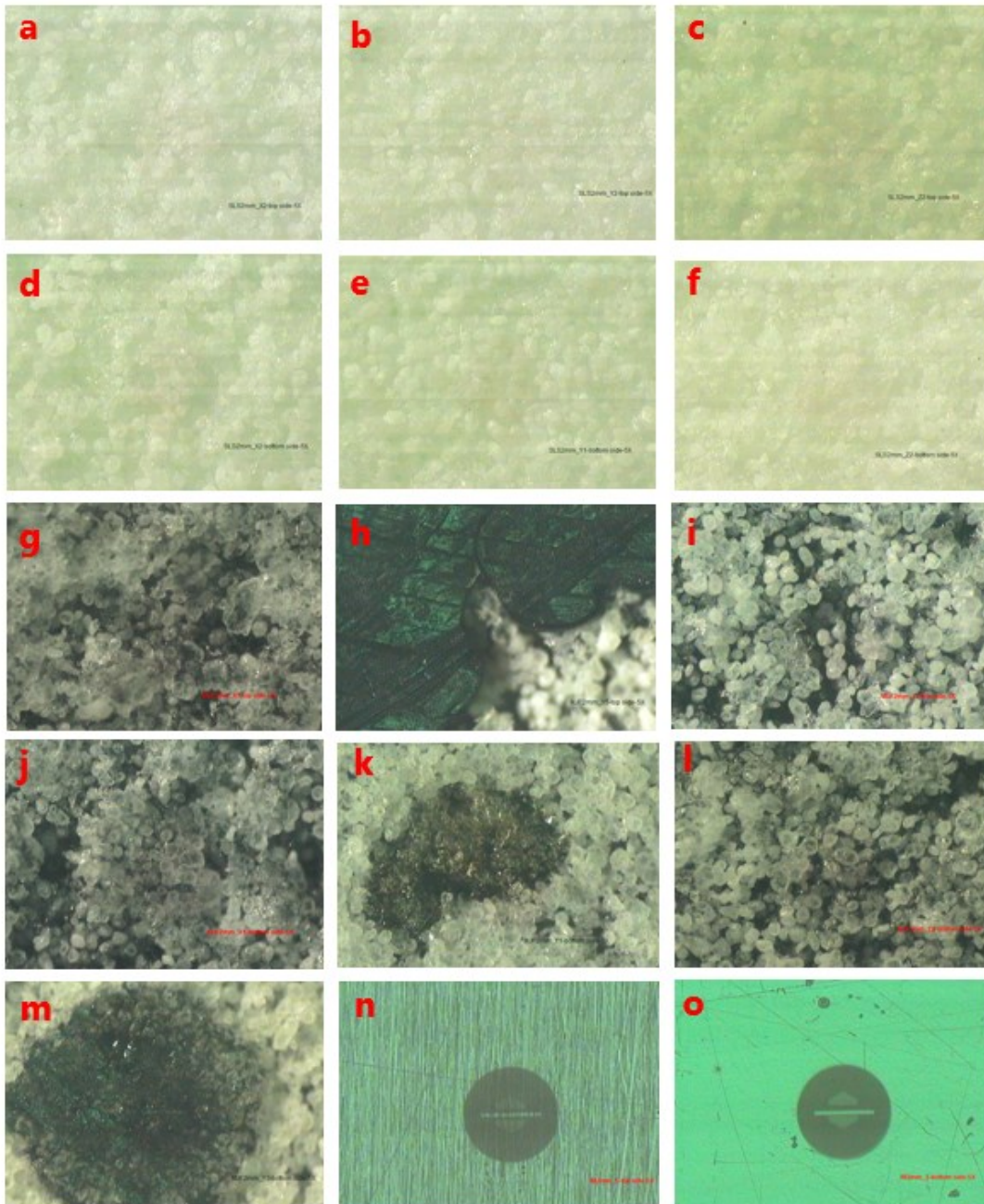

Figure 49: 2mm thick electrical insulation specimens manufactured by SLS, MJF and IM observed with a 5X objective. a: SLS2mm_X2 top side, b: SLS2mm_Y2 top side, c: SLS2mm_Z2 top side, d: SLS2mm_X2 bottom side, e: SLS2mm_Y1 bottom side, f: SLS2mm_Z2 bottom side, g: MJF2mm_X1 top side, h: MJF2mm_ Y5 top side, i: MJF2mm_Z2 top side, j: MJF2mm_X1 bottom side, k: MJF2mm_Y1 bottom side, l: MJF2mm_Z2 bottom side, m: MJF2mm_Y3 bottom side, n: IM2mm_5 top side, o: IM2mm_5 bottom side.

By measuring the densities of both 1mm and 2mm specimens it was observed that specimens belonging to the MJF and IM groups had comparable density values. For SLS the part densities were lower, confirming higher porosity achieved by the process. With the results presented before, together with the ones in Figures 50 and 51, it is possible to assume that porosity alone was not the main factor contributing to the poor insulative performance of MJF specimens, but rather a combination of voids within the parts, poor powder coalescence and the use of the fusing agent. Although it is not clear why the breakdown is predominant for the Y build orientation.
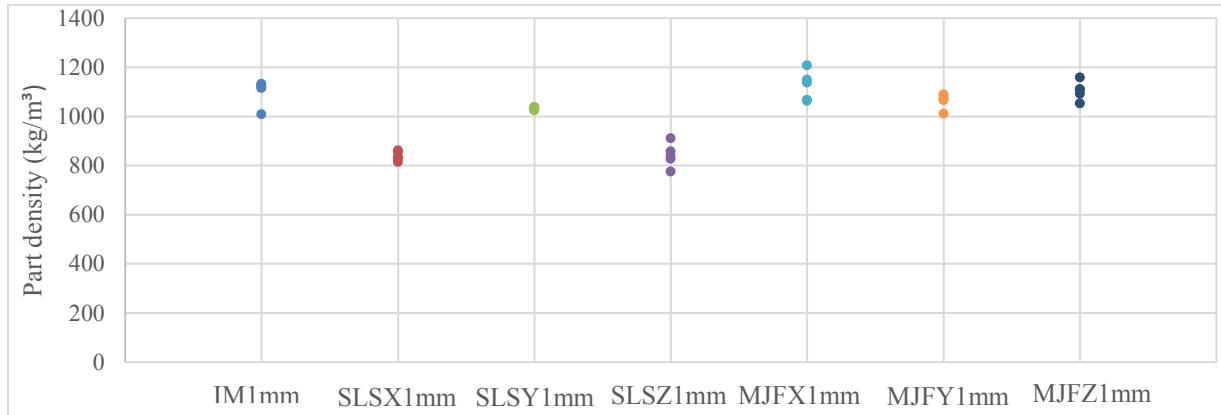
Figure 50: Calculated density of 1mm thick specimens separated by manufacturing process and build orientation.
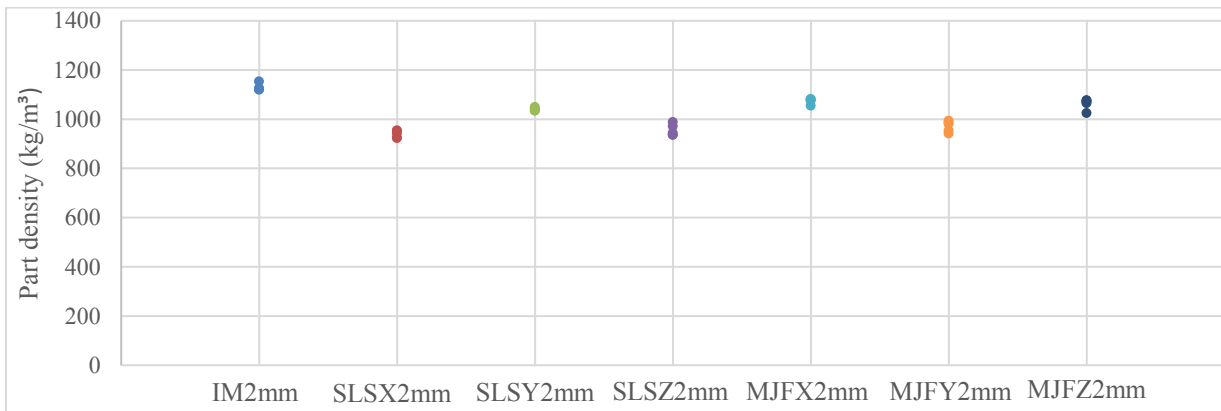
Figure 51: Calculated density of 2mm thick specimens separated by manufacturing process and build orientation.

According to the literature and patents applied by Hewlett Packard, both HSS and MJF processes utilize fusing agents or "inks" that can contain carbon black as one of the active materials for promoting powder fusion [83], [84]. It has been studied before that the presence of carbon black decreases the dielectric strength of some plastic materials as demonstrated by Ueki et. al. [85] for high density polyethylene. In their study, it was found that the areas where carbon black was agglomerated were prone to the formation of rupture channels. SLS does not utilize such radiation-absorbing material (RAM), therefore could offer a performance comparable to injection molding as an electrical insulation above a 2mm thickness at 4kV AC and within the 20-100°C temperature range.

9. Conclusions and future work

The need to identify AM processes for polymers and compare Powder Bed Fusion to Injection Molded parts for potential applications for electromechanical components was addressed on this thesis. This, was done by performing a comparative study through tensile testing and by exposing PA12 specimens to 4kV AC. The processes compared during the experiments were Selective Laser Sintering (SLS), HP-Multi Jet Fusion (MJF) and Injection Molding (IM).

To be suitable for the use in the high voltage environment of an EV, components need to fulfill demanding requirements. Those requirements cover aspects involving environmental conditions, flammability, mechanical and electrical properties among many others, this thesis was intended to be a stepping stone to characterize SLS and MJF parts mechanically but as well to understand how effective they are as electrical insulators. Specimens with thicknesses of 1 and 2mm were tested to identify initial design limitations (for example, minimum wall thickness). More extensive studies would need to be performed to determine the full applicability of PBF parts as electromechanical automotive components and their long-term behavior.

Through the experimental results, this thesis can conclude that Powder Bed Fusion, when characterized by tensile testing, demonstrated lower but comparable mechanical properties as the ones produced by injection molding. Specimens manufactured by SLS from EOS PA2200 demonstrated high stiffness and strength at a low density. One downside was the anisotropic behavior affected by the printing orientation, especially in the vertical direction and due to the inter-layer bonding. This was expected as it is a common characteristic of Additive Manufacturing processes. The best specimens in terms of tensile strength were the ones obtained by SLS printed in Y orientation, which achieved values below 74% from the results obtained by injection molded parts. HP-MJF parts offers the fast production of dense components with relatively similar properties as SLS but showed higher isotropy for tensile strength. Both processes demonstrated to produce PA12 parts that fracture in a brittle and drastic manner with low Elongation at Break (10-25.5%). This could compromise their capability of absorbing energy from impacts or vibration. On the other hand, the injection molded specimens tested, showed brittle behavior as well.

As electrical insulators, according to the HIPOT test results presented in this thesis, SLS PA12 (EOS PA2200) has demonstrated to be potentially suitable for applications up to a maximum voltage of 4kV AC. The SLS process demonstrated comparable short-term capabilities as the ones observed with injection molded samples. The results proved that it could be safe to utilize SLS parts with a minimum wall thickness of 2mm. Although with SLS there exist the possibility of presenting voids that could promote the formation of conductive paths by partial discharges in the long term. The brittle behavior of the parts observed during the tensile tests could also become a contributor of that issue. For serial production applications, long-term testing is recommended and for a larger sample size. Five specimens do not represent a significant population to determine whether SLS parts will always behave in the same way or not. HP-MJF has potential as a

technology due to its processing speed. The technology is relatively new, and more materials and fusing agents will be developed in the future. Although, through the tests performed within the conditions for this thesis, electrical insulation parts manufactured by HP-MJF presented high occurrence of insulation breakdown. Therefore, the risk of electric shock under high voltage stress is high. This could be attributed to the possible presence of carbon black in the fusing agent utilized in the process and voids within the parts. The HP-MJF HP3DHR PA12 material demonstrated to be highly affected by the build orientation on both 1 and 2mm thicknesses. The Y orientation for MJF presented breakdown on 100% for 1mm thick insulators and 60% for 2mm specimens. Apparently, thicker MJF specimens showed improvement in terms of leak current and therefore tests with thicker samples should be performed to determine a minimum wall thickness that could show a stable and safe behavior for the same material.

PBF technologies have great potential for the future of additively manufactured end-products because of processing speed and design freedom. When comparing Powder Bed Fusion with injection molding, it needs to be taken into consideration that both technologies are completely different from each other and the variation between properties are just a reflection of that fact. With this thesis it was not intended to search to replace one process by the other one but to benchmark the technologies.

This thesis cannot determine the full applicability of Powder Bed Fusion processes for their use in Electric Vehicles without being complemented with further research and testing. On the other hand, it gives a good introduction to the topic within Valmet Automotive and fulfills the research questions.

Directly related to the cases studied in this thesis, it is of great importance to make deeper studies on the topic of electrical properties of additively manufactured parts. This thesis only covered voltage withstand test on material thicknesses of 1-2mm without testing insulation resistance. More in-depth tests with a bigger sample size and a wider range of material thicknesses should be performed and at a wider range of voltages to study and determine the safety limits of HP-MJF in multiple printing orientations. As well, this thesis did not include DC voltage tests and many important components of the EV powertrain operate at DC high voltages. For mechanical characterization, impact resistance, bending, compression and flexural properties of the parts would give a wider understanding of the AM parts when compared to injection molding. As well, a wider range of material blends should be studied.

As it was mentioned before, many requirements were not within the scope of this thesis. In order to apply PBF technologies as serial production methods, more studies for the long-term behavior of the parts should be addressed. Some examples for future consideration are: the aging of PBF samples by standard environmental cycle testing and its impact on the mechanical and dielectric properties, the study their reaction to vibration, the moisture absorption of the materials, chemical compatibility with automotive fluids and quality related characteristics such as dimensional accuracy, repeatability of the processes and surface quality to mention some examples.

10. References

1. Gibson I., Rosen D., Stucker B., *Additive Manufacturing Technologies: 3D Printing, Rapid Prototyping and Direct Digital Manufacturing*. 2nd ed. New York, Springer Science+Business Media; 2015.
2. van Barneveld J and Jansson T., *Rapid prototyping: a layered revolution,* part of the series: Impact of game-changing technologies in Europe, Future of Manufacturing in Europe. Working paper, Eurofound, 2017. Reference number: WPFOMEEF18002. Retrieved on 12.03.2019 from: https://www.eurofound.europa.eu/publications/report/2018/game-changing-technologies-in-european-manufacturing
3. Schmid M., *Laser Sintering with Plastics - Technology, Processes and Materials*, Hanser Publishers, 2018. pp. 8, 9, 13-37, 39-64, 65-73, 162-186.
4. European Commission, *Whitepaper on Transport: Roadmap to a Single European Transport Area – Towards a competitive and resource efficient transport system*, Brussels, 2011. Available at: https://ec.europa.eu/transport/themes/strategies/2011_white_paper_en
5. JP Morgan [Internet]. *Driving into 2025: The Future of Electric Vehicles*. October 10, 2018. Retrieved on 05.04.2019 from: https://www.jpmorgan.com/global/research/electric-vehicles
6. European Environmental Agency [Internet]. *Electric vehicles as a proportion of the total fleet.* Retrieved on 05.04.2019 from: https://www.eea.europa.eu/data-and-maps/indicators/proportion-of-vehicle-fleet-meeting-4/assessment-2
7. Greentechmedia.com [Internet]. Hunt T., *The Future of the Electric Car*. Available at: https://www.greentechmedia.com/articles/read/the-future-of-the-electric-car
8. Gershenfeld N., *How to Make Almost Anything*, Foreign Affairs Magazine, Volume 91, Number 6, November/December 2012.
9. European Committee for Standardization. EN13447:2001 *Electrically propelled road vehicles – Terminology*. European Standard. Brussels, 2001. pp. 4,5.
10. Daimler AG. MBN LV123 - *Electrical Characteristics and Electrical Safety of High-Voltage Components in Road Vehicles – Requirements and Tests*. Company Standard. 2014-03
11. Warner J., *Handbook of Lithium-Ion Battery Pack Design - Chemistry, Components, Types and Terminology - 11.3 Use of plastics and composites in battery design*, Elsevier, 2015. pp. 135.
12. Marklines.com [Internet]. Retrieved on 09.08.2019 from: https://www.marklines.com/en/report/rep1104_201209
13. Mann-Hummel.com [Internet]. Retrieved on 06.08.2019 from: https://blog.mann-hummel.com/en/e-mobility-offers-opportunities/
14. Drobny JG, *Polymers for Electricity and Electronics: Materials, Properties, and Applications*, Hoboken: John Wiley & Sons, Incorporated, 2011. pp. 27-102, 138-159.
15. Kutz M., *Applied Plastics Engineering Handbook - Processing and Materials - 1.1.1 Long-Chain Molecules*. Elsevier, 2011. pp. 3.

16. Osswald, T. A., Menges G., *Material Science of Polymers for Engineers,* 3rd edition, Hanser Publishers, Cincinnati, 2012. pp. 3-20, 200-215, 263-270.

17. Zheng R., Tanner R.I., Fan XJ. *Injection Molding: Integration of Theory and Modeling Methods*. Springer, Berlin, Heidelberg, 2011.

18. Shuai Ma, Modi Jiang, Peng Tao, Chengyi Song, Jianbo Wu, Jun Wang, Tao Deng, Wen Shang, *Temperature effect and thermal impact in lithium-ion batteries: A review*, Progress in Natural Science: Materials International Vol. 28, December 2018, pp. 653-666.

19. Discussion with Valmet Automotive Battery Technology Specialist Markku Räjämäki.

20. Dallner C. and Zeiher V., *Electric Cars: Lightweight Construction and More*. Kunstoffe International, 03.2011, pp.66-71. Retrieved on 28.01.2019 from: https://www.kunststoffe.de/en/_storage/asset/626287/storage/master/file/6241619/download/Electric%20Cars:%20Lightweight%20Construction%20and%20%20%20%20%20%20%20%20%20%20%20%20%20%20%20%20%20More.pdf

21. Sabic Presentation: *NORYL™ Resin for BEV & HEV Battery Pack Components*, Held on 16.05.2019 at Valmet-Automotive premises by Sabic Sr Technical Development Engineer Timo Latvakangas.

22. Underwriters Laboratories. UL94 - *Test for Flammability of Plastic Materials for Parts in Devices and Appliances*. Revision May 22, 2001.

23. International Organization for Standardization. ISO 6469-3, *Electrically Propelled Vehicles – Safety Specifications – Part 3: Protection of persons against electric shock*, Second edition 2011-12-01.

24. International Electrotechnical Commission. IEC 60664-1:2007, *Insulation coordination for equipment within low-voltage systems. Part 1: Principles, requirements and tests*. 2007, Geneva, Switzerland. pp. 12, 28-30.

25. Muha V., *E-Mobility T&AP Products and Applications*, presentation on Transportation and Advanced Polymers, ©2018 DowDupont, September 2018, presented at Valmet Automotive by Ilkka Lauttia from Distrupol Nordic AB on 07.02.2019.

26. 3M, Tech brief, *CTI: Comparative Tracking Index Test*. 3M Electrical Markets Division, Austin Texas, USA. Available at: https://multimedia.3m.com/mws/media/1289893O/tech-brief-comparative-tracking-index-test.pdf

27. Thompson M.J., Whalley D. C. and Hopkinson N., *Investigating Dielectric Properties of Sintered Polymers for Rapid Manufacturing*, Department of Mechanical and Manufacturing Engineering, Loughborough University, UK, 2008.

28. Gooch J.W. *Encyclopedic Dictionary of Polymers*, 2nd edition, Springer, New York, 2011. pp. 78, 180.

29. Solvay Amodel®HFFR-4133 Technical Data Sheet. Retrieved on 25.07.2019 from: https://www.solvay.com/en/product/amodel-hffr-4133

30. Dupont Zytel® FR95G25V0NHBK458 Technical Data Sheet. Retrieved on 26.07.2019 from: https://dupont.materialdatacenter.com/en/products/datasheet/SI/Zytel%C2%AE%20FR95G25V0NH%20BK458

31. Dupont Crastin®LW9030FRBK851 Technical Data Sheet. Retrieved on 26.07.2019 from: https://dupont.materialdatacenter.com/en/products/datasheet/SI/Crastin%C2%AE%20LW9030FR%20BK851

32. Sabic NORYL™ RESIN GFN1 Technical Data Sheet. Retrieved on 11.01.2020 from:

https://www.sabic.com/en/products/specialties/noryl-resins/noryl-resin?grade=gfn1

33. Kauffer PH., *Injection Molding: Process, Design, and Applications*. Hauppauge: Nova Science Publishers, Incorporated; 2010. pp. 2.

34. Bryce D. M., *Plastic Injection Molding, Volume I - Manufacturing Process Fundamentals*. Dearborn Michigan, Society of Manufacturing Engineers (SME); 1996, pp. 1-8, 30-65.

35. Kazmer D.O., *Injection Mold Design Engineering*, 2nd edition, Hanser Publications, Cincinnati, 2016. pp. 2.

36. Patil A., Patel A., Purohit R. *An overview of Polymeric Materials for Automotive Applications*, Materials Today Proceedings, Volume 4, Issue 2 Part A, Elsevier, 2017, Pages 3807-3815.

37. International Organization for Standardization. ISO/ASTM 52900:2015 – *Additive Manufacturing – General Principles – Terminology*. 1st edition. Geneva, 2015.

38. Turner BN, Strong R, Gold SA (2014) *A review of melt extrusion additive manufacturing processes*. Rapid Prototyping Journal 2013:192–204, pp- 2.

39. 3dsourced.com [Internet]. *The Complete History of 3D Printing: From 1980 to 2020 - Part 3: 2009 – 2014: FDM & SLA patents expire, worldwide democratization of 3D printing.* Retrieved on 24.07.2019 from: https://3dsourced.com/guides/history-of-3d-printing/

40. 3dhubs.com [Internet]. *Introduction to FDM 3d Printing*. Retrieved on 01.08.2019 from: https://www.3dhubs.com/knowledge-base/introduction-fdm-3d-printing

41. Bagsik A., Schöppner V., *Mechanical Properties of Fused Deposition Modeling Parts Manufactured with Ultem™9085*. Paper 1294 of the 69th annual technical conference of the Society of Plastics Engineers 2011, (ANTEC 2011): Boston, Massachusetts, USA, 1 - 5 May 2011 / [SPE, Society of Petroleum Engineers]; Vol. 1.

42. Knoop F., Schöppner V., *Mechanical and Thermal Properties of FDM Parts Manufactured with Polyamide 12*, Annual International Solid Freeform Fabrication Symposium 2015. pp 935-948.

43. Lederle F., Meyer F., Brunotte G-P., Kaldun C. and Hübner E. *Improved mechanical properties of 3D-printed parts by fused deposition modeling processed under the exclusion of oxygen*, Progress in Additive Manufacturing June 2016 Vol. 1, Issue 1-2, pp 3-7. Springer. https://doi.org/10.1007/s40964-016-0010-y

44. Hoff B., Maestas S., Hayden S., Harrigan D., Grudt R., Ostraat M., et. al., *Dielectric strength heterogeneity associated with printing orientation in additively manufactured polymer materials*, Additive Manufacturing 22, Elsevier 2018, 21-30. https://doi.org/10.1016/j.addma.2018.04.010

45. Monzel W.J., Hoff B.W., Maestas S.S., French D.M., Hayden S.C., *Dielectric breakdown of additively manufactured polymeric materials*, IEEE Trans. Dielectr. Electr. Insul. 22 (2015) 3543–3549, http://dx.doi.org/10.1109/TDEI.2015.005199 .

46. Gonzalez-Henriquez C., Sarabia-Vallejo M., Rodriguez-Hernandez J., *Polymers for Additive Manufacturing and 4D-printing: Materials, methodologies and biomedical applications*. Progress in Polymer Science Volume 94, Elsevier, July 2019, pp-57-116.

47. dsm.com [Internet]. Duis P., *Controlling temperature is key for additive manufacturing*, 10.11.2017. Retrieved on 31.08.2019 from: https://www.dsm.com/markets/engineering-plastics/en/blog/controlling-temperature-additive-manufactoring.html

48. stratasys.com [Internet]. *Stratasys materials*. Retrieved on 05.08.2019 from: https://www.stratasys.com/materials/search.

49. markforged.com [Internet]. Materials for Markforged 3D printers. Retrieved on 30.08.2019 from: https://markforged.com/materials/

50. Ultrafusefff.com [Internet]. BASF Engineering Filaments- technical data. Retrieved on 18.01.2020 from: https://www.ultrafusefff.com/material-data/engineering-technical-data/

51. Sabic.com [Internet]. Sabic ULTEM™ FDM filaments. Retrieved on 18.01.2020 from: https://www.sabic.com/en/products/specialties/filaments/ultem-filament

52. Love L., Duty C., Post B., Lind R., Lloyd P., Kunc V., Peter W, and Blue C., *Breaking Barriers in Polymer Additive Manufacturing*. United States, 2015. Available at: https://www.osti.gov/servlets/purl/1185467

53. 3dsystems.com [Internet]. Our Story. Retrieved on 02.08.2019 from: https://www.3dsystems.com/our-story

54. 3dhubs.com [Internet]. Introduction to SLA 3D Printing. Retrieved on 01.08.2019 from: https://www.3dhubs.com/knowledge-base/introduction-sla-3d-printing#what

55. Salonitis K., *Stereolithography, Advances in Additive Manufacturing and Tooling*, Comprehensive Materials Processing, Reference Work 2014, Elsevier, Volume 10.03. pp.19-67. ISBN 978-0-08-096533-8.

56. Wohlers T., Caffrey T., Campbell I. R., *Wohlers Report 2016: 3D printing and additive manufacturing state of the industry: annual worldwide progress report*. Wohlers Associates, Colorado, 2016. pp 41.

57. Schmid M., Amado A., Wegener K., *Polymer Powders for Selective Laser Sintering (SLS)*, Conference Paper, ETH Zürich 2014. https://doi.org/10.3929/ethz-a-010336188

58. 3dsystems.com [Internet]. *3D Systems Plastic Materials*. Retrieved on 05.08.2019 from: https://www.3dsystems.com/materials/plastic

59. 3D Systems. Selective Laser Sintering (SLS) Material Selection Guide. Retrieved on 24.04.2019. Available at: https://www.3dsystems.com/materials/plastic

60. EOS.com [Internet]. EOS Material Data Center. Accessed on 31.07.2019 and available at: https://eos.materialdatacenter.com/eo/

61. Wegener A., *New polymer materials for the laser sintering process: polypropylene and others*, Elsevier, Physics Procedia 83 2016, pp. 1003-1012.

62. Hewlett Packard Company – hp.com [Internet]. *HP Technical white paper – HP Multi Jet Fusion Technology*. Retrieved on 01.08.2019 from: https://www8.hp.com/us/en/printers/3d-printers/products/multi-jet-technology.html

63. O'Connor H., Dickson A. and Dowling D., *Evaluation of the mechanical performance of polymer parts fabricated using a production scale multi jet fusion printing process,* Additive Manufacturing 22, Elsevier, 2018, 381-387. https://doi.org/10.1016/j.addma.2018.05.035

64. Hewlett Packard Company – enable.hp.com [Internet]. *HP MJF Handbook,* published on April 2019, Retrieved on 31.07.2019 from: https://enable.hp.com/us-en-3dprint-mjfhandbook.

65. Hewlett Packard Company – hp.com [Internet]. *HP – Technical Guideline for Material Development with HP 3D Open Materials Platform*, Published on 01.2018. Retrieved on 01.08.2019 from: https://www8.hp.com/us/en/printers/3d-printers/materials.html

66. Hewlett Packard Company – hp.com [Internet]. *HP Technical note: The HP Multi Jet Fusion Voxel,* Published on 03.2017, retrieved on 01.08.2019 from: http://h20195.www2.hp.com/v2/GetPDF.aspx/4aa6-8157eew.pdf

67. automotivemanufacturingsolutions.com [Internet]. Farish M., *BMW takes additive manufacturing from prototype to serial lines*, Automotive Manufacturing Solutions, December 2019 retrieved on 01.02.2020 available at: https://www.automotivemanufacturingsolutions.com/additive/3d-printing/bmw-takes-additive-manufacturing-from-prototype-to-serial-lines/39753.article

68. Hewlett Packard Company – hp.com [Internet]. Extracted from: https://www8.hp.com/h20195/v2/GetPDF.aspx/4AA7-1532ENE.pdf. pp. 2.

69. engineering.com [Internet]. Molitch-Hou M., *The Coming Proliferation of High Speed Sintering?*, Engineering.com article from interview with Neil Hopkinson, posted on 11.04.2017, accessed on 09.01.2020, available at: https://www.engineering.com/3DPrinting/3DPrintingArticles/ArticleID/14710/The-Coming-Proliferation-of-High-Speed-Sintering.aspx

70. voxeljet.com [Internet]. Voxeljet Whitepaper: *High Speed Sintering as a 3D printing process: flexible, customer-oriented and versatile,* accessed on 09.02.2020. Available at: *https://www.voxeljet.com/3d-printing-systems/vx200-hss/*

71. Van Hooreweder B., Moens D., Boonen R., Kruth J-P., Sas P., *On the difference in material structure and fatigue properties of nylon specimens produced by injection moulding and selective laser sintering,* Polymer Testing 32, Elsevier, 2013, 972-981. https://doi.org/10.1016/j.polymertesting.2013.04.014

72. Flodberg G., Pettersson H., Yang L., *Pore analysis and mechanical performance of selective laser sintered objects*, Additive Manufacturing 24, Elsevier, 2018, 307-315. https://doi.org/10.1016/j.addma.2018.10.001.

73. Sillani F., Kleijnen R., Vetterli M., Schmid M. and Wegener K., *Selective laser sintering and multi jet fusion: Process-induced modification of the raw materials and analyses of parts performance,* Additive Manufacturing 27, Elsevier, 2019, 32-41. https://doi.org/10.1016/j.addma.2019.02.004

74. Morales-Planas S., Minguella-Canela J., Lluma-Fuentes J., Travieso-Rodriguez J. and Garcia-Granada A-A., *Multi Jet Fusion PA12 Manufacturing Parameters for Watertightness, Strength and Tolerances,* Materials 2018, 11, 1472. https://doi.org/10.3390/ma11081472

75. Material datasheet. *EOS Fine Polyamide PA 2200 for EOSINT P*. Provided by Ajatect Prototyping OY on 20.08.2019.

76. Material datasheet. *HP 3D High Reusability PA12*. Provided by Ajatec Prototyping OY on 20.08.2019.

77. Technical datasheet. *EMS Grilamid TR 55 PA12*. Provided by MSK Plast OY on 29.08.2019.

78. International Organization for Standardization. ISO 527-2: 2012 (E), *Plastics – Determination of tensile properties – Part 2: Test conditions for moulding and extrusion plastics*. International Standard, 2nd edition. Geneva, 2012-02-15.

79. International Organization for Standardization. ISO 527-1: 2012 (E), *Plastics – Determination of tensile properties – Part 1: General Principles*. International Standard, 2nd edition. Geneva, 2012-02-15.

80. *International Organization for Standardization. ISO 16750-2:2010(E): Road vehicles – Environmental conditions and testing for electrical and electronic equipment – Part 2: Electrical loads*. 3rd edition, 2010-03-15. Section 4.11.

81. American Society for Testing and Materials. ASTM D149-97a (Reapproved 2004), *Standard test method for Dielectric Breakdown Voltage and Dielectric Strength of Solid Electrical Insulation Materials at Commercial Power Frequencies*. American National Standard, 2004. pp. 3, 4.

82. Gigavac.com [Internet]. Gray J., *Improving Safety and Performance with DC dielectric testing*. Retrieved on 23.11.2019 from: https://www.gigavac.com/application-notes/high-voltage-relays/dielectric-testing

83. Olubummo A, Hartman A. and Zhao L., *Fusing agent(s)*, Patent no. WO 2018/ 194542 A1, Pu. date: 25/10/2018. Hewlett-Packard Development Company, L.P. pp. 2.

84. Emamjomeh A., Prasad K. A., Novick M. A., Montei Fung E*., Detailing agents for three-dimensional (3D) printing*. Patent no.: US 2018/0022923 A1, Pub. date: 25/01/2018. Hewlett-Packard Development Company, L.P., pp. 3.

85. Ueki M.M. and Zanin M., Influence of Additives on the Dielectric Strength of High-density Polyethylene, IEEE Transactions on Dielectrics and Electrical Insulation, Vol. 6 No. 6, December 1999.

86. Material datasheet. DSM Somos ProtoTherm 12120. Available at : https://www.dsm.com/content/dam/dsm/additive-manufacturing/en_US/documents/Sell%20Sheets/Somos%20ProtoTherm%2012120%20SS-PDS%20-%20A4.pdf

Appendix I – Stress – Strain diagrams from tensile tests

Figure I-a: Stress-Stress diagrams for SLS tensile specimens printed in X direction.
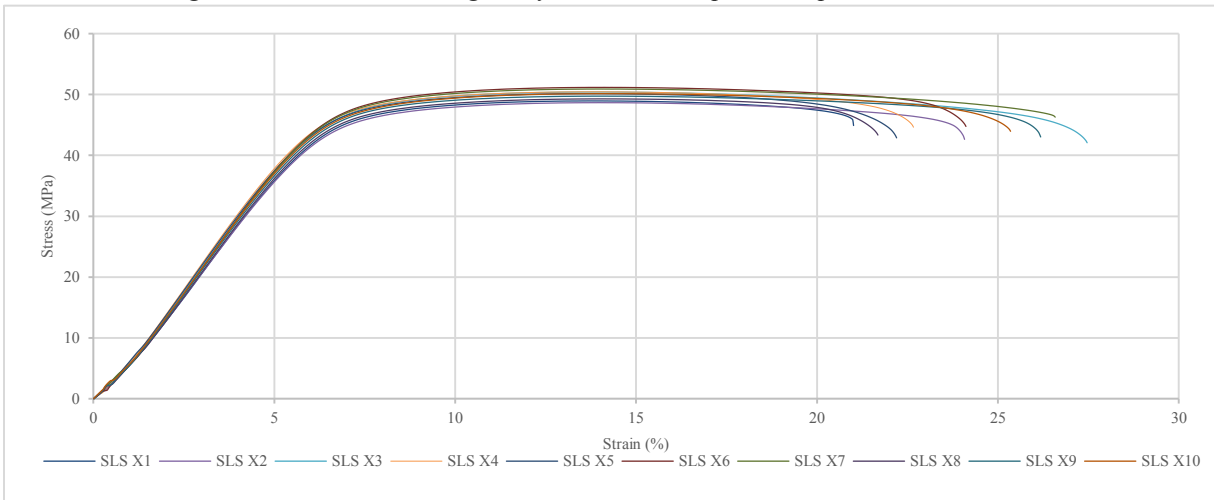

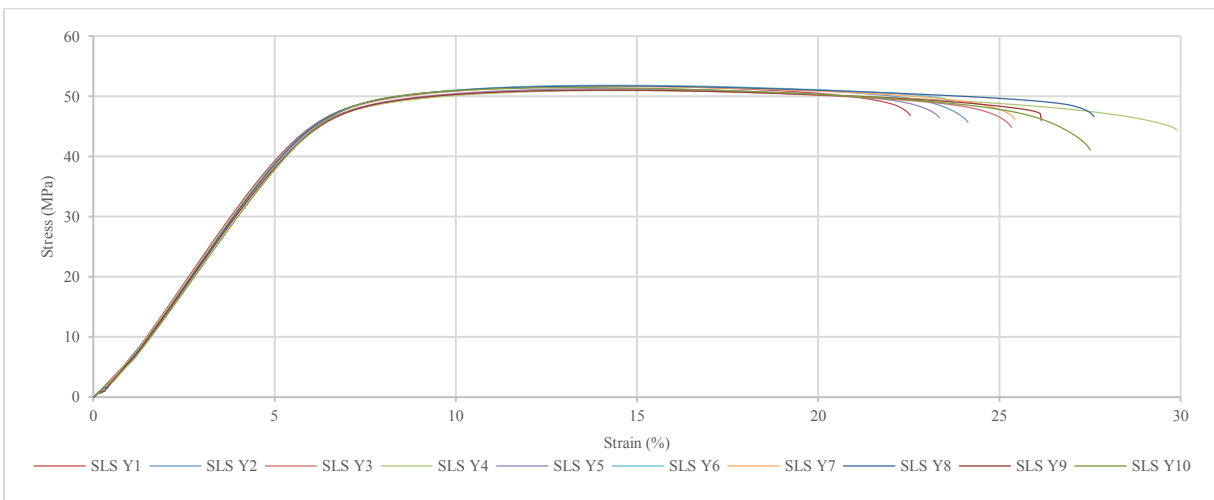*Figure I-b: Stress-Stress diagrams for SLS tensile specimens printed in Y direction.*

Figure I-c: Stress-Stress diagrams for SLS tensile specimens printed in Z direction.
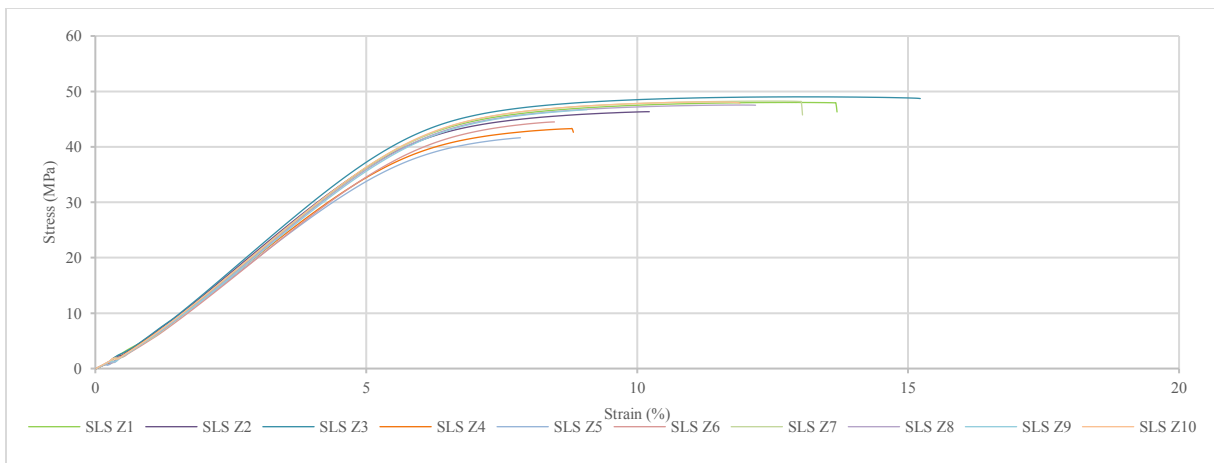
Figure I-d: Stress-Stress diagrams for MJF tensile specimens printed in X direction.
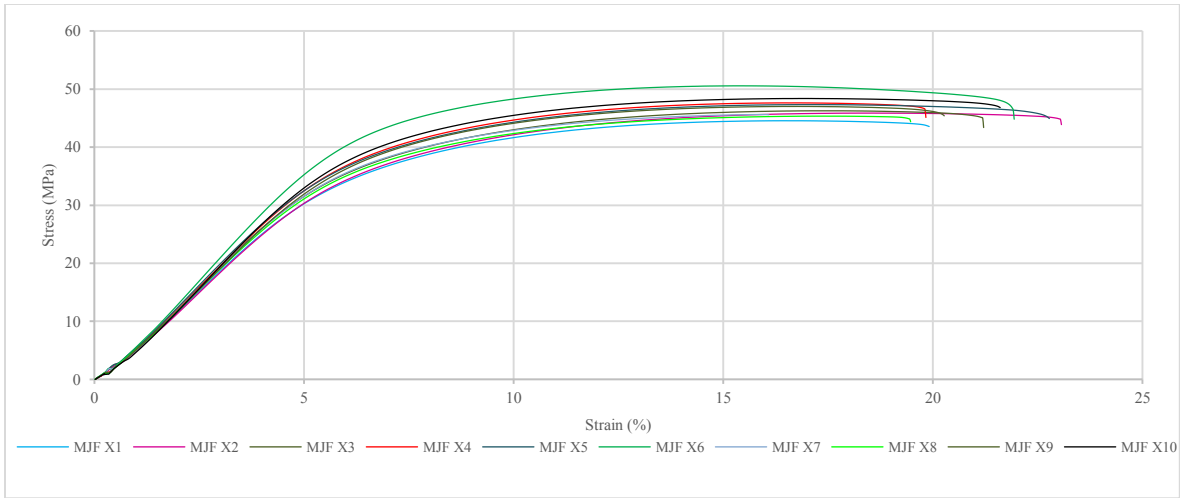

Figure I-e: Stress-Stress diagrams for MJF tensile specimens printed in Y direction.
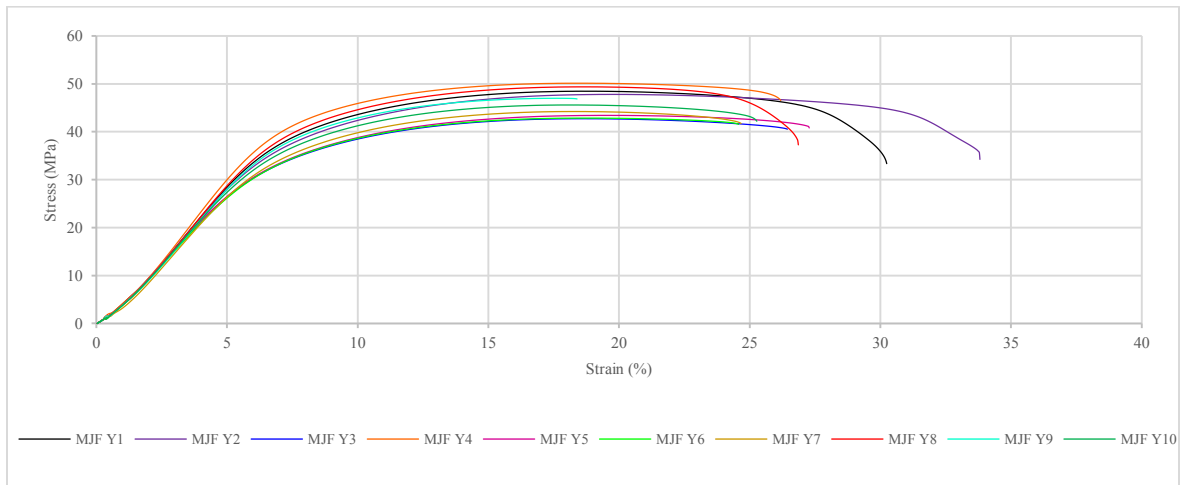

Figure I-d: Stress-Stress diagrams for MJF tensile specimens printed in Z direction.
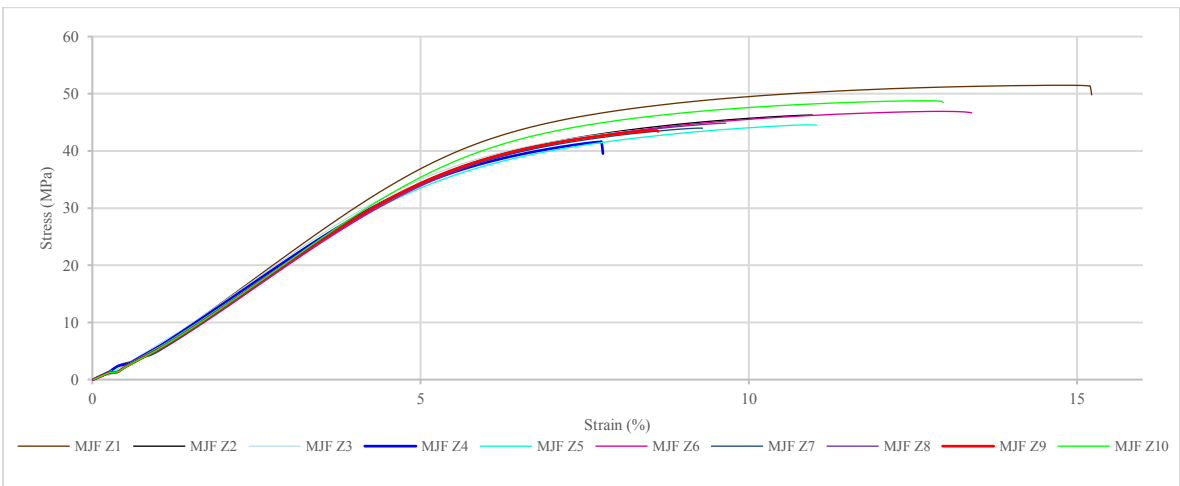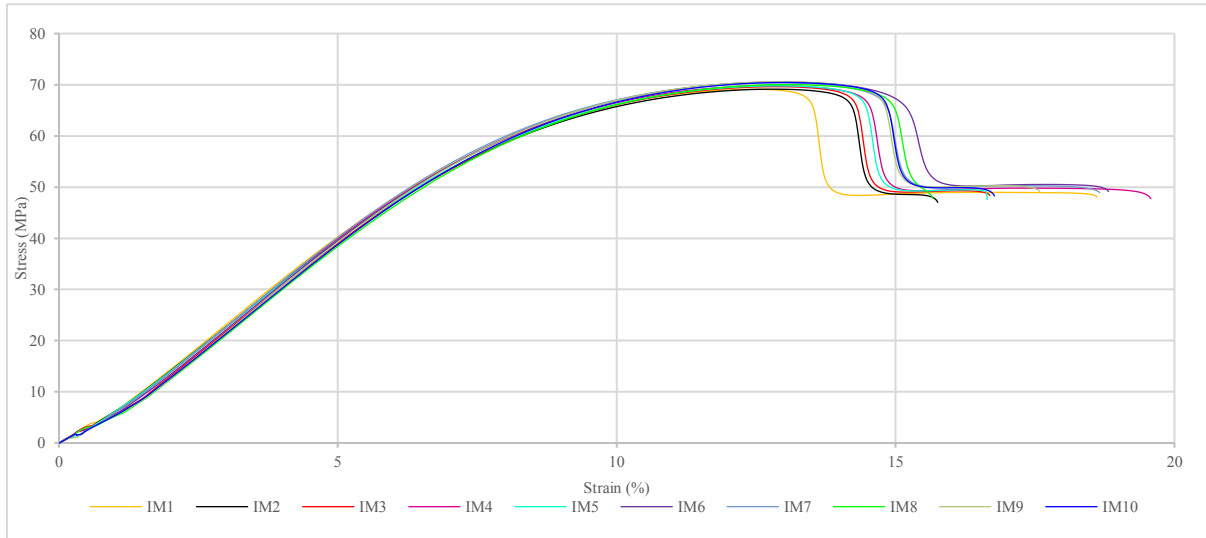
Figure I-e: Stress-Stress diagrams for Injection Molded tensile specimens.

Appendix II – Voltage withstand test results summary.

Table II-a: Summarized results from the voltage withstand tests for all 1 and 2mm specimens.

Specimen	Tester result	Temp. at pass/failure (°C)	Voltage measured at pass/failure temp. (kV)	Leak current range (mA) min.-max.
IM1mm_1	PASS	100	4.000	0.059 – 0.067
IM1mm_2	PASS	100	4.001	0.059 – 0.068
IM1mm_3	PASS	100	3.985	0.058 – 0.07
IM1mm_4	PASS	100	4.001	0.057 – 0.07
IM1mm_5	PASS	100	3.997	0.053 – 0.068
SLS1mm_X1	FAIL	100	3.992	0.061 – 5
SLS1mm_X2	PASS	100	4.002	0.06 – 0.285
SLS1mm_X3	FAIL	100	4.012	0.063 – 5
SLS1mm_X4	FAIL	100	3.989	0.064 – 5
SLS1mm_X5	PASS	100	4.002	0.063 – 0.264
SLS1mm_Y1	PASS	100	3.997	0.061 – 0.25
SLS1mm_Y2	PASS	100	3.982	0.063 – 0.268
SLS1mm_Y3	PASS	100	3.997	0.062 – 0.367
SLS1mm_Y4	PASS	100	3.998	0.058 – 0.226
SLS1mm_Y5	PASS	100	4.002	0.061 – 0.505
SLS1mm_Z1	PASS	100	3.997	0.061 – 0.325
SLS1mm_Z2	PASS	100	3.998	0.066 – 0.344
SLS1mm_Z3	FAIL	100	3.990	0.062 – 5
SLS1mm_Z4	FAIL	100	3.991	0.065 – 5
SLS1mm_Z5	PASS	100	3.974	0.065 – 0.623
MJF1mm_X1	PASS	100	4.000	0.061 – 0.132
MJF1mm_X2	PASS	100	4.003	0.067 – 0.202
MJF1mm_X3	PASS	100	4.001	0.068 – 5
MJF1mm_X4	FAIL	20	3.721 *	5

MJF1mm_X5	SHORT	20	0.045	5
MJF1mm_Y1	FAIL	20	2.805 *	5
MJF1mm_Y2	FAIL	30	3.998	0.24 – 5
MJF1mm_Y3	FAIL	20	4.003	5
MJF1mm_Y4	FAIL	20	3.685 *	5
MJF1mm_Y5	FAIL	20	3.998	5
MJF1mm_Z1	PASS	100	4.002	0.061 – 0.138
MJF1mm_Z2	PASS	100	3.997	0.083 – 0.51
MJF1mm_Z3	PASS	100	4.000	0.069 – 0.185
MJF1mm_Z4	PASS	100	4.001	0.074 – 0.3
MJF1mm_Z5	PASS	100	3.988	0.063 – 0.181
IM2mm_1	PASS	100	4.002	0.054 – 0.061
IM2mm_2	PASS	100	4.000	0.052 – 0.06
IM2mm_3	PASS	100	4.000	0.052 – 0.061
IM2mm_4	PASS	100	4.000	0.052 – 0.059
IM2mm_5	PASS	100	4.000	0.052 – 0.06
SLS2mm_X1	PASS	100	3.993	0.054 – 0.106
SLS2mm_X2	PASS	100	4.002	0.052 – 0.106
SLS2mm_X3	PASS	100	4.000	0.054 – 0.084
SLS2mm_X4	PASS	100	3.998	0.054 – 0.092
SLS2mm_X5	PASS	100	3.998	0.052 – 0.083
SLS2mm_Y1	PASS	100	4.011	0.056 – 0.13
SLS2mm_Y2	PASS	100	4.004	0.052 – 0.091
SLS2mm_Y3	PASS	100	3.998	0.054 – 0.099
SLS2mm_Y4	PASS	100	3.998	0.053 – 0.096
SLS2mm_Y5	PASS	100	4.002	0.053 – 0.09
SLS2mm_Z1	PASS	100	4.005	0.055 – 0.095
SLS2mm_Z2	PASS	100	3.995	0.054 – 0.1
SLS2mm_Z3	PASS	100	4.001	0.052 – 0.097
SLS2mm_Z4	PASS	100	3.996	0.054 – 0.092
SLS2mm_Z5	PASS	100	3.993	0.052 – 0.089
MJF2mm_X1	PASS	100	4.001	0.055 – 0.089
MJF2mm_X2	PASS	100	3.998	0.071 – 0.199
MJF2mm_X3	PASS	100	4.002	0.055 – 0.101
MJF2mm_X4	PASS	100	3.997	0.064 – 0.128
MJF2mm_X5	PASS	100	4.001	0.058 – 0.094
MJF2mm_Y1	FAIL	75	4.002	0.14 – 5
MJF2mm_Y2	PASS	100	4.004	0.196 – 0.472
MJF2mm_Y3	FAIL	80	4.012	0.197 – 5
MJF2mm_Y4	PASS	100	3.997	0.225 – 0.56
MJF2mm_Y5	FAIL	100	3.953	0.231 – 5
MJF2mm_Z1	PASS	100	4.008	0.06 – 0.103
MJF2mm_Z2	PASS	100	4.005	0.062 – 0.138
MJF2mm_Z3	FAIL	100	3.992	0.07 – 5
MJF2mm_Z4	PASS	100	3.997	0.057 – 0.108
MJF2mm_Z5	PASS	100	4.000	0.057 – 0.095

Failure presented during Voltage ramp phase of the test.